International Scientific-Technical and Production Journal

The Paton WELDING JOURNAL

August 2005 # 8

English translation of the monthly «Avtomaticheskaya Svarka» (Automatic Welding) journal published in Russian since 1948

Founders: *E.O. Paton Electric Welding Institute of the NAS of Ukraine*
International Association «Welding»

Publisher: *International Association «Welding»*

Address:
E.O. Paton Electric Welding Institute,
International Association «Welding»,
11, Bozhenko str., 03680, Kyiv, Ukraine
Tel.: (38044) 287 67 57
Fax: (38044) 528 04 86
E-mail: journal@paton.kiev.ua
http://www.nas.gov.ua/pwj

State Registration Certificate
KV 4790 of 09.01.2001

Subscriptions:
$324, 12 issues per year,
postage and packaging included.
Back issues available.

CONTENTS

CURRENT ACHIEVEMENTS OF THE E.O. PATON ELECTRIC WELDING INSTITUTE IN THE FIELD OF WELDING AND RELATED PROCESSES

B.E. PATON
E.O. Paton Electric Welding Institute, NASU, Kiev, Ukraine

Keywords: *vapor-phase technologies, electron beam welding and remelting, growing of single crystals, flash-butt welding, arc and hybrid processes, electroslag technologies, welding of live tissues, mathematical modeling, explosion welding, welding consumables, protective coatings, non-destructive testing, technical diagnostics, welded structures, service life*

In September 2004, the E.O. Paton Electric Welding Institute celebrated its 70-year jubilee. Traditions in its activity laid by Evgeny O. Paton, the founder of the Institute, and differed from many other research institutions, are based on combination of purposeful fundamental theoretical studies with engineering-applied developments, close creative relations with industrial enterprises. Owing to this, the Institute has become the largest research center in the field of welding and related technologies. At the present time its structure and system of management are improving to provide the further progress of welding and related processes and also to solve the basic problems of the industrial production under the new conditions.

Over the previous years the different trends in the Institute activity and its achievements in the scientific-technical progress of the society were elucidated many times. The present article describes some recent research and applied developments of the Institute.

New technological processes. *Vapor-phase technologies*. The new trend in the producing of inorganic materials with amorphous, nano- and microsized structure by a high-speed electron beam evaporation of materials and deposition from a vapor phase in vacuum (EB-PVD) is intensively progressing. New metallic, metal-ceramic and ceramic materials are produced by this technology in the form of functional or structural coatings on the surface of various products in the form of foils, plates (sheet) or some structural elements of a wide range of thicknesses (1–2 μm up to 5–10 mm).

A special attention is deserved by the technology of electron-beam evaporation of composite ingots, in which the composition and structure of gradient materials, deposited from the vapor phase, are «programmed». Figure 1, *a*, *b* shows schematically the structure and general view of a composite ingot, consisting of a ceramic base and separate fragments (inserts) of metallic and non-metallic materials. The inserts of materials of a required shape, sizes and vapor pressure value at temperature of evaporation are arranged in the ingot volume so, that the material with preset gradients of composition and structure could be formed during its continuous evaporation and subsequent condensation of the vapor phase on a substrate.

The hybrid technological processes including ionizing of a vapor flow of the main component and/or adding of inorganic or organic additions, interacting at the surface of condensation with a main component,

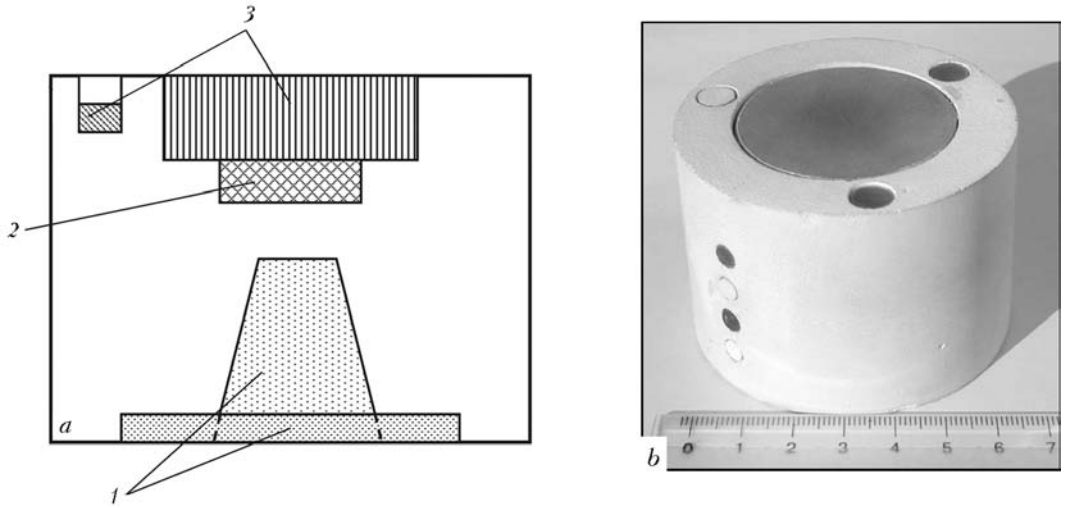

Figure 1. Scheme of structure (*a*) and general view of composite ingot (*b*): *1* — ceramics or mixture of ceramics; *2* — mixture of metals; *3* — metal, alloy, ceramics or organic additions

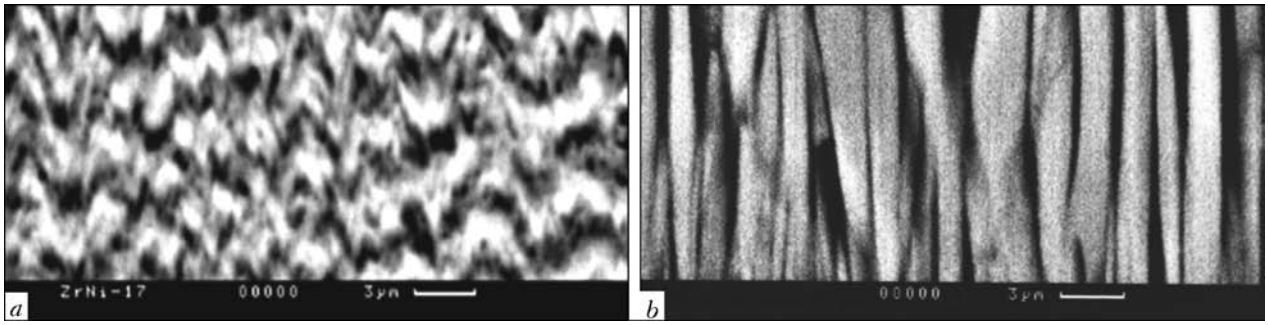

Figure 2. Structure of porous coating ZrO_2 (7 % Y_2O_3) with addition of Ni (*a*) and NaCl (*b*)

into it from a near-arranged source or using a composite ingot are also worthy to mention. In separate variants these can be chemical reactions, accompanied by removal of reaction products from the surface of condensation. This «treatment» of the vapor flow makes it possible to control the condensate structure within wide ranges (Figure 2).

The examples of existing and developing trends of practical application of vapor phase technologies and new materials can be illustrated by protective and structural coatings on different-purpose gas turbine blades, hard-oxide fuel cells, super-hard coatings on tools for materials processing, catalysts in the form of gradient porous coatings on appropriate surfaces (wire, strip, grid, etc.), biomaterials and biocoatings, materials and coatings with special physical properties (optic, electric, magnetic, etc.).

The present obtained experimental results of a high-speed electron beam evaporation of carbon and carbon-containing materials demonstrate also a feasibility of application of this technology for producing nanotubes and diamond-like structures.

Electron beam cold-hearth melting (EBCHM). The works are progressing in the direction of improvement of the technology of electron beam remelting for production of titanium ingots and semi-products using a less expensive initial raw material, such as a titanium sponge. At present the R&P Center «Titan», incorporated into the Institute, is capable to produce the industrial batches of titanium ingots of up to 1500 t per year. Among the recent achievements, the development of technology of melting VT6 alloy ingots-slabs, having a fine-grain equiaxial structure, should be noted.

Using modeling of the process of evaporation of alloying elements, the dependence of degree of evaporation of aluminium on the speed of melting and capacity of electron beam heating of metal in the mould was determined. It was found that aluminium content in the ingot at the capacity of electron beam heating of metal of less than 120 kW and melting speed of more than 200 kg/h is in the compliance with the requirements of standard for the alloy VT6 (Figure 3).

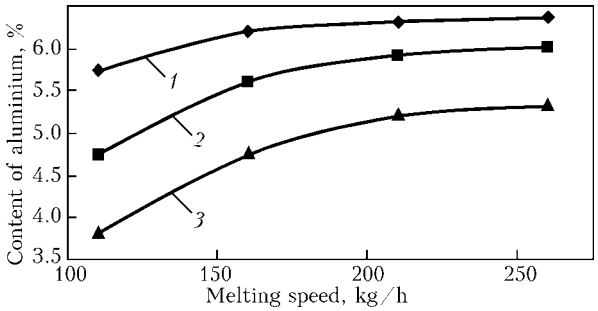

Figure 3. Dependence of degree of aluminium evaporation on melting speed and capacity of electron beam heating of metal in the mould: *1* — *W* = 90; *2* — 120; *3* — 160 kW

The three-dimensional mathematical model of heat transfer during ingots-slabs formation was constructed. The gradients of temperatures, rates of cooling and solidification of molten metal in each point of the VT6 titanium alloy ingot-slab were calculated on the basis of the ingot temperature field. Adequacy of model and feasibility of ingot structure prediction were proved.

Optimum technological conditions (90 kW capacity of electron beam heating of metal and 200 kg/h melting speed) were defined that allows producing a fine-grain equiaxial structure in the entire cross-section of the slab that is confirmed by the analysis of macrostructure of VT6 titanium alloy ingots-slabs of 150 × 950 mm section and 2 m length (Figure 4).

At the E.O. Paton Electric Welding Institute the method of electron beam melting was used for producing PT-3V titanium alloy ingots-slabs with a homogeneous chemical composition and structures, from which the welded structures of hydrofoil mechanisms of 200–250 mm thickness for sea ships without welding edge preparation were manufactured at the Feodosiya Ship-Building Company «More». The use of ingots-slabs could increase the efficient metal yield by 10 % and decrease the cost of manufacture by 20 % as compared a with traditional technology.

In addition, in the field of EBCHM the scientists of the Institute have created, for the first time in the world, the technologies and equipment for melting ingots from uncrushed blocks of spongy titanium, for producing high-quality ingots of complexly-alloyed titanium alloys, for melting hollow ingots for production of large-sized titanium pipes, where the technology of lateral surface melting is successfully used instead of their mechanical treatment.

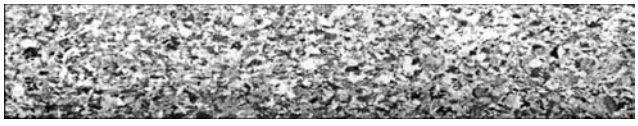

Figure 4. Macrostructure of VT6 ingot-slab of 150 × 950 mm section

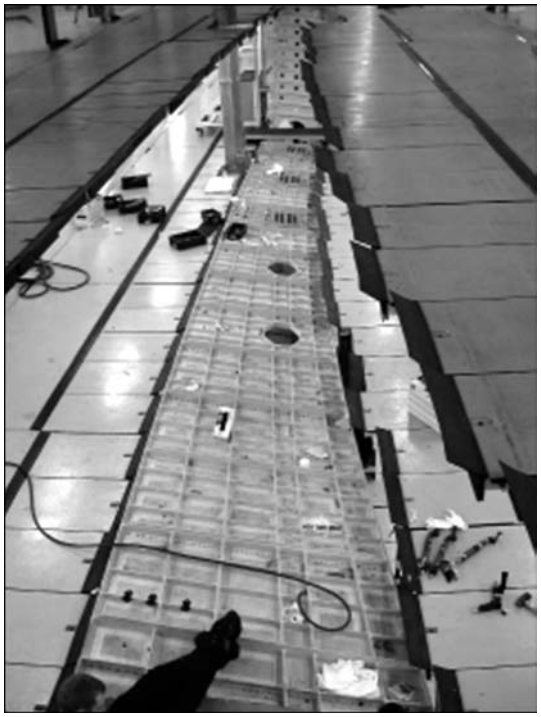

Figure 5. Assembly of airbus A-380 wing in AIRBUS UK using large-sized panels welded by electron beam (photo was given by company AIRBUS)

Electron beam welding of thick materials. For the first time the theoretical and experimental investigations of a spectrum of natural oscillations of molten metal in vapor-gas channels of large depth have been carried out. It was established that disturbances occurring under the effect of reaction of recoil of the evaporating metal in the form of capillary waves on the internal surface of the channel have a discrete spectrum of oscillations, whose first harmonic, characterized by the least frequency and highest amplitude, has a determinant influence on the stability of geometric sizes of vapor-gas channel and formation of defects in the form of different discontinuities in the middle and root parts of the welds. It was shown on this basis that the above-mentioned stability of vapor-gas channels of a large depth can be increased by inclination of the butt plane and electron beam at 10–12° angle to horizon. At such space reorientation of the weld pool the mode of natural oscillations of the molten metal is changed in the field of gravity force, i.e. their transformation from purely capillary waves, typical of a vertical channel, into capillary-gravitational waves. Similar transformation of molten metal oscillations in an inclined vapor-gas channel leads to a significant increase in frequencies of the lowest harmonics of oscillations, that causes the decrease in amplitude of disturbances of molten metal surface at the front wall of the channel, and, as a consequence, the increase in stability of the welding process as a whole.

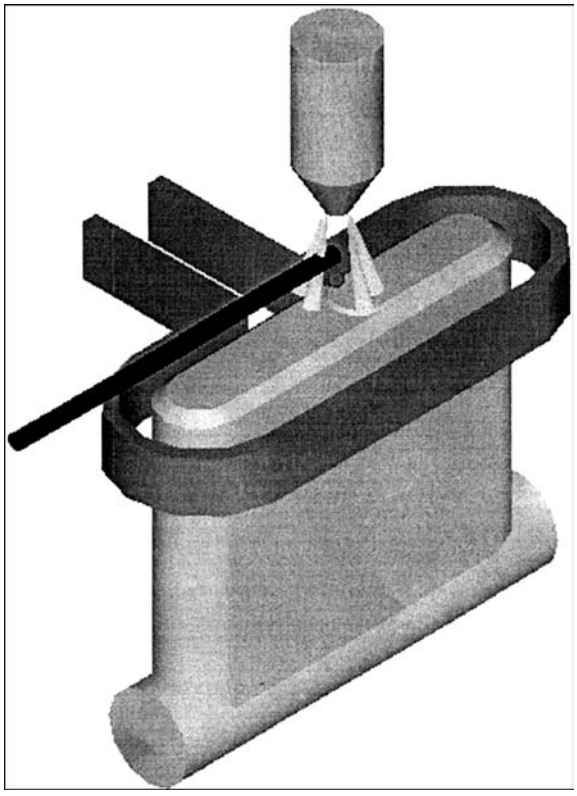

Figure 6. Scheme of process of plasma-induction growing of super-large single crystals of refractory metals

In addition, the effective means of increase in stability of formation of deep welds occurred to be the application of a scanning with a parallel transfer of beam along and across the welding direction. This leads to the reduction in averaged concentration of power, generated at the walls of the vapor-gas channel, and also to the decrease in number of primary electrons, reaching the channel bottom, that has a favorable influence on the increase in stability of the vapor-gas channel as a whole. For this case, the optimum range of frequencies of scanning of high-power electron beam in EBW of metal and alloys of large thickness was defined.

The results of investigations became the basis of technological processes of EBW of aircraft structures (Figure 5) manufactured from high-strength aluminium alloys of up to 150 mm thickness.

Growing of single crystals. Single crystals of refractory metals (tungsten, molybdenum) are the products of high technologies and the most of programs in the space nuclear power and aerospace engineering depend greatly on the progress in science and technology of high-temperature materials. The problem of growing large single crystals of refractory metals was seemed to be unsolvable over many years due to their high temperature of melting. Method of plasma-induction zonal growing of single crystals, developed at the Institute, allowed radical solution of this problem. The specifics of this method consists in the fact that there are no limitations for it both in sizes and also in shape of a cross section (circle, square, plate, pipe, etc.).

The combination of plasma and induction heating (Figure 6) can maintain the molten metal pool in electromagnetic field without the contact with copper being cooled that predetermined the challenging prospects of the method in growing large and super-large

($20 \times 140 \times 170$ mm and more) single crystals of refractory metals, as the increase in their sized has a determinant effect on widening the scale of their application in industry. Oriented single crystals of tungsten and molybdenum, in particle shaped ones, can be a perfect pre-fabrication for large rolled refractory metal products.

Electroslag processes in the production of composite billets. Among the methods of producing composite, including multi-layer and bimetal, billets and products used in industry, a special place is occupied by the methods based on application of the electroslag process: electroslag cladding (ESC), welding (ESW) and remelting (ESR), which are differed from other methods by their versatility and efficiency.

Over the recent years the new opportunities were open up for the improving the technology of producing the bimetal billets and products of different purposes, such as composite billets of mill rolls, bimetal reinforcement bars, hearth steel-copper electrodes of arc furnaces, etc. owing to the development of the new technological process at the E.O. Paton Electric Welding Institute of electroslag cladding with liquid metal (ESC LM) and the new technological diagram of ESR with two power sources (ESR DC) using of a current-carrying mould.

One of the most important conditions of producing a composite billet is a minimum change in chemical composition of clad layer metal by its dilution by a metal of the billet being clad. The study of isotropy of the chemical composition in height and section of composite billets of rolls of ESC LM (samples were cut out from lower, middle and upper parts of the billet) showed almost uniform distribution of basic alloying elements both in height and also in section of the deposited layer. Similar results were obtained in measurement of hardness on clad billets, that proves the isotropy of properties of the working layer of composite billets of rolls produced by ESC LM.

The investigation of technological capabilities of ESC LM showed that this method has a large number of advantages as compared with traditional methods of cladding. The application of ESC LM makes it possible to clad the external surfaces of cylindrical billets of almost any diameter, the thickness of the clad layer is defined exclusively by the requirements of the customer and can be 20–100 mm and more. ESC LM is characterized by the high efficiency of the process, which ten times exceeds the efficiency of traditional methods of cladding and amounts to 200–800 kg/h and more, depending on the sizes of parts being clad and materials being used.

In the scope of joint efforts with NKMZ Ltd. the first in the world industrial unit for ESC LM (Figure 7) has been created, which is designed for production of composite billets of mill rolls of up to 1000 mm diameter, up to 2500 mm length of barrel being clad and up to 20 t mass. A great experience has been gained in manufacture of billets with a high-chromium clad layer, first of all, for working rolls of

Figure 7. Appearance of industrial ESC LM installation at NKMZ Ltd. and billet of 740 mm diameter composite mill roll after cladding using ESC LM method

continuous wide-band mills. Tests of these rolls showed that their resistance was 2–3 times increased as compared with standard cast iron rolls used earlier.

Owing to the developed technology of ESC LM and a special design of a current-carrying mould, a constant regular rotation of slag-metal melt is realized in the process of cladding of the bimetal billet. This enables maximum averaging of the temperature and chemical composition of the metal pool in its cross-section, thus promoting more uniform melting of the base layer and producing a preset thickness of the cladding layer. Technology of ESC LM was realized in manufacture of bimetal billets of 350 mm diameter with a corrosion-resistant cladding using austenitic steel of 316L type and base layer of 20GS steel for 16 mm bimetal reinforcement bar (Figure 8). Metallographic examinations did not show any defects (laminations, cracks, slag inclusions, etc.) in the line of fusion of dissimilar steels.

Composite bimetal billets (steel + copper) are used as hearth electrodes of modern arc DC furnaces. In service of the furnace the steel part of the electrode contacts with molten melt, while its copper part serves as a lower current connector, to which all measuring instruments are connected. Reliability of hearth electrode and efficiency of the arc furnace service depend greatly on the quality of a dissimilar joint (steel + copper).

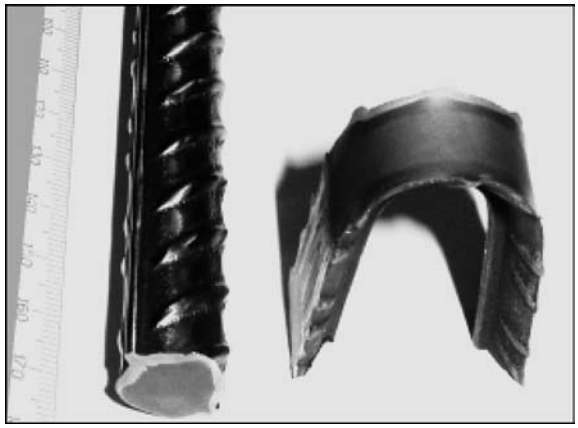

Figure 8. Appearance of bend-test sample (longitudinal macrosection) of 16 mm diameter bimetal reinforcement bar

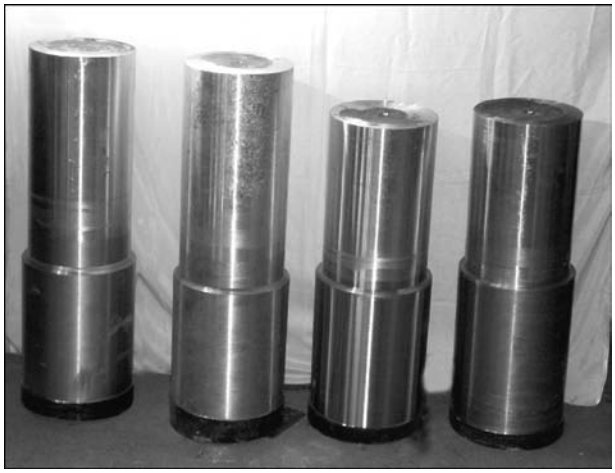

Figure 9. Industrial batch of 350 mm diameter steel-copper bimetal ingots of ESR DC for hearth electrodes of arc furnace

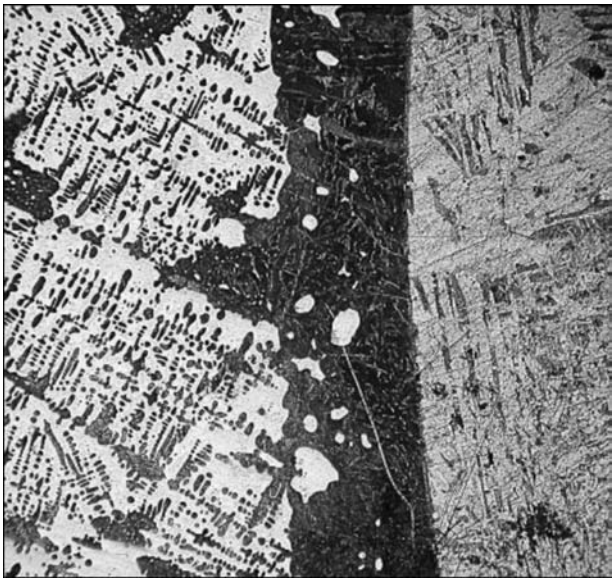

Figure 10. Microstructure of joining zone of dissimilar metals (steel + copper) in 350 mm diameter bimetal ingots of ESR DC for hearth electrodes of arc furnace (×320)

At the E.O. Paton Electric Welding Institute a radically new technological diagram of producing bimetal steel-copper ingots for hearth electrodes of arc DC furnaces, based on use of the electroslag process in a current-carrying mould by a double-circuit (ESR DC) allowing variation not only in depth, but in shape of the metal pool, has been developed. In this case, all the basic problems, connected with provision of a minimum length of transition zone of dissimilar metals and producing of high-quality billet with a guaranteed strength of layers joining, are solved. Technology, based on ESR DC, can produce monoblock bimetal ingots (steel + copper) for hearth electrodes of up to 350 mm diameter and up to 1300 mm length (Figure 9). The conducted complex of investigations of metal of bimetal ingots, including macro- and microexaminations (Figure 10) of the zone of joining the dissimilar metals (steel + copper) confirmed their high metallurgical quality and compliance with requirements specified to the heath electrodes of the arc DC furnaces.

Flash-butt welding. The flash-butt welding is referred to the number of most effective methods of metal joining. This direction continues to progress successfully and its capabilities have not yet been exhausted. A new variety of method of welding with a continuous flashing, named as welding with a pulsing flashing, has been developed. This method, patented in leading countries of the world, allows twice decreasing in the duration of welding process and tolerances for flashing (Figure 11), providing a highly-concentrated heating. This opens up the opportunities for joining hard-to-weld, softening materials, and also for widening the fields of application of the flash-butt welding. New technologies of welding high-strength steels and alloys, dissimilar metals were developed on its basis. In particular, the new technology of welding rails of infinite length in repair of continuous railway tracks has been developed and implemented. The required tolerance for welding is compensated in this case by tension of rails welded. Computer-aided systems of automatic control of main parameters, providing the reproduction of preset conditions of welding independently of tension forces in rails have been developed. In addition, the control system makes it possible in welding to set the preset level of stresses in rail sections of the continuous track with account for the surrounding temperature. New generation of rail welding machines of K922 type has been developed for welding with a tension, in which new technologies

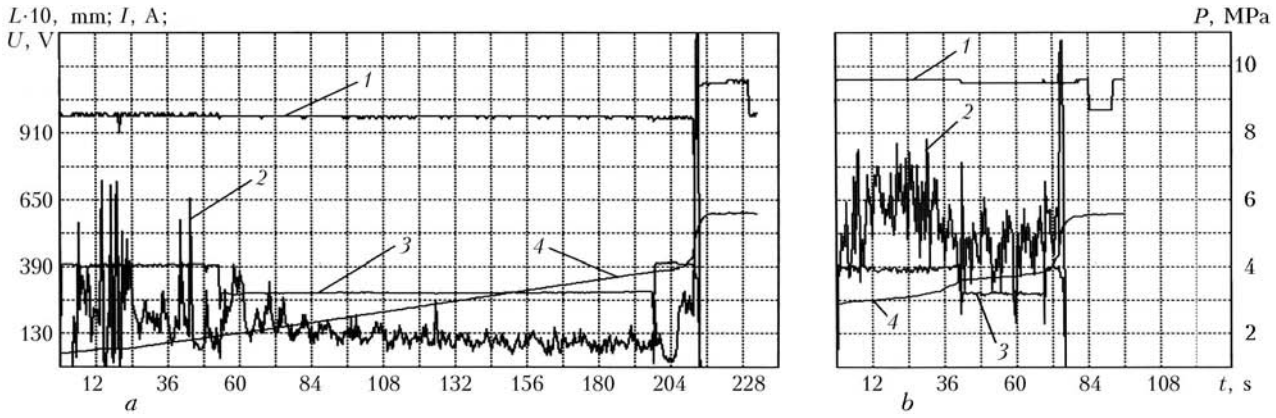

Figure 11. Main parameters of flash-butt welding of R65 rails with continuous (*a*) and pulsing (*b*) flashing: *1* — pressure; *2* — welding current; *3* — welding voltage; *4* — displacement

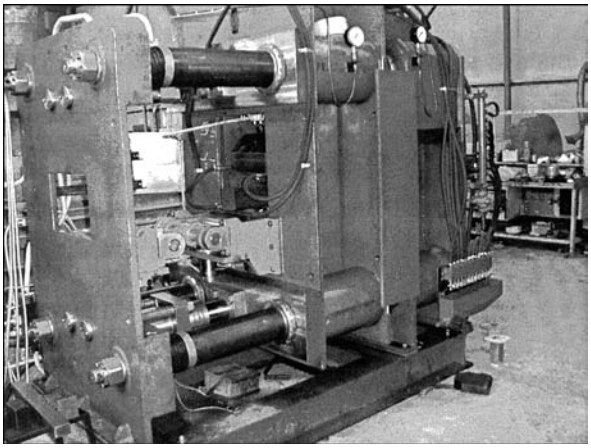

Figure 12. Flash-butt welding machine K1003 for joining massive rolled sections

and control systems were realized. The manufacture of these machines, having demand at the world market, is organized at Kakhovka Plant of Electric Welding Equipment.

Based on the method of a pulsing flashing, the new technologies of joining rolled prefabrications of a large cross-section area (more than 20,000 mm^2) have been developed. To realize these technologies, the new flash-butt welding machine K1003 has been designed and manufactured (Figure 12).

The radically new processes of magnetically impelled arc butt welding have been developed, widening significantly the capabilities of the process. In particular, the MIAB technology of welding pipes of up to 219 mm diameter and up to 12 mm wall thickness has been developed (traditional process allows welding pipes of up to 100 mm diameter and wall thickness of not more than 6 mm). A series of universal and specialized equipment for the realization of this technological process has been created.

Hybrid processes. Over the recent years a new trend in the creation of science intensive technologies, i.e. hybrid methods of welding, has been formed at the Institute. The research works are carried out on the study of processes based on use of a laser radiation and arc with consumable electrode, and also a laser radiation and plasma (Figure 13). Technologies of laser-arc welding of steels and aluminium alloys, and also the technologies of a combined and hybrid surfacing and surface alloying of steels have been developed. Technology of multi-pass hybrid welding (laser + arc with consumable electrode) of thick steels has been suggested (Figure 13, *a*). At a limited power of a laser radiation (up to 3 kW) this method makes it possible to weld low-alloy steel of up to 20 mm thickness for three-four passes (laser radiation up to 10 kW is necessary for a single-pass laser welding of steels of such thickness). It was established that the speed of hybrid welding of aluminium alloys can reach up to 300 m/h (for $\delta = 2$ mm) and more (Figure 13, *b*). At the same power parameters of arc and laser beam the speed of arc welding is 30–50 m/h, while

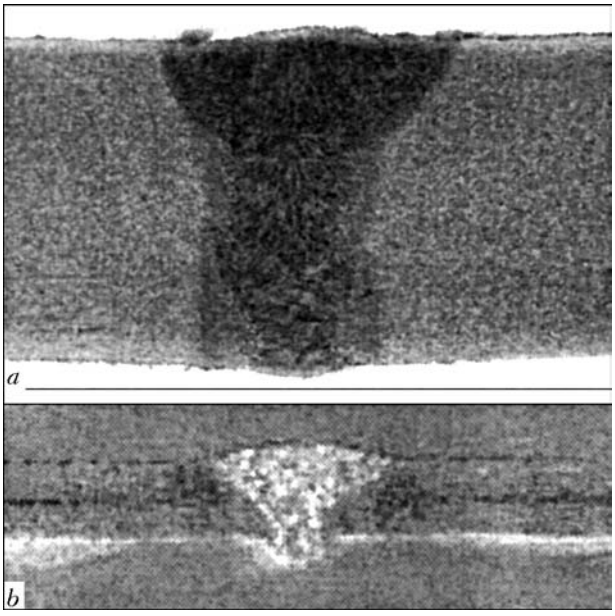

Figure 13. Macrostructure of butt joints made by laser-arc welding: *a* — steel X70 of 18.7 mm thickness, 4 passes (2.7 kW radiation power, 25 m/h welding speed, 400 m/h wire feed speed (1.2 mm dia.), 200 A welding current, 25 V voltage, CO_2 shielding (×2.5); *b* — alloy AMg6 of 1.9 mm thickness (2.5 kW radiation power, 300 m/h welding speed, 760 m/h wire feed speed, 200 A welding current, Ar shielding) (×5)

that of laser welding is 60 m/h. Increase in speed is stipulated by a synergic effect (mutual effect and increase in stability of hybrid process constituents).

To deposit the ultrathin layers of wear- and corrosion-resistant coatings, a combined process, consisting in combining of microplasma spraying and laser surfacing, has been developed. It can eliminate a main

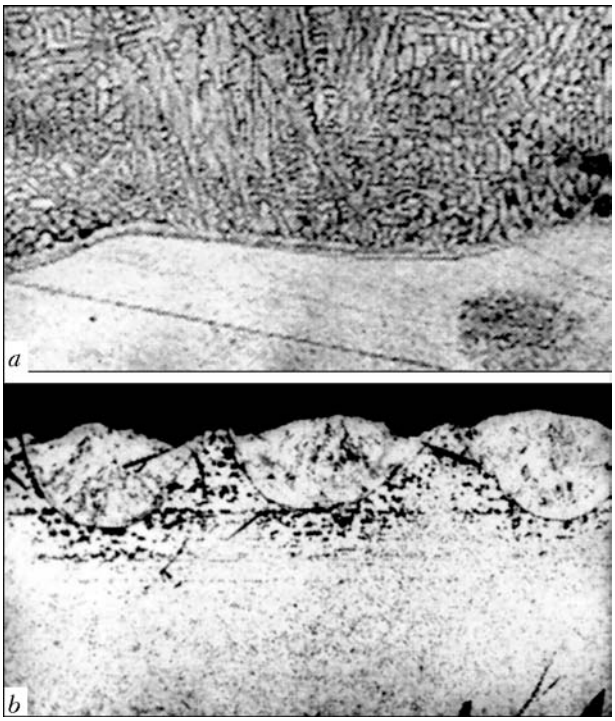

Figure 14. Microstructure of coating from alloy of Ni–Cr–B–Si system deposited on carbon steel (*a* — ×1000) and paths of laser-microplasma surface alloying of low-carbon steel with chromium (*b* — ×32)

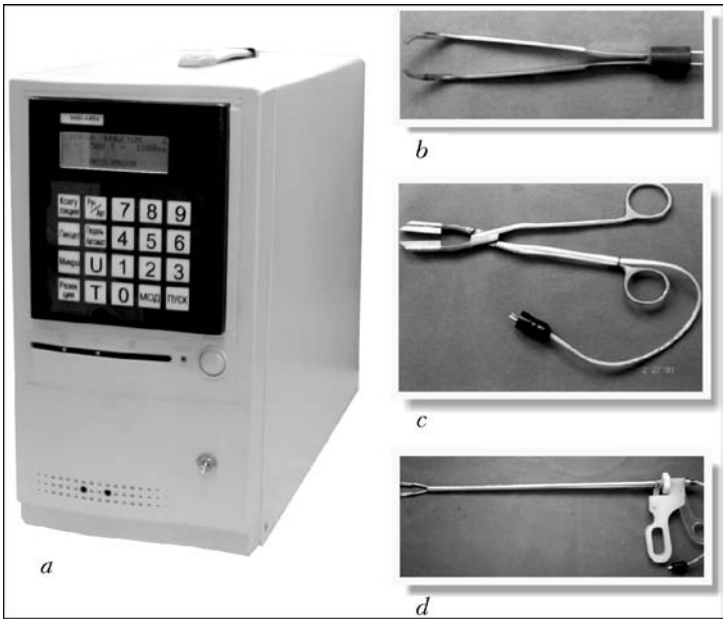

Figure 15. Equipment and instrument for welding live tissues: *a* — high-frequency welding power source; *b* — medical welding forceps; *c* — medical welding clamp; *d* — medical laparoscopic clamp

drawback of laser surfacing, such as crack formation, and also increase the density of sprayed coatings and strength of their adhesion with a base (Figure 14, *a*). Here, there is no need in preliminary preparation of surface, necessary in case of application of microplasma spraying. The similar combined process was suggested for surface alloying of steels to increase their hardness and heat resistance (Figure 14, *b*). Making hard paths of alloying in a softer and ductile matrix allows decreasing the susceptibility to formation of a grid of fire cracks in service, for example, of artillery barrels.

Welding of animal and human soft tissues. This is a quite new direction for the Institute. Application of high frequency currents for hemostasis, i.e. blood-vessel occlusion to interrupt or prevent bleeding in surgical operations, has been known since long ago. It was proved by us that there is one more field of using high-frequency currents for joining the areas of tissues and organs, without threads and metallic staples, reduction of time of patient staying under narcosis, reduction to minimum of decomposition products enter the wound, minimizing the blood losses, reduction of bactericidal action and pains during operation, reduction of probability of metastatic spreading and blood losses. Technique of producing joints resembles the technology of resistance welding of metal parts and partly polymeric materials. Surely, the mechanism of joint formation is differed radically. Tissue heating by passing of high-frequency current along it leads to denaturation of protein, acceleration of its thermal movement and formation of a common albuminous space with forming a joint after its cooling. The cooling is accompanied by renaturation of protein, i.e. by the recovery of structure. However, the protein structure is recovered not completely. A part of molecules undergoes irreversible changes and does not renaturate. The degree of renaturation depends on the highest temperature and time of tissues duration at it. As the irreversible change of protein is not desirable, the welding should be performed in relatively narrow temperature and time intervals that requires automatic control with appropriate feedbacks.

Models of electrosurgical equipment have been designed (Figure 15), which can be used not only for welding, but also for hemostasis and thermal cutting of tissues. This equipment is used in several Ukrainian hospitals not only for experimental operations, but also in a routine practice. The application of welding occurred to be effective in general surgery, operative gynecology, oncology, otolaryngology, operations on liver, lungs and other organs.

We have intention to further develop works in the field of electrosurgery as one of the most important trends in modern medicine.

Improvement of technologies and materials. *Mathematical modeling*. A great attention in investigation and optimization of welding technologies is paid to the mathematical modeling of typical physical (chemical) processes (phenomena), on which the quality of products depends greatly. The progress of computer engineering creates good prospects for application of rather complex models, reflecting multiple factors and interrelation of phenomena proceeding in welding and related technologies, that is very important to extent knowledge in this field. In addition, the computerization of the mathematical modeling makes it accessible for a wide circle of users, dealing not only with research works, but also with development and optimization of the engineering solutions.

The priory directions include the development of information-calculation systems for typical problems, representing interest for the practical work, in particular, systems for the selection of a rational method of arc welding, welding consumables and conditions

for welding a definite structural steel; determination of stress-strain state in welding of circumferential multi-pass welds of similar and dissimilar thick-walled elements of structures; determination of stresses and strains in tube sheet of heat exchangers in welding-in of tubes; prediction of stresses and strains, microstructure and properties in surfacing of bodies of rotation of shaft type by a spiral line of a small pitch with account for complex thermal cycles in HAZ metal and deposited layer; creation of system for flash-butt and resistance welding for modeling the coupled fields of electrical potential, heat evolution, temperatures, strains and stresses on the basis of process parameters, measured in time (current voltage, compression forces, upset displacements).

Welding of structures from high-strength low-alloy steels. The works of the recent years are devoted to the solution of problems of welding structures made from HSLA steels. This is, first of all, the prevention of a brittle fracture of welded joints, caused by structural transformations and hydrogen-induced embrittlement.

A new physically-grounded criterion, characterizing the degree of deterioration of brittle strength of metal under the hydrogen effect, has been suggested and procedure of use of the new criterion, allowing for the data of mechanical tests, has been developed.

The main link of the hydrogen embrittlement is the behavior of an initiated microcrack, appeared during deformation, in the presence of hydrogen.

Localizing of a negative charge on adsorbed atoms of hydrogen leads to the decrease in the level of a normal stress required for microcrack transition into autocatalytic propagation in the field of stresses, that is considered at the macrolevel as an effect of embrittlement.

The most important factors of hydrogen embrittlement are the evolution of dislocation structure in plastic deformation, and also the properties of grain boundaries, particles of the second phase, non-metallic inclusions. A special role of dislocations in the mechanism of hydrogen brittleness is stipulated by the fact that their displacement is the main mechanism of plastic deformation and simultaneously the most effective method of hydrogen transportation in the metal volume.

Non-metallic inclusions, depending on their binding with a matrix, can act from the very beginning of deformation as cracks, and the brittle inclusions can initiate themselves the initiation of sharp cracks.

Hydrogen in metal of weld and HAZ decreases the specific energy of a submicrocrack surface. Reduction in stress of a brittle fracture, caused by the submicrocrack, initiated by a dislocation scheme, is proportional to decrease in specific surface energy under the hydrogen effect.

It is possible to decrease the susceptibility of the welded joint to cold cracking by introducing the hydrogen traps into the weld metal. Hydrogen traps are different structural defects, such as vacancies, dissolved atoms, dislocations, boundaries of grains and phases, micro- and macropores, non-metallic inclusions, particles of the second phase, etc. The adding of rare-earth elements to the weld metal is effective. Compounds of these elements are sorbing the hydrogen, releasing matrix from it, thus retarding the mass transfer of hydrogen in the most stressed areas of weld and HAZ.

Investigations of mechanism of hydrogen absorption by metal during welding were carried out, the role of arc temperature, current polarity, temperature of molten metal, air medium and equipment for hydrogen determination in welding consumables and welded joints was evaluated. Absorption of hydrogen from plasma of arc discharge is defined by the degree of its ionizing and depends on arc temperature. The assessment of behavior of hydroxide and hydrogen fluoride in arc atmosphere showed that fluorine and oxygen interact effectively with hydrogen at the arc column periphery. Main hydrogen sources in welding consumables were found, metallurgical and technological measures were offered to decrease the hydrogen content in metal of welded joints and to prevent the formation of hydrogen-induced cracks.

The results of investigations were used for the development of welding consumables, such as electrodes and agglomerated fluxes, guaranteeing the ultralow contents of hydrogen in weld metal (up to 1 $cm^3/100$ g). This makes it possible to decrease significantly the temperature of products preheating.

A series of grades of flux-cored wires for welding of thick-walled structures of the metallurgical equipment has been created.

The application of new low-hydrogen welding consumables is rather challenging in ship and railway car building, in manufacture of heavy-loaded machine metal structures, and also in construction of pipelines and in many other branches.

A series of electrodes for welding low-alloy steels of increased and high strength has been developed:

- ANO-101, ANO-102 (for steels with a yield strength up to 460 MPa, with Si–Mn and Si–Mn–Ni–Cu systems of alloying);
- ANO-100 (for steels of up to 550 MPa yield strength, with Si–Mn–Cr–Ni–Cu system of alloying);
- ANO-103 (for steels of up to 650 MPa yield strength, with Si–Mn–Mo system of alloying).

New agglomerated fluxes for welding low-alloy steels have been developed:

- ANK -561 (flux of aliminate-basic type for welding steels of up to 490 MPa yield strength, with Mn–Si–Ni system of alloying);
- ANK-57 (flux of fluorite-basic type for welding steels of up to 590 MPa yield strength, with Mn–Si–Ni–Mo–Ti system of alloying).

Electroslag welding. Machines of the new generation for ESW with wire electrodes have been designed and manufactured: AD381 is the twin-electrode machine for site welding of 30–60 mm thicknesses, and ASh 115M is designed for welding of curvilinear welds of up to 200 mm metal thickness.

The AD381 type machine was used successfully in repair and construction of casings of blast furnace jackets and converter casings made from low-alloy steels, and can perform all vertical increments and site joints, thus increasing significantly the productivity of site jobs.

The works were carried out for 2 or more times increase in ESW speed with a simultaneous reduction in heat input to increase the efficiency and to refuse the postweld heat treatment. The basic principle is the control of the heat generation zone and electrodynamics of the slag and metal pools. The control is realized by varying the path of current passing in a slag pool by an appropriate connection and commutation of current connectors to the electrodes and workpiece being welded.

The investigations are carried out for the development of the method of electroslag welding or cladding using fixed consumable sectional large-section electrodes in a narrow gap for thick metal.

The method allows producing thick welds without use of a complicated welding equipment and a scarce welding wire. The process can be controlled by a preset program. At the present time the thickness of 600 mm can be welded.

Systems of stabilization of current, voltage and level of metal pool are being developed and implemented successfully.

Welding of high-alloy steels and alloys. Aircraft engines, as well as gas turbine units (GTU) of land or off-shore application are the very important and most science intensive part of the modern transport engineering. The updating of their technical characteristics (effective power, cost, effect on ecology, service life, etc.) represents a complex designing, materials science and technological problem. The intensive work is going on in all the world for its solution. The key technologies are necessary to open up the new opportunities both for the application of advanced materials with special properties and to find the new design solutions on their basis.

The Institute in collaboration with such leading specialized organizations of Ukraine as «Progress» and «Motor Sich» (Zaporozhie), «Zarya-Mashproekt» (Nikolaev), M.V. Frunze MNPO (Sumy) carries out research and experimental-industrial works in two directions, namely development of repair technologies to extent the service life of aircraft and gas turbine engines and development of technologies for realization of conception for producing all-welded monoblocks of GTU of the new generation on the basis of permanent joints of GTU elements made from challenging materials.

Extension of GTU life is based on grounding a feasibility and development of technologies of multiple recovery of service characteristics of nozzle vanes and blades, elements of disc, heating chambers, sealing elements and other highly-loaded parts of GTU. The new technologies have been developed at the Institute in collaboration with industrial enterprises for restoration and repair of almost all types of products from heat-resistant nickel alloys, including alloys of the new generation with content of γ-phase up to 70 % and more (on the base of intermetallics) (Figure 16).

Technologies of joining alloys with polycrystalline directed and monocrystalline structure without violation of their structural orientation in the site of joining and with preservation of the preset level of properties have been mastered.

In combination with special types of heat treatment and deposition of advanced functional coatings it is possible to 1.5–3 times increase the life of element in operating units.

Creation of all-welded monoblocks of GTU became possible by application of new technologies of joining, accounting for the weldability of materials. These technologies include microplasma surfacing and spraying, reactive-diffusion bonding, welding with use of hybrid types of a microdischarge. The Institute has offered a new conception of assessment of weldability of materials of various types on the basis of fact that the weldability is a physical property of the material which can be controlled. Using this approach, the new processes have been developed, allowing producing monoblocks of blades with a disc (Figure 17) or impellers (Figure 18) with exclusively high service characteristics and operating life.

Welding of titanium and titanium alloys. The works are carried out for the development of new structural titanium alloys with a good weldability for the aerospace engineering, chemical machine building, medicine, etc. A pilot alloy T-110 (Ti–5.5Al–1.2Mo–1.2V–4Nb–1.8Fe) has been developed, which is not inferior to the known alloy VT22 by the level of strength, but it possesses a good weldability both in arc and electron beam methods of welding. After heat treatment the welded joints of alloy T-110 have good characteristics of ductility at the level of strength of not less than 95 % of that of the parent metal (1100 MPa), and fatigue life of welded joints at 600 MPa load is $5 \cdot 10^6$ cycles.

Resistance in aggressive media is one of the most important characteristics of titanium, defining its wide application in chemical machine building. The highest corrosion resistance is observed in commercial titanium and its alloys with palladium. However, the strength of these alloys does not exceed 500 MPa. Corrosion resistance of high-strength industrial titanium alloys is inferior to commercial titanium by this characteristic.

The investigations showed that it is possible to increase the strength of titanium without decrease in its corrosion resistance if to use isomorphous β-stabilizers, in particular, molybdenum, vanadium and niobium as alloying elements. Titanium alloy of Ti–4.5Al–2.5V–2.5Mo–3.5Nb–1.5Zr has been developed on this basis. The strength of alloy (950 MPa) almost 2 times exceeds the strength of the commercial tita-

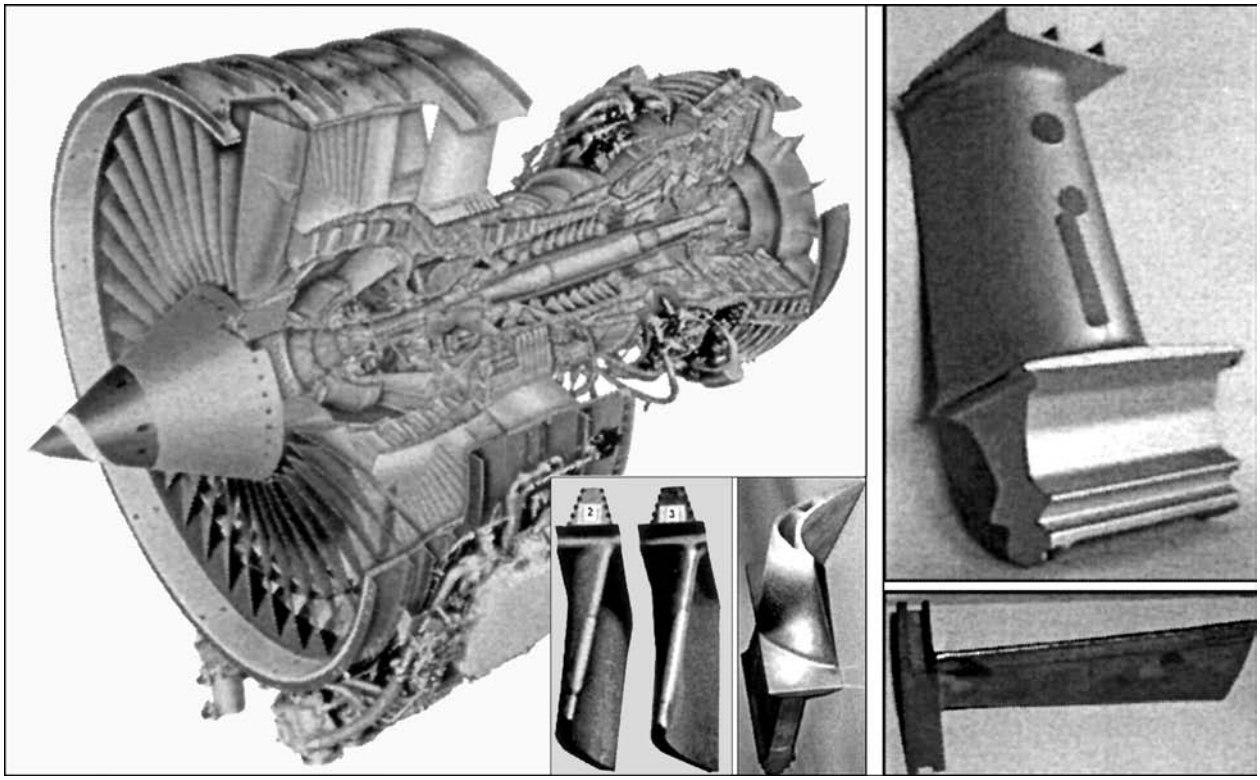

Figure 16. Blades and nozzle vanes made from nickel superalloys

nium, and its stress corrosion resistance is not inferior to that of the commercial titanium.

Theoretical and experimental investigations in the field of chemically pure halogenide fluxes for welding titanium and its alloys contributed to the creation of the radically new methods of welding (as regards to titanium). They include automatic consumable electrode submerged arc welding, electroslag welding of titanium, argon-arc tungsten electrode welding over the slag layer (A-TIG), narrow-gap magnetically impelled arc welding.

Flux-cored titanium wires and technologies of titanium welding with tungsten electrode in argon have been developed. This process can perform single-pass welds without edge grooving on titanium of up to 16 mm thickness. Technologies of mechanized welding of titanium with non-consumable electrode and appropriate equipment have been developed for welding under the shop and site conditions. The works are carried out for activation of metallurgical processes in EBW of titanium using the proper fluxes.

Welding of composite, dissimilar and hard-to-weld metals. Joints of dissimilar and hard-to-weld metals require a dosed highly-concentrated input of heat to the zone of joining to minimize the thermal effect on the properties of parent metal and to decrease the possibility of formation of brittle intermetallic phases. It was suggested to solve this problem by use of the composite inserts and nanoactivators, arranged between the parts being welded, in the resistance pressure welding. Composition of material and shape of inserts are designed so that to have a feasibility to increase the transient resistance in the butt, that leads in its turn to the highly-concentrated heating of parts being welded. This prevents their hardening and provides mechanical properties at the level on one of metals being welded. A nanoactivator, used simultaneously with inserts, protects the weld metal and promotes also the formation of structures, free from oxides, around the near-weld zone, thus decreasing the probability of formation of brittle intermetallic phases in the joint. The developed technology has found its application in welding dispersion-strengthened copper, aluminium with steel and copper with tungsten alloys (Figure 19).

Explosion welding. Concerning the development of theory of explosion welding, the conditions of joint formation in collisions at minimum allowable rates

Figure 17. Disc with blades

Figure 18. Fragment of GTU blade

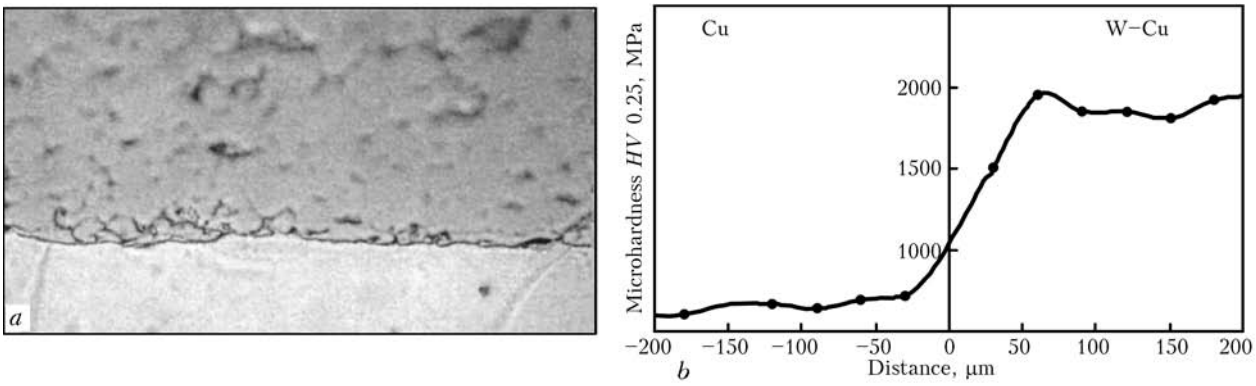

Figure 19. Microstructure of copper-tungsten alloy joint (*a*) and distribution of microhardness in it (*b*)

were studied. The results of these investigations are used in the development of «partial load» technological conditions of welding for manufacture of elements of metal structures sensitive to the level of residual plastic deformations and risk in their fracture. The effect of difference in density and hardness in joining dissimilar materials was defined. The effect of roughness of surfaces joined was studied and recommendations for rational selection of degree of cleanness of their mechanical treatment were formulated. Procedures of chemical preparation of the surfaces joined in welding high-strength aluminium alloys with a decreased capability to a high-speed plastic deforming were optimized. It was shown that preliminary chemical treatment allows joining these alloys directly, without interlayers of more ductile metal.

The results of investigation are shown in Figure 20, where a typical region of weldability by explosion for metals is shown in system of coordinates «angle of collision–rate of contact point». Optimum are the conditions adjacent to the lower boundary of this region. The obtained results made it possible to develop the technological conditions of explosion welding in the band of width of several degrees lower than the traditional lower boundary (see dashed band of «precision explosion welding» in Figure 20).

The main consumers of technologies developed on the basis of investigations are the electrical industry and non-ferrous metallurgy, which need, first of all, the reliable bimetal adapters for high-current electric circuits. Technologies of manufacture of tubular transition pieces of variable section from dissimilar metals (Figure 21) and deposition of protective coatings (anti-corrosion, wear- and heat-resistant) on large-sized products have been developed for machine building and metallurgy.

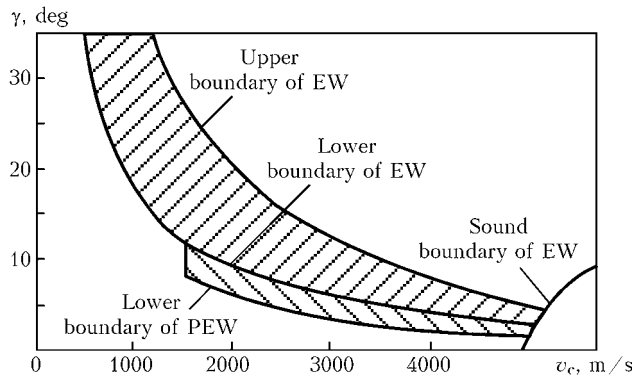

Figure 20. Region of weldability in use of explosion

Brazing. A great attention is paid traditionally at the Institute to the fundamental and applied investigations in the field of brazing, in particular, joining of promising hard-to-weld materials (intermetallic, dispersion-strengthened, heat-resistant nickel alloys), joining of thin-walled, including multi-layer, structures. New brazing filler alloys have been developed for high-alloy nickel alloys (for example, on the base of Ni–Cr–Zr system). They have new qualitative level as compared with traditional ones and allow significant widening of volume of application of construction and repair brazing in the modern engine construction.

Brazing filler alloys and technology of brazing alloys on the intermetallics base, in particular γ-TiAl, have been developed. The strength of joints produced with use of the developed brazing alloys are close to the strength of the parent metal at room and high (700 °C) temperature, and also at long-time strength test.

Brazing filler alloys, technology and equipment have been developed for vacuum brazing of lattice structures, for example, rocket rudders. Creation of a carrousel type unit made it possible to solve the

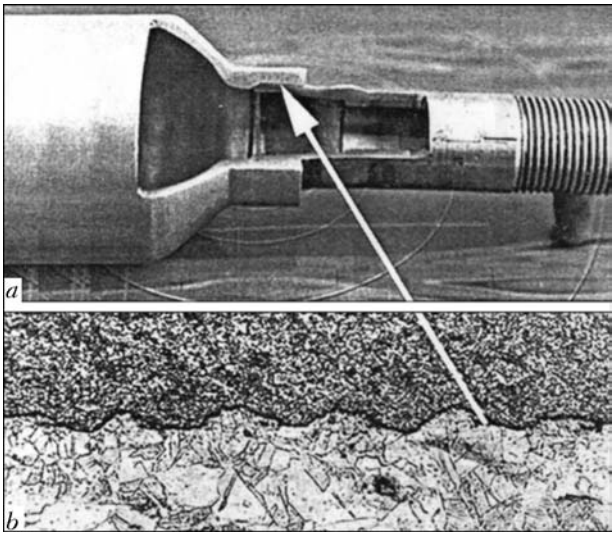

Figure 21. Tubular transition piece (*a*) and microstructure of joint (*b*)

most important problem, such as significant increase in productivity of the vacuum brazing.

Arc brazing opens up the large prospects for manufacture of thin-walled structures. Significant reduction in heat input, absence of spattering, undercuts, a good surface of welds are far from a full list of advantages. In particular, it can join the zinc-plated iron without deterioration of the protective layer.

Results of investigations in the field of brazing of aluminium and its alloys are very promising for the industrial application. Thus, the reactive flux allows aluminium brazing without brazing filler alloys. The latter is formed due to a reaction of flux components with aluminium. The new flux is a good basis for the development of highly-effective technologies in a serial manufacture of automobile radiators, radiating aerial and other products.

Protective coatings. The works are intensively progressing in the field of deposition of different-purpose functional coatings (wear-, corrosion-, heat-resistant, bioactive, etc.) using the thermal spraying, diffusion saturation and electric-spark alloying. Unique equipment, materials (powders, flux-cored wires) and technologies are being developed for producing coatings.

The designed installation of MPN-004 type for microplasma spraying, characterized by small dimensions (14 kg mass), low level of noises (30–50 dB), small size of spraying spot (1–5 mm) allows spraying coatings of a wide range of materials (metals, alloys, oxides, carbides, etc.). Technology of microplasma spraying of bioceramic coatings is used for deposition of bioactive coatings from hydroxyapatite on different types of endoprostheses (Figure 22). A feasibility was found to produce textured bioceramic coatings by the same way. The presence of texture stimulates of the process of resorption (dissolution) of the coating material. The developed technology makes it possible to control the phase composition and texture of the bioceramic coating that provides the feasibility of producing coatings with optimum properties.

Works in the field of quasi-crystalline coatings, deposited by the method of a supersonic air-gas spraying (unit «Kiev-S») have led to the creation of coatings, possessing heat conductivity of 1.5–2.0 W/(m·deg) and promising for use as heat-protective coatings, in particular, in internal combustion engines manufactured from aluminium alloys.

The works are carried out for the development of a hybrid laser-arc technology of producing coatings, characterized by a feasibility to combine the process of coating deposition with a process of synthesis in a gas phase, for example, for deposition of diamond and diamond-like coatings.

Resource of safe service of welded structures. The definite resource of a safe service of modern welded structures is designed even at the stage of their designing and manufacture. However, at a long-time service of critical structures (bridges, main pipelines, large oil- and gas storages, etc.) their resource of service is periodically determined on the basis of:

- monitoring of a real load capacity of structures;
- technical diagnostics of their conditions from the point of view of the presence of discontinuities and defects of shape, level of residual non-relaxed stresses, degree in change of characteristics of material resistance in hot points under the effect of different types of loading;
- design codes, binding the load capacity and results of technical diagnostics for the integrated determination of the safe service resource.

In many cases the «hot points» of the welded structures are the welded joints. The intensive works are carried out at the Institute, connected with the development of design codes for welded joints on the basis of existing approaches of fracture mechanics with account for recommendations of the International Institute of Welding, American Petroleum Institute and others. Example of this work is the development in collaboration with Gosneftegazprom of official building standards of Ukraine «Strength Design of Operating Main Pipelines with Defects» (VBN V.2.3-00018201.04–2000).

The Institute pays a lot of attention traditionally to the determination of residual stresses in different

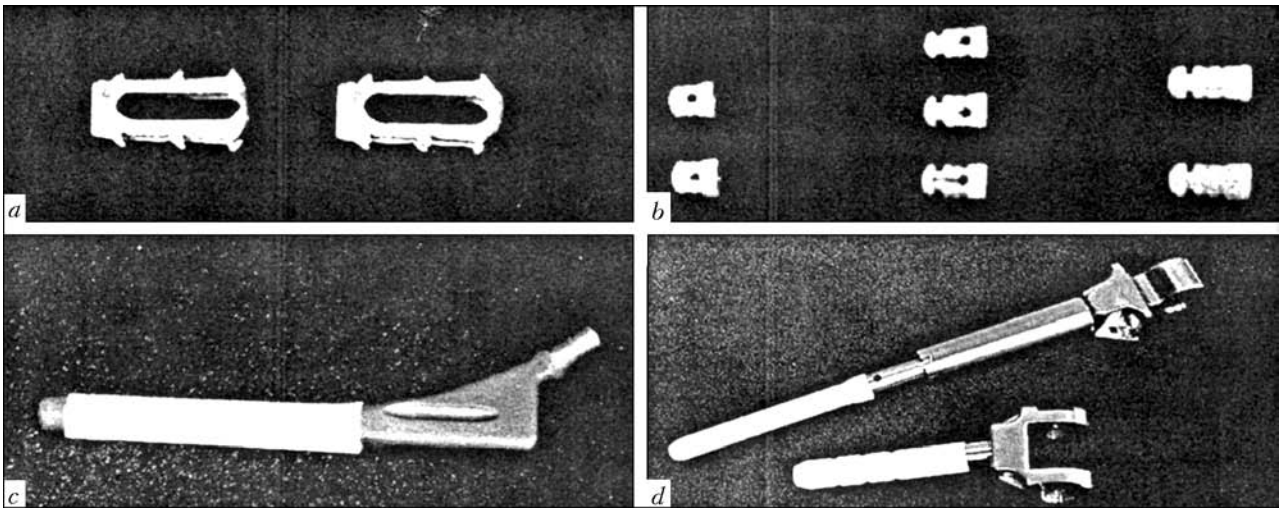

Figure 22. Endoprostheses with microplasma bioceramic coatings: *a* — intervertebral; *b* — dental; *c* — coxofemoral; *d* — knee

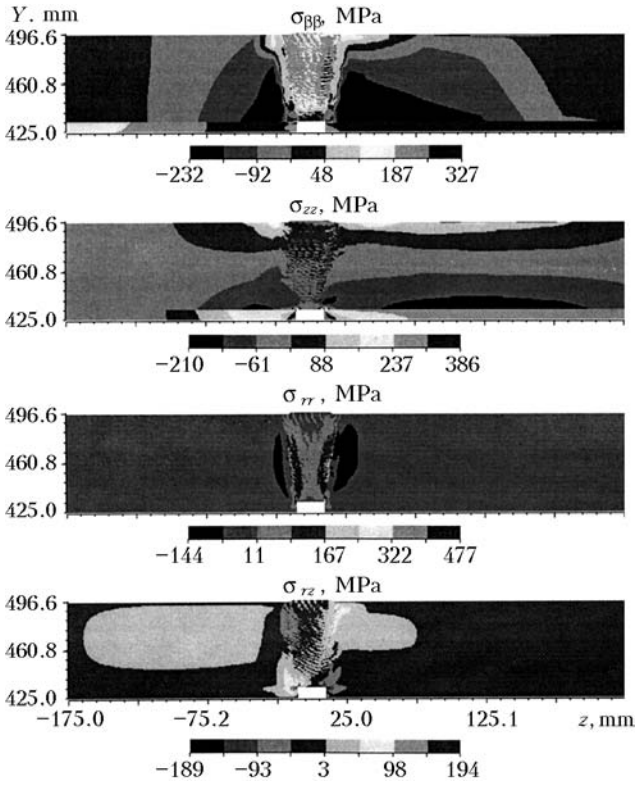

Figure 23. Design data on distribution of residual welding stresses after welding and tempering of circumferential weld of pipes Dn 850

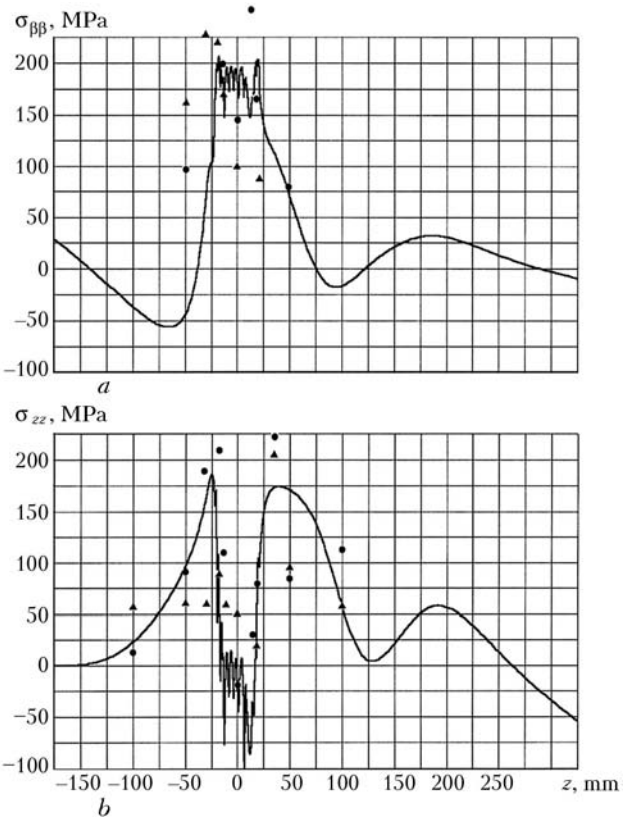

Figure 24. Comparison of design curves of residual stresses $\sigma_{\beta\beta}$ (*a*) and σ_{zz} (*b*) on the external surface in the zone of weld of pipes Dn 850 after high tempering with experimental data

welded joints and assemblies. A combined method, based on mathematical modeling of kinetics of formation of residual stresses in welding and post heat treatment in the entire volume of the welded assembly in combination with experimental measurements in accessible surfaces of the assembly examined, is used successfully. This approach was realized, for example, as regards to welded joints of pipes Dn 850, used for fastening the steam generator of the nuclear reactor WWER-1000 to the pipeline of the first contour.

Figure 23 gives the design data for distribution of residual stresses $\sigma_{\beta\beta}$ (circumferential), σ_{zz} (transverse), σ_{rr} (radial), σ_{rz} (tangent).

Figure 24 shows a sufficiently good agreement of design and experimental data for external surface (accessible for measurements) with respect to $\sigma_{\beta\beta}$ and σ_{zz} that is a basis of validation of the design data.

A new express method and compact equipment have been developed for non-destructive examination of stressed state in structures, stipulated both by their manufacture and also by service loads. The principle of the technology consists in the creation of a new non-destructive method of an elastic relaxation of stresses on the basis of introducing a high-density pulse of current into the examined area and no-contact determination of a field of displacements in the relaxation zone using a method of electron speckle-interferometry (Figure 25).

A computerized automated systems makes it possible to calculate the values of stresses on the basis of data about displacements in a local zone of relaxation.

One of the new technologies of evaluation of welded structure performance, developed at the Institute, is the technology based on a quantum fracture mechanics. Technology uses, in parallel with traditional parameters characterizing the condition of material, the data of its acoustic emission, emitted by the material in the process of deforming. This technology is rational in use of AE in the volume of 100 % control of structures and their assemblies. Works on control with use of the given technology can be performed without interruption of manufacturing and intended for the automatic assessment of hazard of the revealed defects.

The application of the developed technology for control of materials makes it possible to realize 100 % control of structures and their assemblies without destruction, to determine preliminary the rupture load, to assess the residual life of the structure material. Over the recent 12 years of application of the developed technology in different branches of industry of different countries, more than 1000 structures were tested (objects of power engineering, chemical industry, gas transport, ammonia pipelines).

The challenging, in our opinion, are the diagnostic systems of a continuous monitoring of structures, allowing continuous obtaining of information about the condition of structures during a long time. These systems have been already operated for more than 3 years at some enterprises of Ukraine. Figure 26 shows a

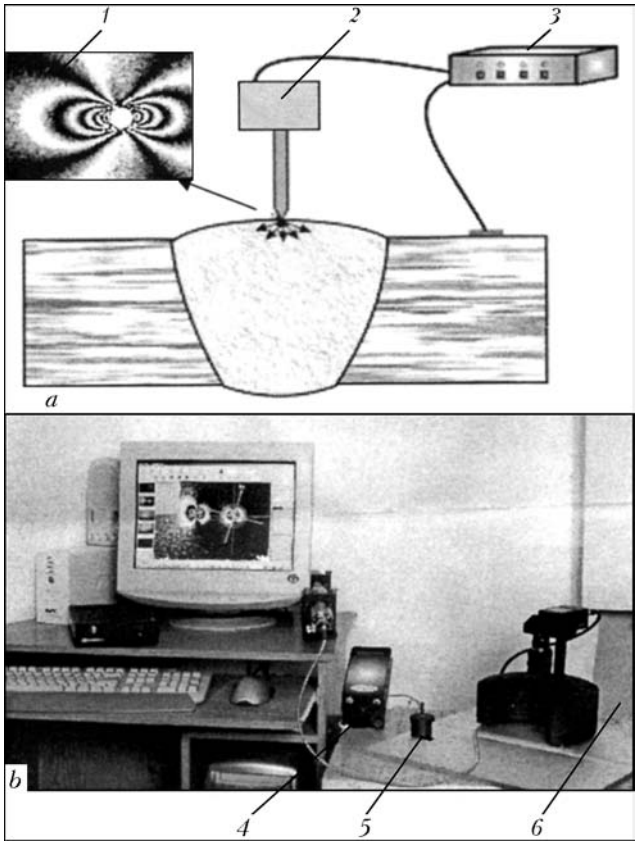

Figure 25. Scheme (*a*) and hardware (*b*) of the method of stressed state assessment: *1* — interference pattern characterizing the residual stresses; *2* — device for input of current pulses; *3*, *4* — generator of pulses; 5 — device for input of pulses; *6* — speckle-interferometer

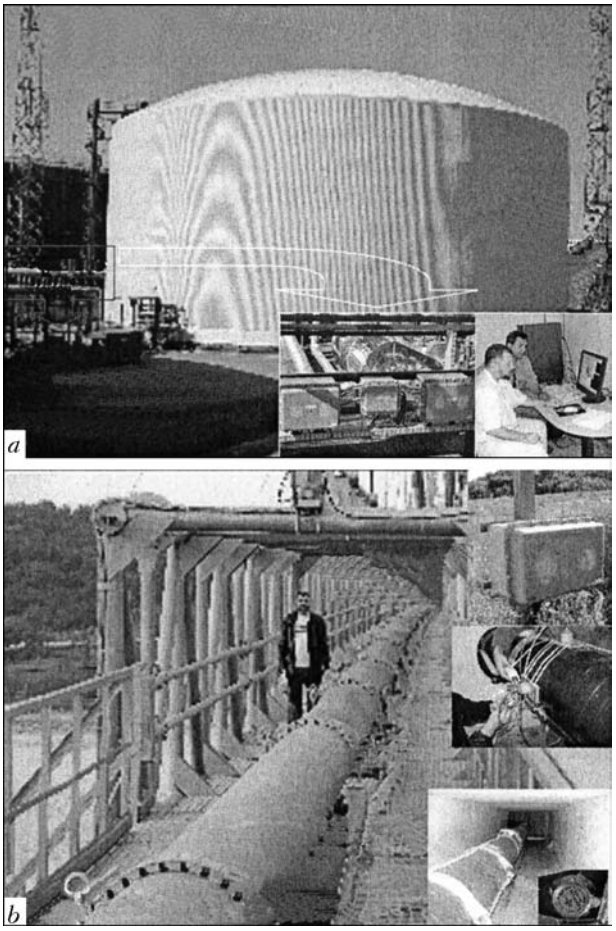

Figure 26. Continuous monitoring of storage tank of ammonia (*a*) and ammonia pipeline on bridge (*b*)

continuous monitoring of a typical structure of a large-sized storage tank of ammonia of 34,000 m^3 and ammonia pipeline of 1000 m length on bridge across the Dnieper river.

The widening of fields of application of aluminium alloys in welded structures depends on guarantee of the required resistance of joints to the fatigue fractures. The cyclic fatigue life of aluminium alloy welded joints is about 40 % of that of joints of structural steels. Therefore, the aluminium structures need the postweld treatment to a greater extent as compared with steel structures. The investigations showed that the effective method of postweld treatment of welded aluminium alloys can become a surface plastic deformation of the zone of transition from weld to the parent metal using a high-frequency mechanical peening. Figure 27 shows the results of fatigue tests of butt welded joints of aluminium alloy AMg6 in initial state, after machining of convexity and high-frequency mechanical peening using technological equipment of a relatively low consumed power (up to 0.3 kW) with a piezo-ceramic transducer. Increase in fatigue resistance of aluminium alloy AMg6 butt joint was 45–100 % after treatment as compared with initial state depending on the cycle asymmetry.

Ultrasonic testing (UST). The UST is one of the main methods of flaw detection in welded joints. This method is realized traditionally using piezo-electric transducers. The successful application of UST can be illustrated by a series of automated installations having a UST system with computer control, designed and manufactured at the Institute for Vyksunsk Metallurgical Works (Figure 28). They provide automated UST of ends of pipes of 508–152 mm diameter across the entire thickness of 7–50 mm wall, revealing defects of «lamination» type at 60 mm width from the edge, longitudinally-oriented defects of «crack» type on 30 mm width from the pipe edge, and also longitudinal welds of straight welded pipes.

It was found for the first time at the Institute, that it is rational to apply electromagnetic-acoustic

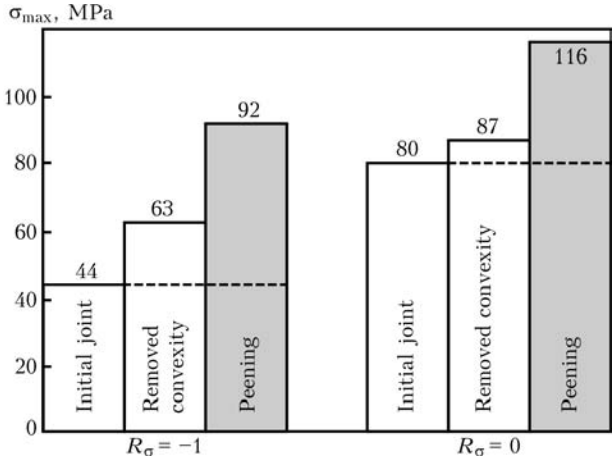

Figure 27. Change in values of limited endurance limit σ_{max} at $1 \cdot 10^6$ cycles depending on method of treatment of welded joint of AMg6 alloy and asymmetry of cycle R_σ of alternating stresses

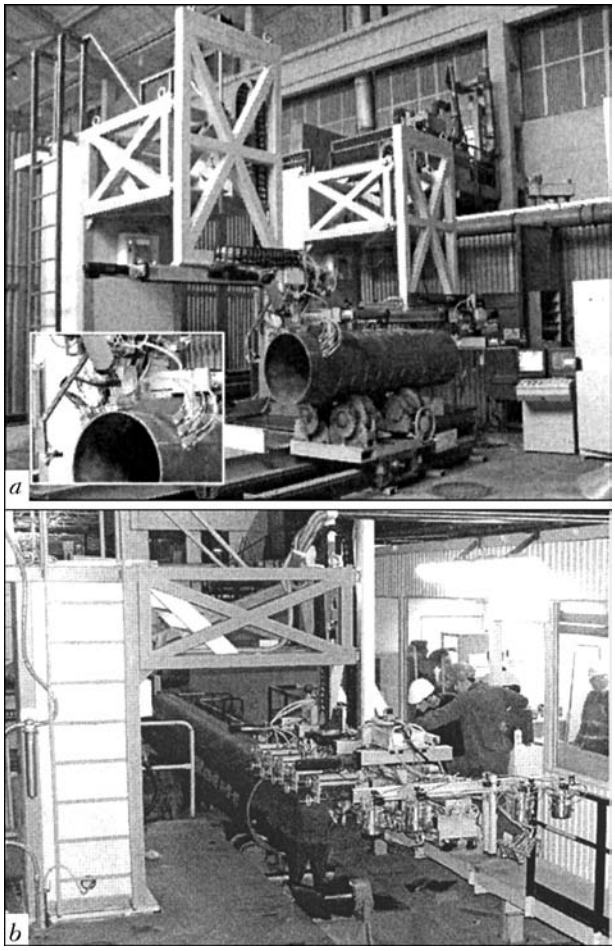

Figure 28. Installation NK 360 (*a*) and NK 362 (*b*) for automated UST of pipes

transducers (EMAT) in some case for UST of welded joints and sheet structures, which avoid the need in use of an intermediate acoustic medium (couplant) and allow exciting of special horizontal-polarized transverse waves. This gives an opportunity to perform UST of products with a rough surface, in the presence of remnants of insulation, without empting the object and in the presence of foreign deposits. The tests showed that all the natural defects (rounded, extended, of different orientation) are revealed at 97 % validity without effect of bead shape of welded joint on UST results. In addition, there is no need in waiting for metal structure cooling after welding. EMAT can operate at temperature from –50 up to 170 °C. The obtained results prove the promising widening of field of UST application.

Some problems of natural gas transportation. The Institute is dealing with the improvement of site welding of main pipelines, welding consumables, with the design and manufacture of machines for arc welding and flash butt welding. Except the above-given trends, it is dealing also with others trends, related only partially to welding.

Increase in efficiency of gas transportation systems. It is known that the gas transportation systems of Russia and Ukraine are the power objects of a planetary scale. The natural gas, transported by the main pipelines, satisfies the need in power of industry and social infrastructure of the whole continent.

Thus, only one pipeline of 1.4 m diameter is transporting gas of up to 800 kg/s at a mean rate of gas flowing in the pipeline of about 40 km/h. The pipeline is transporting annually the mass of gas equivalent by power to 340 billion kW·h (approximate efficiency of pipeline is 10,000 (kW·h)/s).

At such a scale of power transporting and consuming, the problems of reduction of any types of losses and increase in efficiency of operation of gas transportation system, from the one hand, and utilization of heat secondary energy resources, connected with losses in gas pumping equipment, from the other hand, are very actual. The latter is especially important also for keeping the ecological requirements specified for the powerful objects (Kyoto Protocol).

A compressor station of about 50 MW total mechanical shaft capacity is installed for transportation of gas in the above-mentioned gas pipeline per each 120–150 km on average.

At the present time, the use of shaft capacity of 10, 16 and 25 MW is effective at the compressor stations of gas turbine units. The present consumption of fuel gas per one gas turbine engine up to $(2–3)\cdot10^3$ kg/h is effective. The specific gas consumption for producing a mechanical capacity is within 0.33–0.35 m/(kW·h). Expenses only for the fuel gas for the operation of turbines of gas pumps of compressor stations of one pipeline of up to 1500 km length is about 150 million US dollars. In this case, the gas turbine engines reject approximately 180 kg/s of combustion products at temperature of 450–550 °C into the surrounding atmosphere from a hot path. Efficiency factor of these power units is not more than 32 %, that shows the scales of rejections of heat power by the compressor stations into atmosphere, amounting to about 60–70 % of the power consumed by them (or up to 100 MW of heat power). Moreover, the hot path of gas turbine engines rejects directly from the hot path up to 60 MW of heat power. This power can be used at each compressor station for an additional-generation of about 16–25 MW of electric power and many other purposes.

The another effective way is the generation of cold using units utilizing the heat of gas turbine engines. Application of these units for cooling the transporting gas will increase the efficiency of main pipelines approximately by 8–10 %, compensate the consumption of electric power for a drive of fans of apparatuses for air cooling of gas, guarantee own needs of compressor station in electric power, and also save the fuel gas consumed by the gas turbine engines.

In winter, the generation of additional power is possible for needs of enterprises, living complexes or agricultural facilities located near the compressor stations.

The saving of expenses for gas transportation by 5–10 % only in the gas transportation system of Ukraine will give a significant effect, improve the

ecology of environment, power provision and living conditions of population near the compressor stations. Moreover, the flow capacity of pipelines will be increased. For the gas transportation system of Russia this effect will much greater.

Alongside with the scientists of the E.O. Paton Electric Welding Institute, the associates of the Institute of Engineering Thermophysics and Institute of gas of the NAS of Ukraine, and also Odessa State Academy of Cold, OJSCs IGSh VNIPITRANSGAZ and Sumy M.V. Frunze MNPO, are working now for the solution of this problem.

Light-weight metal-plastic cylinders for transportation vehicles (Figure 29). The world autopark rejects more than 70 % of pollutions into atmosphere, therefore, the whole world pays a great attention to the application of natural gas-methane as an alternative, ecologically clean motor gas. In parallel with ecological safety the application of the natural gas is stimulated by its price and large natural resources. One of the reasons, restricting the wide application of gas on transport means, is a large weight of high-pressure cylinders.

At present, there are three types of cylinders at the market: metal, plastic and metal-plastic.

Cylinders of the first type, the best designs of which have a coefficient of mass perfection M/V of about 1.25 kg/l, are manufactured from seamless all-drawn tubes.

This index in cylinders of the second type is much better (about 0.3 kg/l), but the high prices for structural materials and labor intensity for manufacture stipulate their high cost, i.e. up to 20 US dollars per litre.

The cylinders of the third type are more universal. They have a load-carrying gas-proof metal casing and strengthening composite sheath. The significant reduction in mass and labor intensity for manufacture can be attained by application of high-strength steels and composite materials possessing a high specific strength. The E.O. Paton Electric Welding Institute has developed the new technology of manufacture of relatively inexpensive light cylinders, whose casings are made from high-strength steels, and the strengthening composite sheath is made by a circular coiling. The cylinders are designed for 20 MPa operating pressure with a safety factor of 3.1 at M/V of about 0.6 kg/l for the service period of more than 15 years, and have a splinter-proof failure at pressures of less than 60 MPa and shot of 7.62 mm bullet.

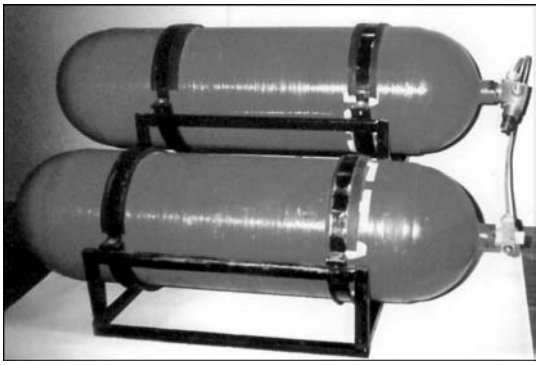

Figure 29. Light-weight metal-plastic cylinders for transport vehicles

Metallic casing of these cylinders is manufactured from high-strength sheet steel. Welding of shells, bottoms and necks is made using technology which guarantees the welded joints equal in strength to the parent metal.

Reinforcement of a cylindrical part of the cylinder by a composite material makes it possible to reduce the mass and to increase the serviceability of the cylinder at multiple fillings without reduction in safety coefficient, and also to avoid the feasibility of fragment failure.

As to the design, materials, labor consumption and mass parameters, the cylinder of the E.O. Paton Electric Welding Institute is not inferior to the best world standards and differed from them by use of non-scarce materials, stability of mass, cleanness and uniformity of internal surface, increased corrosion resistance and long life at multi-cycle loads. The technological process makes it possible to manufacture cylinders of different types and sizes without significant modification of the existing facility. Cylinders can be used not only in transport, but also in the public utility spheres, agricultural machinery, in emergency-rescue works. At present, a serial manufacture of these cylinders is mastered by three enterprises of Ukraine.

It should be noted in conclusion that welding and related processes continue their intensive and comprehensive progressing. Theoretical premises are created for the development and application of new technologies, upgraded materials in manufacture of products both in traditional fields of welding industry and also in other fields considered earlier exotic. Over the XXI century the welding and related technologies will preserve their role as a leading and mass technology in all the branches of the human activity, and the Institute will keep up to date.

EFFECT OF NON-RELAXED RESIDUAL STRESSES ON LOAD-CARRYING CAPACITY AND RESIDUAL LIFE OF WELDED JOINTS OF PIPINGS AND EQUIPMENT OF NUCLEAR POWER ENGINEERING OBJECTS

V.I. MAKHNENKO, E.A. VELIKOIVANENKO, G.F. ROZYNKA and **N.I. PIVTORAK**
E.O. Paton Electric Welding Institute, NASU, Kiev, Ukraine

The non-relaxed residual stresses in the presence of crack-like defects can influence greatly the decrease in load-carrying capacity and safe service of welded joints of pipings and elements of equipment of nuclear power engineering objects. This influence is growing largely in degradation of characteristics of resistance to brittle fracture K_{IC}, K_C and growth of corrosion cracks K_{ISCC} in the process of service (repairs).

Keywords: *nuclear power engineering, pipings and equipment, welded joint, non-relaxed residual stresses, diagram of fracture estimation, defects, growth of cracks, service life*

In modern designs of pipings and equipment of objects of nuclear power engineering the low- (10G2NMFA type) and high-alloy (austenitic) steels, which are characterized by sufficiently high resistance to stress relaxation at operating temperatures in the process of service of the mentioned equipment, are widely used. Therefore, the non-relaxed residual stresses in the zone of welded joints (after manufacture or repair) are preserved almost during the whole period of service and can influence the load-carrying capacity and residual life of safe service of the appropriate objects.

The above-described circumstance predetermines the application of proper technologies of welding in manufacture and repair of elements of equipment of low-alloy steels, when the final high-temperature tempering is an obligatory condition of the mentioned technologies. However, it is known [1 et al.] that the degree of relaxation of residual welding stresses in thick-walled parts even at furnace tempering is far from 100 % and, depending on technological factors, can vary in certain limits. In cases of a local high-temperature tempering of site welded joints the level of non-relaxed residual stresses depends greatly on technological parameters of process and geometry of the product [2, 3 et al.], therefore, it is important to obtain data about the real non-relaxed stresses and to account for their effect on residual safe service life of definite joints and assemblies using appropriate algorithms (methods) in estimation of residual safe life of welded structure of the above-said purposes.

It is known that the most significant effect of non-relaxed residual stresses is observed in the presence of sharp geometric stress raisers (defects) of a crack type. Starting from the work of Wells [4], the estimated algorithms, based on approaches of fracture mechanics of bodies with cracks [5, 6 et al.], are used for quantitative estimation.

At static loading of welded elements from structural materials the allowance for residual stresses is sufficiently illustrative on the base of diagram of fracture assessment (DFA), developed by British power engineers in the form of so-called procedure R-6 [5–7 et al.]. According to this procedure the defects of discontinuity, described by an appropriate equivalent crack (for example, by [8]), are remained in equilibrium state in a preset field of non-relaxed residual stresses σ_{ij}^{res} and stresses σ_{ij} from service load ($i, j = x, y, z$), if the condition is true

$$f(K_r, L_r) = 0, \qquad (1)$$

where K_r is the value characterizing the particularly brittle rupture in the zone of defect being considered; L_r is the same in case of a pure tough rupture. Parameters K_r and L_r consist of characteristics (invariants) of stress-strain state, shape and sizes of a defect, geometry of welded assembly, and also properties of material in «hot point», determining resistance, respectively, to brittle and tough rupture.

There are different representations (1) based on generalization of experimental data (of type given in Figure 1), obtained for structural steels [5].

Curves in Figure 1 are well enough approximated by the relationship from [5]

$$K_r(L_r) = (1 - 0.14L_r^2)\,[0.3 + 0.7\exp(-0.65L_r^6)];$$
$$K_r(L_r) = 0 \text{ at } L_r > L_r^{\max}, \qquad (2)$$

where $K_r = K_I / K_{IC}$; $L_r = \sigma_{ref} / \sigma_y$; K_I is the coefficient of intensity of stresses on the contour of crack-like defect in the field of stresses σ_{ij} and σ_{ij}^{res}; σ_{ref} is the value of invariant of current operating stresses σ_{ij} in the defect zone, determining the beginning of a plastic instability; σ_y is the yield strength of material; $L_r^{\max} = (\sigma_y + \sigma_t) / 2\sigma_y$; σ_t is the ultimate rupture strength of material.

In case of multi-axial stressed state at the apex of a crack-like defect, the relationship (2) can be used

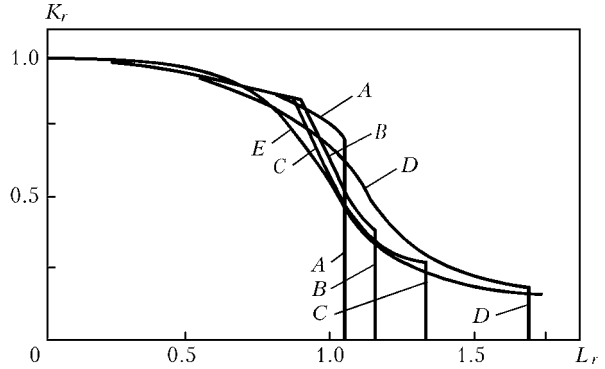

Figure 1. Diagrams of limiting state of $K_r = f(L_r)$ for structural steels of different type: *A* — high-strength steel EN408; *B* — steel A533V for high-pressure vessels; *C* — low-carbon steel with manganese; *D* — austenitic steel; *E* — estimated curve by (2)

in the scope of theory of a generalized normal rupture [9], substituting parameter $K_{\omega\theta}^{\max}$ instead of K_I into (2). Here, $K_{\omega\theta}^{\max}$ is maximum value of $K_{\omega\theta}$ at $\omega = \omega_*$ and $\theta = \theta_*$, determined by relationships

$$K_{\omega\theta} = \left[(K_I + K_I^{res}) \cos^3 \frac{\omega}{2} - 3(K_{II} + K_{II}^{res}) \cos^2 \frac{\omega}{2} \sin \frac{\omega}{2}\right] \times$$

$$\times \cos^2 \theta + (K_{III} + K_{III}^{res}) \cos \frac{\omega}{2} \sin 2\theta; \qquad (3)$$

$$\frac{\partial K_{\omega\theta}}{\partial \theta} = 0 \text{ at } \theta = \theta_*, \quad \frac{\partial K_{\omega\theta}}{\partial \omega} = 0 \text{ at } \omega = \omega_*.$$

Here, K_I, K_{II}, K_{III} are the modes of coefficient of intensity of stresses from external load; K_I^{res}, K_{II}^{res}, K_{III}^{res} is the same from residual non-relaxed stresses σ_{ij}^{res}. It is typical that the values σ_{ref} do not depend on residual stresses, as σ_{ij}^{res} has no time to relax completely before starting the state of a plastic instability (tough rupture).

In the process of service the vector of sizes a_i of defect is growing, and also the degradation of material properties occurs to a certain degree (reduction in K_{IC} in particular), that leads to increase in values K_r and L_r. From DFA (Figure 2) [7] the state from point *A*, being considered, is transferred to point *B* closer to the limiting curve, determined by (2), i.e. to point *C*. Strength safety factor in point *A* is determined by relation $n(A) = OC/OA$, in point *B* by $n(B) = OC/OB$, and in point *C* by $n(C) = 1.0$.

Consequently, if to express the residual stresses $\sigma_{ij}^{res}(A)$ by $K_r^{res}(A)$ in the form

$$K_r^{res} = [K_{\omega\theta}^{\max} (\sigma_{ij}^{res} \neq 0) - K_{\omega\theta}^{\max} (\sigma_{ij}^{res} = 0)] \frac{1}{K_{IC}} \qquad (4)$$

and they increase $K_r(A)$ and do not influence $L_r(A)$, then it is not difficult to determine the effect of $K_r^{res}(A)$ at preset $L_r(A)$ and $K_r(A)$ on n.

Figure 3 shows the dependence of $n_{res}(A)/n(A)$ on $L_r(A)$ and relation $K_r^{res}(A)/K_r(A)$ for the most extreme case, when $K_r(A) + K_r^{res}(A) = f_1[L_r(A)]$, i.e. $n_{res}(A) = 1$, $f_1(L_r)$ is the right part in (2). It is seen from the Figure that at $L_r(A) < 0.7$ the role of residual

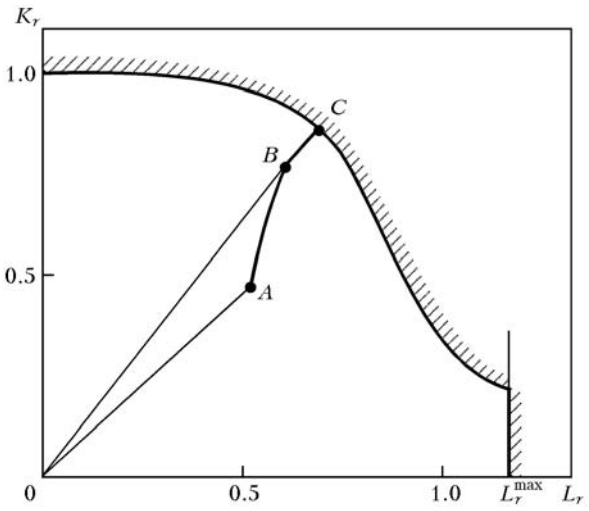

Figure 2. DFA and scheme of *ABC* trajectory of kinetics of fracture propagation in «hot point»

stresses is remarkable sufficiently even at $K_r^{res}(A)/K_r(A) > 0.2$.

It is known that at high tempering of welded joints of pipings and equipment of structural steels for the nuclear power engineering the values of non-relaxed residual stresses are preserved at the 50–120 MPa level. In case of service loads, corresponding to working stresses 200–350 MPa, the effect of non-relaxed residual stresses in estimation of life of safe operation of load-carrying elements even at static loading should not be neglected. It can be shown that at degradation of fracture toughness K_{IC} in the process of service (that is typical in radiation of welded joints of bodies of power reactors of WWER type) the accounting for non-relaxed residual stresses reduces the life of a safe service of the body.

In accordance with [10] K_{IC} can be presented in the form

$$K_{IC} = A + D \exp [C(T - T_{cr0}) - C\Delta T_{cr}], \qquad (5)$$

where for reactor body steels $A = 23$ MPa·m$^{1/2}$; $C = 0.019$ 1/°C; $D = 48$ MPa·m$^{1/2}$; T is the temperature of metal in hot point; T_{cr0} is the critical temperature of brittleness (CTB) of material in initial state; ΔK_{cr} is the shifting of initial CTB due to material embrittlement under the action of radiation.

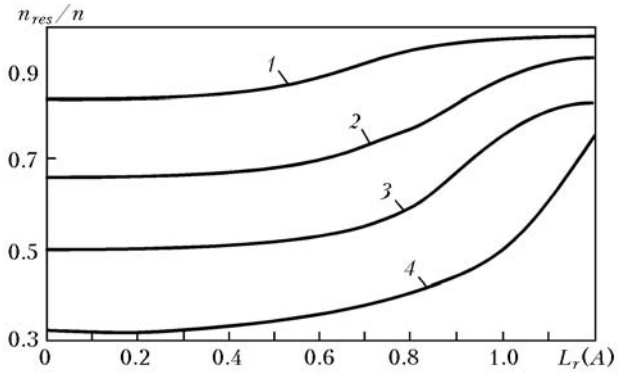

Figure 3. Effect of residual stresses on n_{res}/n depending on $L_r(A)$ at $K_r + K_r^{res} = f_1[L_r(A)]$: *1* — $K_r^{res}/K_r(A) = 0.2$; *2* — 0.5; *3* — 1.0; *4* — 2.0

Using (5) together with (2), it is possible to obtain relationship for allowable shifting of CTB, not accounting for residual stresses σ_{ij}^{res}. For crack-like defect under conditions of normal rupture we shall obtain

$$\Delta T_{cr}^{res} = -\frac{1}{C}\ln\left[1+\frac{K_I^{res}}{K_I^{max}-Af_1(L_r)}\right] = \\ = -52.6\ln\left[1+\frac{K_I^{res}}{K_I^{max}-23f_1(L_r)}\right]. \quad (6)$$

As for the thick-walled bodies the product $23f_1(L_r)$ is usually much less than K_I^{max} at thermal shock, then it follows from (6):

$\frac{K_I^{res}}{K_I^{max}}$	0	0.1	0.2	0.5	1.0
ΔT_{cr}^{res}, °C	0	−5.0	−9.6	−21.3	−36.4

It is seen that at the most probable values of relation K_I^{res}/K_I^{max} within the 0.2–0.5 ranges in case of non accounting for σ_{ij}^{res}, the decrease in allowable shifting of CTB by 10–20 °C is required, that is rather significant if to take into consideration that the allowable design value of CTB for material for the most radiated welded joints does not exceed 100 °C for all the term of service (about 40 years).

The problems of growth of geometric sizes of crack-like defects are widely described in modern literature. Three typical mechanisms of growth are distinguished mainly: fatigue, corrosion and creep. The first is associated with alternate loads, while two others can be manifested also at static load.

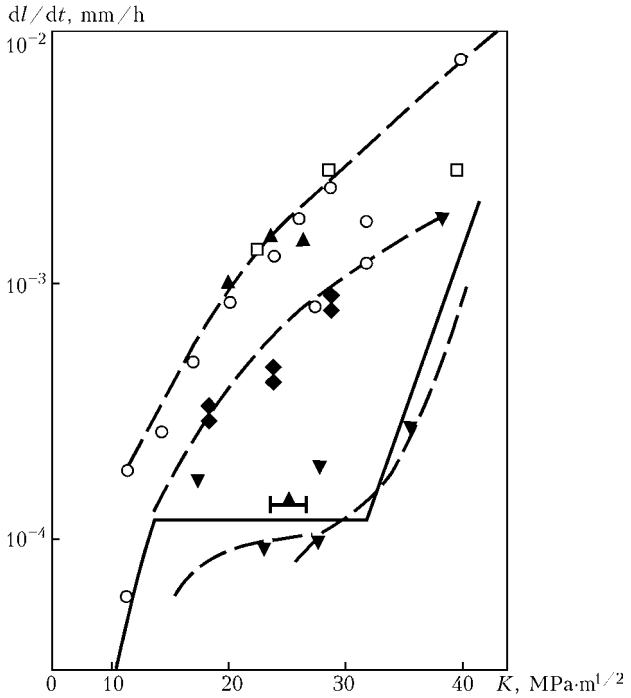

Figure 4. Kinetics of growth of size dl/dt of cracks of intercrystalline stress corrosion at long-time static loading in Cr–Ni steels: ▼ — sensitization, 650 °C, 2 h, $O_2 \approx 0.2$ mg/l; ▲ — sensitization, 650 °C, 2 h, $O_2 \approx 0.2$ mg/l (another melting); ◆ — different sensitization, $O_2 \approx 0.2$ mg/l; ❍ — sensitization, 650 °C, 24 h, $O_2 \approx 8$ mg/l; ❒ — sensitization, 24 h, $O_2 \approx 0.2$ mg/l [13]

For the pipings and equipment of nuclear power engineering considered the role of creep is not large under service temperature conditions of operation, however, fatigue and corrosion in particular, are the factors, influencing greatly the service safety. Role of residual stresses in the growth of defects by a fatigue mechanism can be shown using known experimental data of [11 et al.].

On the example of a crack of a normal rupture

$$\frac{da}{dN} = C(\Delta K_I u)^m \text{ at } \Delta K_I > \Delta K_{th}(R); \\ \frac{da}{dN} = 0 \text{ at } \Delta K_I < \Delta K_{th}(R), \quad (7)$$

where $\Delta K_{th}(R) = (190-144)R$, but not lower than 65 MPa·mm$^{1/2}$ according to [12]; $C = C_0F(R)$; C_0, m are the characteristics of material; N is the number of cycles; $\Delta K_I = K_I^{max} - K_I^{min}$ — from the external load; $R = \dfrac{K_I^{min}+K_I^{res}}{K_I^{max}+K_I^{res}}$;

$$F(R) = 1,\ u = \frac{1}{1.5-R} \text{ at } R \le +0.5; \\ F(R) = \frac{1}{1-R-\Delta K_I/K_C} \text{ [12]},\ u = 1 \text{ at } R \ge +0.5. \quad (8)$$

It follows from (7) and (8) that at $\Delta K_I > \Delta K_{th}(R)$ in the area of positive values of K_I^{res}, R is increased and, respectively, the values u at $R \le +0.5$, i.e. the rate of crack growth, is da/dN.

In the region of high values R and positive values K_I^{res}

$$F(R) = \frac{1}{(1-R)\left[1-\dfrac{K_I^{max}+K_I^{res}}{K_C}\right]}$$

is increased (especially at $K_I^{max} + K_I^{res} \to K_C$), thus increasing da/dN.

In the region of negative values K_I^{res} the crack growth is delayed due to decrease in R and u at $K_I^{max} + K_I^{res} > 0$ up to a complete its arresting at $K_I^{max} + K_I^{res} < 0$.

Thus, at cyclic loads the residual stresses can play a significant role from the positions of rate of growth in sizes of crack-like defects (theoretically the rate is varied from 0 up to ∞ due to K_I^{res}).

For corrosion cracks the role of non-relaxed residual stresses and stresses from external load is equal. Experimental data of type given in Figure 4 of work [13] showed that the rate of growth of these cracks depends on the coefficient of intensity of summed stresses, i.e. in several cases the role of K_I^{res} can be rather important.

As an illustration to the above-given information, let us consider data, obtained in 2004, about the de-

fects in the zone of welded joint No.111/1 of steam generators of PGV-1000M type of the first block of South-Ukrainian nuclear power station (Figure 5).

Defectogram of transverse cracks, revealed in welded joint approximately after a year of a local repair of this joint, is given in Figure 6. The cracks were formed in a non-repaired zone, which during the previous repair was not subjected to welding effect, however, simultaneously with the zone repaired it was subjected twice to a local high tempering with a total holding of approximately 16 h at 650 °C. The cause of initiation of these transverse (with respect to weld axis) cracks has a clearly expressed corrosion nature, the rate of their growth reached approximately 30–40 mm/year, that proves the presence of sufficiently high stresses. At working circumferential stresses of 50–60 MPa and above-mentioned high tempering, at which the welding stresses should relax to the level not above 100 MPa, without determination of real stresses, connected with a local tempering, the appearance of the mentioned defects is impossible to explain. It should be noted here that after the previous repair all the welded joints passed the non-destructive testing of discontinuity, that is, naturally, did not excluded the omission of separate small cracks, especially in a non-repaired zone, however, to attain the above-mentioned values of rate of crack growth a high level of stresses is required.

Using a package of computer applied programs WELDPREDICTIONS, developed at the E.O. Paton Electric Welding Institute, the field of residual circumferential $\sigma_{\beta\beta}$ and transverse σ_{zz} stresses was determined by study the developing elastic deformations in the zone considered with account for main technological operations. It was established that the local tempering is a cause of occurrence of sufficiently high residual stresses (Table 1), which in combination with service stresses (Table 2) lead to the occurrence of significant K_I in the defects considered (Table 3). Recommendations of work [8] were used in calculation of K_I [8].

It is seen from Table 3 that for the stressed state (with respect to $\sigma_{\beta\beta}$ by Table 2) the values K_I, corresponding to the commencement of the so-called stages of a corrosion crack growth with a domination of a mechanism of hydrogen embrittlement, when $K_I > K_{ISCC}$ (Figure 7), and at a rate of growth, corresponding approximately to the above-mentioned values (30–40 mm/year), are determined not only by the initial sizes, omitted in a previous repair of defects, but also by degradation of properties of the material sensitive to tempering cracks [14].

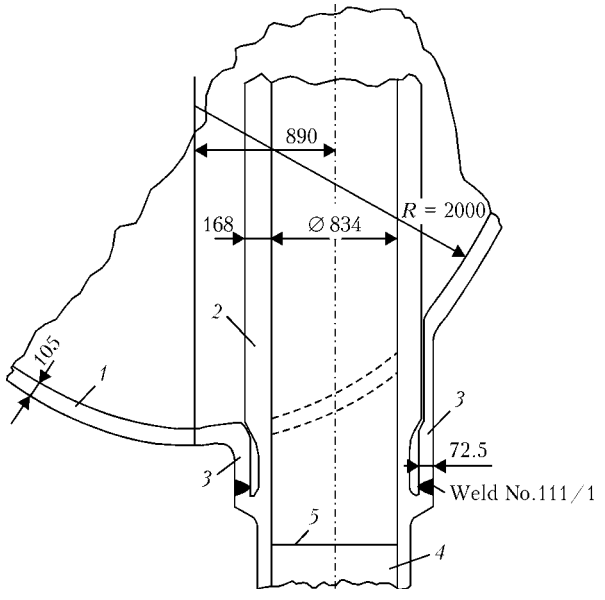

Figure 5. Scheme of arrangement of weld No.111/1 of steam generator of PG-1000M type: *1* — body; *2* — collector; *3* — branch pipe; *4* — piping of «hot» water; *5* — site weld with Dn 850

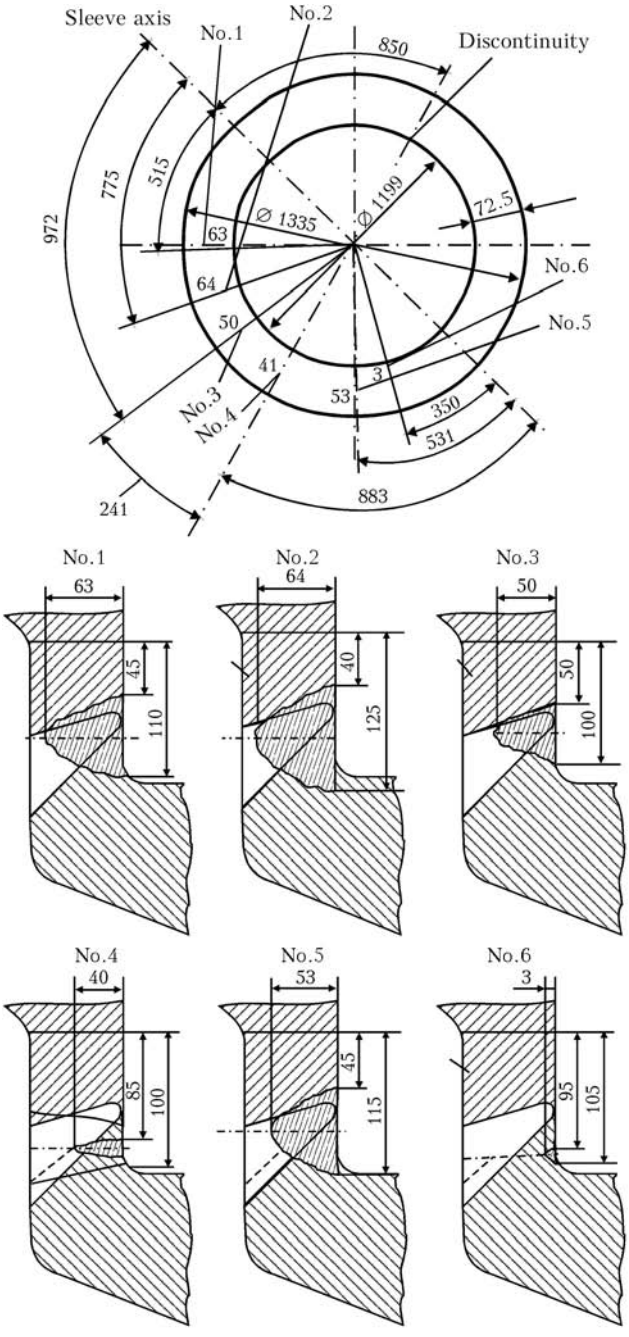

Figure 6. Defectogram of welded joint No.111/1 of «hot» collector of 1PG-1 type: Nos. 1–6 — numbers of defects (see Table 3)

Table 1. Residual stresses, MPa

z, mm	*r, mm*							
	597.00	*607.00*	*617.00*	*627.00*	*637.00*	*647.00*	*657.00*	*667.00*
				$\sigma_{\beta\beta}$				
5.000	86.85	86.16	79.91	69.22	56.83	45.29	36.04	29.33
15.000	78.68	73.50	67.96	61.79	55.16	48.58	42.70	38.36
25.000	68.66	64.57	62.28	60.81	58.88	55.92	52.38	49.80
35.000	60.43	59.21	60.62	62.98	64.64	64.71	63.52	62.49
45.000	54.47	56.44	61.17	66.49	70.96	73.82	75.29	76.35
55.000	50.49	55.20	62.84	70.49	77.27	82.77	87.32	91.32
65.000	48.13	54.79	65.22	74.84	83.40	91.44	99.35	107.16
75.000	47.85	55.10	68.98	79.36	89.29	99.98	111.13	123.36
85.000	49.83	65.62	74.51	84.07	95.50	108.96	122.86	138.84
95.000	130.20	99.19	86.20	91.58	103.41	119.35	135.39	151.88
105.000	149.72	130.69	126.18	123.01	125.53	134.43	149.64	165.11
115.000	186.77	180.50	171.04	165.63	160.97	161.55	170.41	183.02
125.000	220.56	218.10	212.87	209.39	202.83	197.88	197.18	194.71
135.000	225.94	224.91	222.37	214.19	210.05	204.41	200.93	196.45
145.000	168.58	156.43	149.18	153.81	160.58	171.71	182.66	194.74
155.000	157.85	145.07	145.82	154.03	164.00	175.81	191.44	202.23
165.000	149.33	139.96	139.98	145.89	158.92	178.75	197.80	212.97
175.000	140.76	132.79	132.63	141.22	157.36	179.27	203.90	220.17
185.000	129.27	121.76	123.57	132.08	148.67	173.68	206.78	229.28
195.000	115.26	108.45	107.98	113.02	126.15	151.31	198.05	249.03
205.000	100.57	93.09	87.86	85.61	86.63	89.35	86.97	47.65
215.000	86.60	77.67	69.64	61.95	53.59	40.48	14.86	-48.71
225.000	73.60	63.97	53.83	42.38	28.19	8.36	-24.61	-63.10
235.000	62.82	52.91	41.57	28.06	11.29	-10.67	-37.26	-68.46
245.000	55.26	45.35	33.47	19.13	1.78	-18.47	-41.81	-69.35
255.000	51.64	41.86	29.84	15.47	-1.39	-20.33	-41.67	-66.95
265.000	52.50	42.84	30.93	16.66	0.27	-17.83	-38.00	-61.50
275.000	57.95	48.35	36.39	22.10	5.83	-12.13	-31.81	-54.00
285.000	68.16	58.42	46.21	31.63	14.85	-3.83	-23.83	-45.07
295.000	83.11	73.00	60.38	45.24	27.06	6.80	-14.46	-35.42
305.000	102.56	92.08	79.19	62.15	42.36	20.35	-2.92	-25.70
315.000	126.93	116.79	103.69	87.15	67.68	46.29	24.70	3.41
				σ_{zz}				
5.000	0.00	0.00	0.00	0.00	0.00	0.00	0.00	0.00
15.000	0.00	0.00	0.00	0.00	0.00	0.00	0.00	0.00
25.000	-1.95	-2.22	-1.82	-1.44	-1.13	-0.94	-0.74	1.08
35.000	-4.00	-4.55	-3.61	-2.82	-2.36	-2.13	-1.65	0.45
45.000	-5.28	-5.54	-4.11	-3.38	-3.36	-3.60	-3.51	-2.53
55.000	-4.79	-4.29	-2.67	-2.92	-4.16	-5.59	-6.68	-8.01
65.000	-0.98	0.10	0.79	-1.75	-5.09	-8.22	-11.22	-15.72
75.000	9.25	8.48	5.54	-0.74	-6.46	-11.37	-17.05	-25.03
85.000	32.00	20.30	9.06	-0.62	-8.14	-14.73	-23.57	-35.33
95.000	77.13	25.73	10.57	-0.15	-9.62	-17.85	-29.56	-46.46
105.000	77.15	38.92	16.74	2.45	-10.52	-21.20	-35.35	-56.82
115.000	72.34	55.81	24.91	6.80	-14.09	-30.21	-42.14	-60.70
125.000	75.02	58.64	31.26	7.83	-12.88	-30.98	-44.28	-70.82
135.000	71.89	59.03	39.01	12.81	-8.29	-30.50	-50.93	-78.54
145.000	71.18	62.12	34.91	18.29	-4.80	-29.46	-57.14	-80.27
155.000	73.07	55.38	37.69	19.15	-3.37	-30.38	-56.17	-80.64
165.000	70.90	51.62	37.78	20.00	-2.80	-28.33	-56.96	-77.92
175.000	70.13	47.18	31.88	17.42	0.28	-24.37	-53.05	-75.94
185.000	64.36	41.92	28.38	15.90	2.36	-18.57	-48.92	-73.00
195.000	54.66	37.11	24.34	13.21	3.03	-10.10	-36.41	-74.85
205.000	45.79	31.68	19.44	8.44	-0.92	-7.59	-7.82	-79.78
215.000	38.92	26.40	16.02	7.04	-0.66	-10.18	-32.65	-37.64
225.000	31.55	20.91	11.88	3.72	-4.71	-15.71	-28.52	-9.33
235.000	23.90	14.94	7.02	-0.47	-8.05	-15.34	-14.46	2.01
245.000	16.37	9.09	2.42	-3.70	-8.89	-10.27	-4.54	7.53
255.000	9.65	4.00	-1.18	-5.41	-7.62	-5.51	1.66	10.68
265.000	4.36	0.13	-3.49	-5.86	-5.90	-2.12	5.18	12.71
275.000	0.80	-2.26	-4.58	-5.58	-4.41	-0.18	6.75	13.79
285.000	-0.86	-3.35	-4.65	-4.79	-3.33	0.42	6.62	13.80
295.000	-0.97	-3.38	-3.77	-3.57	-2.58	0.04	4.96	12.38
305.000	-0.25	-2.56	-2.11	-2.30	-1.91	-0.55	2.49	8.50
315.000	0.30	-0.76	-1.01	-1.10	-1.00	-0.35	1.30	-0.28

Note. Here and in Table 2 the values $\sigma_{\beta\beta}$ and σ_{zz} referring to weld section, are given on dark background.

Table 2. Stressed state, MPa, in periphery zone at T = 300 °C and working pressure 6 MPa

z, mm	*r, mm*							
	597.00	*607.00*	*617.00*	*627.00*	*637.00*	*647.00*	*657.00*	*667.00*
				$\sigma_{\beta\beta}$				
5.000	86.85	86.16	79.91	69.22	56.83	45.29	36.04	29.33
15.000	78.68	73.50	67.96	61.79	55.16	48.58	42.70	38.36
25.000	68.66	64.57	62.28	60.81	58.88	55.92	52.38	49.80
35.000	60.43	59.21	60.62	62.98	64.64	64.71	63.52	62.49
45.000	54.47	56.44	61.17	66.49	70.96	73.82	75.29	76.35
55.000	50.49	55.20	62.84	70.49	77.27	82.77	87.32	91.32
65.000	48.13	54.79	65.22	74.84	83.40	91.44	99.35	107.16
75.000	47.85	55.10	68.98	79.36	89.29	99.98	111.13	123.36
85.000	49.83	65.62	74.51	84.07	95.50	108.96	122.86	138.84
95.000	130.20	99.19	86.20	91.58	103.41	119.35	135.39	151.88
105.000	149.72	130.69	126.18	123.01	125.53	134.43	149.64	165.11
115.000	186.77	180.50	171.04	165.63	160.97	161.55	170.41	183.02
125.000	220.56	218.10	212.87	209.39	202.83	197.88	197.18	194.71
135.000	225.94	224.91	222.37	214.19	210.05	204.41	200.93	196.45
145.000	168.58	156.43	149.18	153.81	160.58	171.71	182.66	194.74
155.000	157.85	145.07	145.82	154.03	164.00	175.81	191.44	202.23
165.000	149.33	139.96	139.98	145.89	158.92	178.75	197.80	212.97
175.000	140.76	132.79	132.63	141.22	157.36	179.27	203.90	220.17
185.000	129.27	121.76	123.57	132.08	148.67	173.68	206.78	229.28
195.000	115.26	108.45	107.98	113.02	126.15	151.31	198.05	249.03
205.000	100.57	93.09	87.86	85.61	86.63	89.35	86.97	47.65
215.000	86.60	77.67	69.64	61.95	53.59	40.48	14.86	-48.71
225.000	73.60	63.97	53.83	42.38	28.19	8.36	-24.61	-63.10
235.000	62.82	52.91	41.57	28.06	11.29	-10.67	-37.26	-68.46
245.000	55.26	45.35	33.47	19.13	1.78	-18.47	-41.81	-69.35
255.000	51.64	41.86	29.84	15.47	-1.39	-20.33	-41.67	-66.95
265.000	52.50	42.84	30.93	16.66	0.27	-17.83	-38.00	-61.50
275.000	57.95	48.35	36.39	22.10	5.83	-12.13	-31.81	-54.00
285.000	68.16	58.42	46.21	31.63	14.85	-3.83	-23.83	-45.07
295.000	83.11	73.00	60.38	45.24	27.06	6.80	-14.46	-35.42
305.000	102.56	92.08	79.19	62.15	42.36	20.35	-2.92	-25.70
315.000	126.93	116.79	103.69	87.15	67.68	46.29	24.70	3.41
				σ_{zz}				
5.000	0.00	0.00	0.00	0.00	0.00	0.00	0.00	0.00
15.000	0.00	-0.01	0.00	0.00	0.00	0.00	0.00	-0.39
25.000	-6.05	-2.18	-4.46	-3.49	-2.30	-1.10	2.07	5.06
35.000	-13.61	-12.26	-11.32	-8.55	-5.65	-2.58	4.06	8.52
45.000	-21.11	-21.31	-18.24	-13.76	-9.34	-4.76	4.80	9.18
55.000	-27.32	-28.27	-24.05	-18.36	-13.02	-7.62	3.62	6.68
65.000	-30.85	-31.99	-28.35	-22.01	-16.49	-11.11	0.11	1.02
75.000	-29.86	-39.72	-31.49	-24.38	-19.79	-15.37	-5.95	-7.51
85.000	-22.89	-68.06	-31.90	-25.93	-23.41	-20.82	-14.66	10.87
95.000	-22.68	-69.60	-31.90	-25.96	-23.46	-20.89	-14.77	-29.46
105.000	-2.11	-37.85	-32.66	-28.48	-28.54	-27.99	-26.20	-40.60
115.000	11.63	-1.99	-20.18	-25.45	-34.99	-41.67	-36.33	-51.56
125.000	23.30	9.47	-11.01	-24.20	-36.00	-45.67	-49.43	-74.95
135.000	28.99	18.70	2.21	-17.64	-33.03	-49.94	-63.24	-88.98
145.000	37.85	30.95	3.89	-10.84	-31.27	-53.39	-74.51	-96.23
155.000	44.80	29.15	10.40	-8.40	-31.08	-57.14	-83.27	-105.24
165.000	50.41	33.55	16.29	-5.55	-31.65	-59.83	-90.90	-109.98
175.000	57.59	37.07	15.40	-6.07	-29.92	-60.09	-97.49	-116.01
185.000	61.40	41.32	17.75	-4.73	-28.67	-60.12	-103.28	-121.62
195.000	62.74	47.33	20.83	-3.36	-27.44	-56.06	-109.18	-153.69
205.000	63.73	51.51	22.98	-3.10	-27.81	-50.90	-113.56	-167.82
215.000	64.43	53.60	24.87	-0.30	-24.77	-60.09	-113.39	-150.73
225.000	61.89	52.84	24.70	0.77	-22.78	-44.92	-120.08	-105.76
235.000	55.27	47.78	21.04	-1.77	-23.28	-48.67	-87.33	-71.17
245.000	45.67	39.76	15.56	-4.94	-24.35	-41.18	-61.96	-49.74
255.000	34.70	30.37	9.76	-7.26	-21.82	-31.76	-43.62	-34.17
265.000	23.80	20.88	4.61	-8.09	-17.94	-23.20	-30.20	-21.98
275.000	13.99	12.30	0.49	-8.06	-14.07	-16.23	-20.34	-12.44
285.000	5.91	4.91	-2.62	-7.56	-10.81	-11.16	-13.33	-5.15
295.000	-0.24	-0.99	-4.65	-6.82	-8.44	-8.03	-8.75	-0.06
305.000	-4.43	-4.87	-5.58	-6.29	-6.98	-6.64	-6.42	0.49
315.000	-6.40	-6.40	-6.40	-6.40	-6.40	-6.40	-6.40	-6.40

Table 3. Results of calculation of intensity factor for semi-elliptic cracks, corresponding to defectogram of steam generator (welds No.111/1)

Type of collector	*No. of defect*	*a, mm*	*c, mm*	$K_I(G)$, $MPa \cdot m^{1/2}$	$K_I(D)$, $MPa \cdot m^{1/2}$	*Scheme of semi-elliptic crack*
1PG-1	1	63	32.5	46.8	27.3	
	2	64	42.5	46.9	34.0	
	3	50	25.0	46.2	23.4	
	4	40	7.5	18.9	6.5	
	5	53	35.0	54.4	30.4	
	6	3	5.0	10.6	12.1	
1PG-2	1	48	36.0	50.8	31.9	
	2	10	12.5	19.3	19.6	
	3	35	15.0	30.7	17.0	
	4	40	7.5	18.9	6.5	
	5	50	25.0	46.2	23.4	
	6	8	7.5	16.9	15.0	

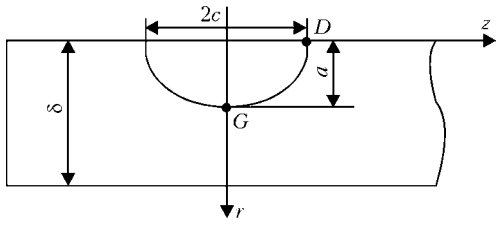

Coming from data of Table 3 with account for real sizes of omission of similar defects (of No.6 type), it can be assumed that value K_{ISCC} of material in the zone considered decreased to 10–15 MPa·m$^{1/2}$ at temperature of about 300 °C and the presence of aggressive medium, corresponding to a feed-water in a pocket (see Figure 5).

It is natural that decrease in values of residual stresses (see Table 1), for example, to 100 MPa at initial defects of No.6 type (Table 3), will lead to the fact that the process of their growth ($K_I << K_{ISCC}$) will be determined mainly by a mechanism of an electromechanical corrosion and will be valid for much larger time comparable with a standard period of service of steam generators of PGV-1000M type.

CONCLUSIONS

1. The role of residual non-relaxed stresses is rather important in the load-carrying capacity and safe service life of welded joints of pipings and elements of equipment for the nuclear power engineering. The effect of residual stresses is most noticeable in the presence of crack-like defects in the zone of welded joints.

2. Using DFA, the effect of residual stresses on a risk of spontaneous growth of defects is estimated, while using the kinetic diagrams of growth of sizes of defects at cyclic loading and stress-corrosion it is possible to obtain data about safe service life of the considered welded joints with account for non-relaxed residual stresses.

3. In-service (repair) degradation of material characteristics, determining the resistance to brittle fracture (K_{IC}, K_C) and also the limit of changing the mechanisms of growth of corrosion cracks K_{ISCC}, increases the effect of non-relaxed residual stresses on the decrease in load-carrying capacity and residual life of welded joints.

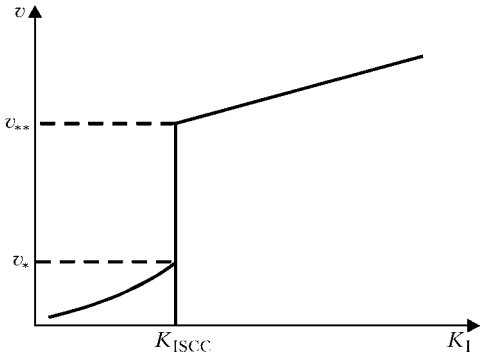

Figure 7. Schematic diagram of rate v of growth of stress corrosion cracks

1. Vinokurov, V.A. (1973) *Tempering of welded structures for stress relaxation*. Moscow: Mashinostroenie.
2. Lu, H., Wang, J., Murakawa, H. (1999) Mechanical behavior in local post weld heat treatment. Rep. 4. *Transact. of JWRI*, 28(**1**), 55–60.
3. McEneney, J.W. (1998) Recommended practices for local heating of welds in pipe and tubing. *ANSI/AWS. D10-9X.*
4. Wells, A.A. (1977) Effect of residual stresses on brittle fracture. In: *Fracture*. Vol. 5. Ed. by G. Libovits. Moscow: Mashinostroenie.
5. Harrison, R.P., Loosemore, K., Milne, J. et al. (1980) Assessment of the integrity of structure containing defects. In: *Rep. R/H R6-Rev. 2. Central Electricity Generating Board*. Berkeley.
6. Makhnenko, V.I., Makhnenko, O.V. (2000) Development of calculation procedures for assessment of allowable defects in welded joints of critical structures. *The Paton Welding J.*, **9/10**, 79–87.
7. Makhnenko, V.I. (2003) Improvement of methods for estimation of residual life of welded joints in durable structures. *Ibid.*, **10/11**, 107–116.
8. *MR 125-01-90*. Calculation of coefficients of stress intensity and section weakening for defects in welded joints. Kiev.
9. Andrejkiv, A.E. (1982) *Three-dimensional problems of the ory of cracks*. Kiev: Naukova Dumka.
10. *RD EO 0353-02*. Procedure of assessment of service life of bodies of nuclear WWER reactors during service of MRK-SKhP-2000. St-Petersburg-Moscow.
11. (1987) *Current research on fatigue cracks* Ed. by T. Tanaka et al. London-New York: Elsevier Appl. Sci.
12. Hobbacher, A. (1996) Recommendations for fatigue design of welded joints and components. IIW Doc. *XIII-1539-96/XV-845-96*.
13. Horn, R.M., Kass, J.N., Rangantath, K. (1984) Evaluation of the growth and stability of stress corrosion cracking in sensitized austenitic pipings. *J. Pressure Vessel Techn.*, 106(**2**), 201–208.
14. Hrivnyak, I. (1984) *Weldability of steels*. Moscow: Mashinostroenie.

WELDABILITY OF AIRCRAFT ALUMINUIM ALLOYS OF GREAT THICKNESS IN EBW

O.K. NAZARENKO[1], **V.M. NESTERENKOV**[1] and **R.V. ILYUSHENKO**[2]
[1]E.O. Paton Electric Welding Institute, NASU, Kiev, Ukraine
[2]Airbus UK Company, Bristol, England

Weldability of high-strength aluminium alloys 2024-T351 and 7010-T7651 100 mm thick in electron beam welding has been studied. It is shown that EBW can be used to produce sound welded joints with a high static strength and sufficiently reliable service properties.

Keywords: *electron beam welding, high-strength aluminium alloys, welded joints, weldability, great thickness, microstructure, physico-mechanical properties*

Application of advanced high-strength aluminium alloys of 2000 and 7000 series alloyed with zinc, copper, magnesium and manganese is promising to lower the weight of passenger and transport aircraft by replacing the bolted and riveted joints by welded joints. Although most of the aircraft alloys of these two series are usually regarded as difficult-to-weld, the most recent achievements of welding science and technology (development of advanced welding processes, upgrading welding equipment, improvement of the methods of welding process monitoring and control) allow looking forward to actual welding of the alloys of these series.

This study presents some results of evaluation of weldability of high-strength alloys of 2000 and 7000 series designed for use in load-carrying structures of modern aircraft wings. All the investigations were conducted in close co-operation of the E.O. Paton Electric Welding Institute of NASU and Airbus UK Company, which is fully responsible for design, manufacturing technology and production of the wings for all types of aircraft of European Airbus Concern.

Materials and welding equipment. Aircraft alloys 2024-T351 and 7010-T7651 were studied, typical composition of which is given in Table 1. Butt joints of 100 mm thick plates were welded proceeding from the existing and advanced wing designs. Welding direction coincided with that of plate rolling.

Work on electron beam welding was performed in two machines with vacuum chambers of $2.5 \times 2.5 \times 3.5$ and $12 \times 6 \times 5$ m with welding guns mobile inside the chambers. Vacuum in the first chamber was $2 \cdot 10^{-4}$, in the second $1 \cdot 10^{-3}$ mm Hg. Batch-produced ELA 60/60 power unit [1] with accelerating voltage of 60 kV was used. Gun cathode was of LaB_6, vacuum in the gun cathode area being $2 \cdot 10^{-5}$ mm Hg.

Considering intensive evaporation of metal in the direction of the welding gun cathode in EBW of aluminium alloys, special attention was given to monitoring cathode wear and admissibility of its further service, as cathode wear has great influence on the reproducibility of the geometry and stability of weld quality. A system of beam diagnostics developed at the E.O. Paton Electric Welding Institute was used for objective evaluation of the degree of cathode wear and obtaining valid information on the spatial-energy parameters of the beam [2]. Electron beam diagnostics was conducted by the method of «direct edge of the plate» [3], when the beam is briefly deflected towards the sensor. The sensor proper and the massive target are located in a specially allocated place of the welding chamber some distance from the item being welded.

Electron beam diagnostics enables comparing the initial maximum current density in the case of a new cathode and its current value during the entire operating life of the cathode, until the maximum current density has dropped significantly, and the initial position of beam focal plane has shifted by more by than 5 to 10 mm.

Table 1. Composition of alloys to be welded, %

Alloy grade	*Cu*	*Zn*	*Mg*	*Mn*	*Zr*	*Ti*	*Other*
2024	3.8–4.9	0.25*	1.2–1.8	0.3–0.9	–	0.15*	0.5Si 0.5Fe 0.1Cr
7010	1.5–2.0	5.7–6.7	2.1–2.6	0.1*	0.10–0.16	0.06*	0.12Si 0.15Fe

*Maximum content of elements.

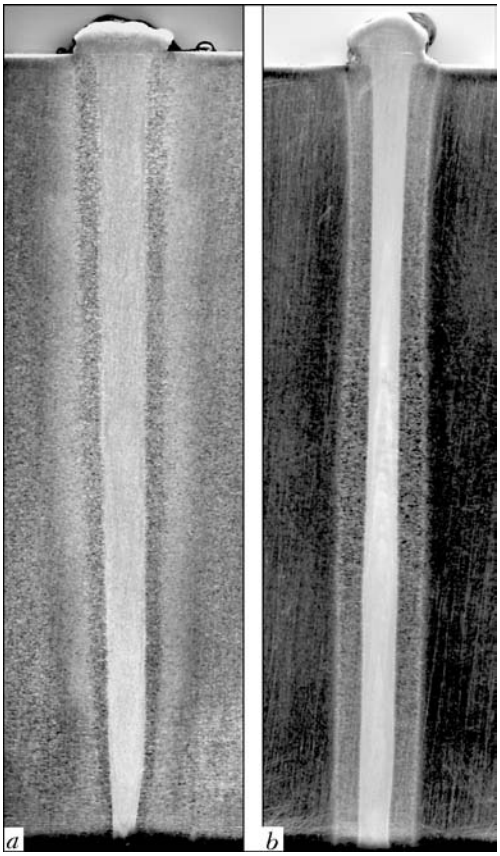

Figure 1. Macrostructure of the cross-section of a welded joint of alloy 2024 (*a*) and 7010 (*b*) 100 mm thick

Automatic tracing of butt trajectory during welding was performed using RASTR system [2], which also enables performing preparatory operations before welding, namely visualization of the working space on the system monitor screen, determination of the actual beam position in the working space zone and its alignment with the butt, selection of zero point of the future welding program and monitoring the accuracy of the gun returning to it. Possibility of real-time visual observation of EBW process creates more comfortable working conditions for the operator and gives him complete guarantee of normal weld formation.

Technological features and welding modes. During preparation for welding the samples and blanks were machined to surface finish not lower than $\nabla^{3.2}$ without using any lubricating cooling liquids with subsequent degreasing using aircraft petrol or acetone. Before loading into the vacuum chamber, the welded edges and the adjacent region of 15 to 20 mm width were scraped. The time between scraping and welding was never longer than 4 h. The welding electron beam gun was in all the cases located in the vacuum chamber at 150 mm distance from the item being welded. At complete penetration of the blanks run-off tabs were used, which were mechanically clamped to the item. In the selected sequence the item was rigidly fixed on the table, and the gun was moved along the butt at the working speed. Welding was conducted in the downhand position, using a vertical electron beam. Butt joints of 1 m length were assembled using a rigid frame-type device, providing both a tight fit of the blanks to be welded, and close contact of the run-off root backing with the items being welded. Tack welding of the butt joint was performed in two stages, namely first from the weld root side, and then from the face side of the butt after turning the blanks.

Welding with complete penetration of the butt joints (I_f = 875 A, which corresponds to the focal position at mid-depth of penetration) was conducted in the following mode: I_p = 480 and 410 A; v_w = 6 and 4 mm/s for alloys 2024, 7010, respectively. During welding a sawtooth beam scanning along the butt with 180 Hz frequency and 2.7 mm amplitude was performed simultaneously with sinusoidal scanning across the butt with 110 Hz frequency and 1.8 mm amplitude.

Visual inspection did not reveal any irregularities of weld surface formation. After removal of root backing the penetration width was measured in the weld lower part, which was equal to 3.0–3.5 mm. Such a small scatter of weld root width values is indicative of a high stability of the EBW process and weld pool stability.

The welded joints were then subjected to ultrasonic testing, metallographic investigations, mechanical and corrosion testing.

Study of welded joints of alloys 2024 and 7010. Conducted ultrasonic testing did not reveal any coarse defects in welded joints of both the alloys. Transverse macrosections of weld start, middle and end were prepared to study the weld geometry (Figure 1).

Welds of alloy 2024 have practically parallel walls in the transverse section with a slight convergence towards the weld root. Width of the cast zone is 5.8 to 6.1 mm. In the transverse section the welds of alloy 7010 are closer to the cross-section of the electron beam, the cast zone width being 4.5 to 5.1 mm. Macrosections cut out at the start, in the middle and at the end of welds have practically the same shape, which is indicative of a stable weld formation. A typical microstructure of the weld and fusion zone of welded joints on alloys 2024 and 7010, is shown in Figures 2 and 3, respectively.

Welds of alloy 2024 are characterized by a predominantly dendritic structure, although a structure with a non-uniform grain size is observed in the root part (Figure 2, *b*). The latter is attributable to insufficient stirring of the weld pool metal and a high temperature gradient in the weld root of 100 mm depth. Welds of alloy 7010 have a fine-crystalline structure, uniformly distributed across the entire thickness of the butt, grain size being approximately 10 μm. Analysis of welded joints of alloy 2024 (Figure 2, *c*) in some cases revealed microcracks along the grain boundaries in the HAZ metal (liquation cracking) [4], characteristic of fusion welding of many high-strength steels. No such microdefects were found in the HAZ metal, when studying welded joints of 7010 alloy. Comparative chemical analysis of the weld

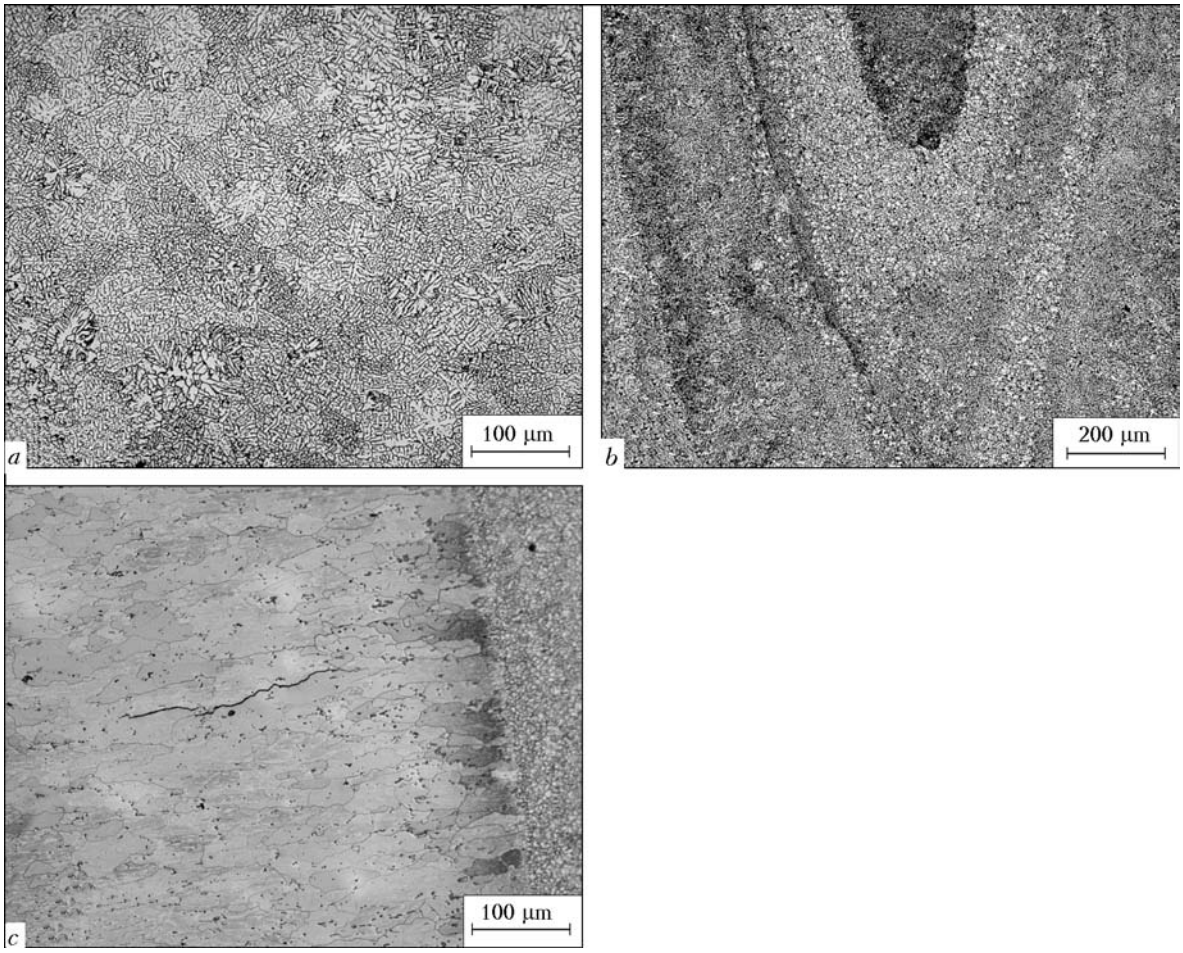

Figure 2. Microstructure of the main cast zone (*a*), weld root (*b*) and fusion zone (*c*) of alloy 2024

and base metal in welding of alloys 2024 and 7010 (Table 2) showed no loss of the main alloying elements for evaporation [1].

Nature of softening of the weld and HAZ metal under the impact of the EBW thermal cycle was evaluated by measuring the material hardness on transverse sections of welded joints. Vickers hardness was measured at 1 kg load in the interval between the adjacent measurement points of 0.5 mm. In this case for each studied welded joint the hardness was measured on three levels by weld depth, namely $t/4$, $t/2$ and $3t/4$ (where t is the welded joint thickness equal to 100 mm).

As is seen from Figure 4, metal hardness practically does not change by penetration depth for both the alloys. For 2024 alloy it is equal to approximately 100 units, which is much lower compared to weld metal of alloy 7010 (approximately 140 units.). The nature of alloy softening is also different. While for alloy 2024 softening is the most pronounced in the weld metal, for alloy 7010 the minimum of material hardness is in the HAZ metal zone located at approximately

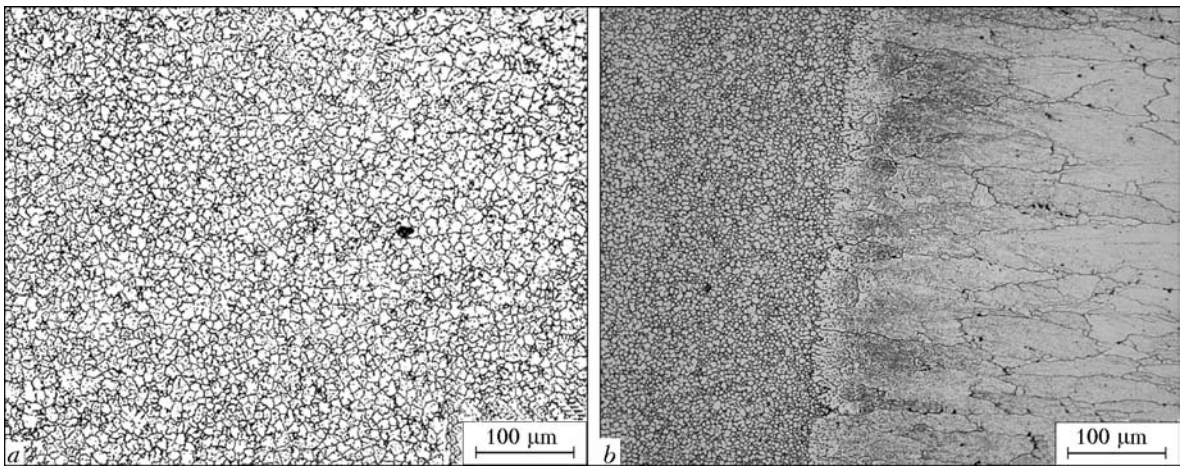

Figure 3. Microstructure of the weld (*a*) and fusion zone (*b*) of alloy 7010

Table 2. Composition of welded joint metal, %

Test object	*Cu*	*Mg*	*Mn*	*Zn*
Alloy 2024				
Base metal	3.81	1.48	0.41	–
Weld upper part	4.01	1.45	0.42	–
Weld middle (by thickness)	3.90	1.49	0.41	–
Weld root part	4.05	1.50	0.41	–
Alloy 7010				
Base metal	1.61	2.28	–	5.74
Weld upper part	1.77	2.32	–	5.77
Weld middle (by thickness)	1.70	2.31	–	5.97
Weld root part	1.78	2.35	–	5.86

7 mm from the middle plane of the weld. Total width of the HAZ including the weld is approximately the same for both the welds and is equal to about 28 mm.

Mechanical properties of welded joints of alloys 2024 and 7010 were evaluated at testing of standard samples for static tension, fatigue strength and fatigue crack propagation rate (FCPR). Similar testing of base metal samples was performed for comparison.

Static strength. Testing was conducted in keeping with the requirements of EN 2002-1 standard. Cylindrical samples were cut out across the weld to study the welded joints and across the plate rolling direction for the base metal. Samples were cut out of different sections by the thickness of the plates welded ($t/4$, $t/2$, $3t/4$ — similar to the above-described hardness measurement procedure). Table 3 gives the results of tensile testing of samples. Result analysis showed that the average values of ultimate strength of welded joints on alloys 2024 and 7010 are equal to approximately 82 and 85 % of base metal strength, being quite high values in welding of thick heat-hardenable aluminium alloys. It should be noted that while samples of welded joints of alloy 2024 fail along the weld in testing, welded joints of alloy 7010 are characterized by fracture running mostly through the HAZ metal, which is in good agreement with the results of hardness

Table 3. Mechanical properties of base metal and welded joints of aluminium alloys 2024 and 7010 100 mm thick

Object of study	$\sigma_{0.2}$, *MPa*	σ_t, *MPa*	δ, %	*Fracture site*
Alloy 2024				
Base metal	314	460	18	
Welded joint	279	379	6	Weld
Alloy 7010				
Base metal	461	527	11	
Welded joint	340	452	6	HAZ/fusion zone

Note. Averaged data are given by the results of testing 4 samples of fase metal and 9 of welded joints.

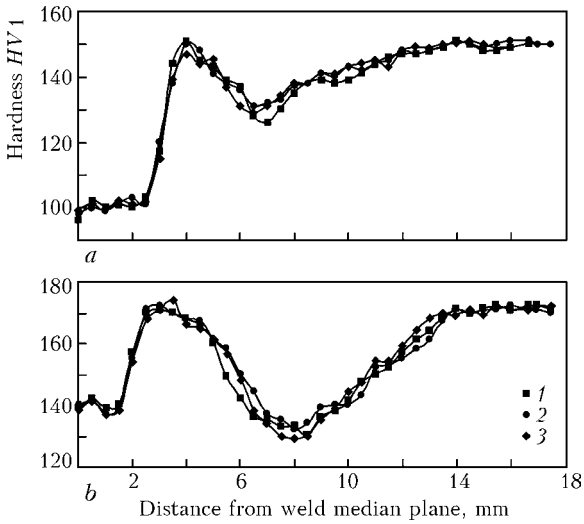

Figure 4. Hardness profile of alloy 2024 (*a*) and 7010 (*b*) at different distances from the weld median plane: *1* — $t/4$; *2* — $t/2$; *3* — $3t/4$

measurements. No significant differences in the results of tensile testing of samples cut out of different sections across the weld thickness was found for either of the alloys.

Fatigue strength. Fatigue testing at constant amplitude loads was conducted in keeping with the requirements of EN 6072 standard, the load coefficient being $R = 0.1$ in all the cases. Cylindrical samples with the gauge length of 11 mm diameter and theoretical coefficient of stress concentration $K_{th} = 1$ were cut out across the weld for welded joints and across the plate rolling direction for the base metal. Samples of welded joints were cut out of different sections across the weld thickness ($t/4$, $t/2$, $3t/4$), and base metal samples — only from the plate mid-thickness ($t/2$). Fatigue strength studies of welded joints were conducted on three levels of loading for alloy 2024 and five levels for alloy 7010. Base metal of both the alloys was tested at three loading levels. Testing re-

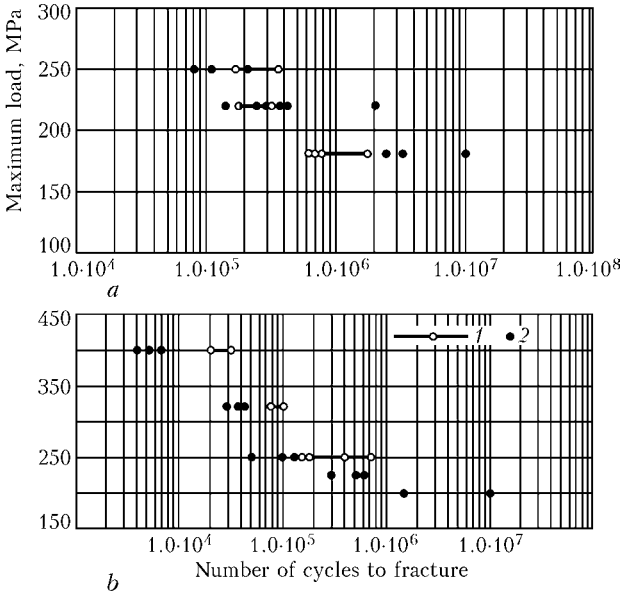

Figure 5. Fatigue strength of base metal and welded joints of alloy 2024 (*a*) and 7010 (*b*): *1* — base metal; *2* — area of sample cutting out is $t/2$

Table 4. Results of fatigue strength testing of base metal and welded joints of aluminium alloy 2024 100 mm thick

Material	*Sample cutting out zone (by metal/weld thickness)*	*Maximum load, MPa*	*Number of cycles to fracture*	*Note*
Base metal	$t/2$	250	366340	
	$t/2$	250	183380	
	$t/2$	250	170330	
	$t/2$	220	190370	
	$t/2$	220	312360	
	$t/2$	180	181740	
	$t/2$	180	1756270	Fracture in the threaded part
	$t/2$	180	692500	
	$t/2$	180	991030	
Welded joint	$t/4$	250	82450	
	$t/2$	250	204350	
	$3t/4$	250	107050	
	$t/4$	220	249990	
	$t/2$	220	380250	
	$t/2$	220	425600	
	$3t/4$	220	297460	
	$t/4$	180	24314450	
	$t/2$	180	3332740	
	$3t/4$	180	10000000	No fracture
	$t/4$	180	10000000	Same
	$t/2$	180	782510	
	$3t/4$	180	634690	

Table 5. Results of fatigue strength testing of the base metal and welded joints of aluminium alloy 7010 100 mm thick

Material	*Sample cutting out zone (by metal/weld thickness)*	*Maximum load, MPa*	*Number of cycles to fracture*	*Note*
Base metal	$t/2$	400	20510	
	$t/2$	400	31190	
	$t/2$	320	79500	
	$t/2$	320	96860	
	$t/2$	320	77670	
	$t/2$	250	689000	Fracture in the threaded part
	$t/2$	250	178080	Same
	$t/2$	250	157610	»
	$t/2$	250	402960	»
Welded joint	$t/4$	400	4100	
	$t/2$	400	5310	
	$3t/4$	400	6770	
	$t/4$	320	38880	
	$t/2$	320	29520	
	$3t/4$	320	41730	
	$t/4$	250	51440	
	$t/2$	250	137610	
	$3t/4$	250	102020	
	$t/4$	225	299420	
	$t/2$	225	602440	
	$3t/4$	225	519560	
	$t/4$	200	10000000	No fracture
	$t/2$	200	1495030	
	$3t/4$	200	10000000	No fracture

sults are given in Tables 4 and 5. As shown by the results, in alloy 2024 the fatigue properties of the welded joint and base metal are very close at all the evaluated loading levels (Figure 5, *a*), which is indicative of practically the same process of fatigue damage accumulation both in the base metal and in the weld.

Samples of welded joints of alloy 7010 fail much faster at high loads that the base metal samples. With load lowering a tendency is observed for reduction of the difference in the fatigue life of welded joints compared to the base metal. However, the welded samples still fail faster than base metal samples (Figure 5,*b*). On the other hand, at loads in the range of 200 to 250 MPa (range close to the actual maximum loads on many load-carrying structures of the aircraft wing) welded joints of alloy 7010 look sufficiently sound and fatigue-resistant.

Rate of fatigue crack propagation. Testing was conducted in keeping with the requirements of ASTM E647 standard at the loading coefficient $R = 0.1$. Compact samples of C(T) type to ASTM E647 were cut out so that the fatigue crack would propagate along the weld for welded joints, and along the plate rolling direction for the base metal. On welded joint samples the notch was oriented both towards the weld center, and in the fusion zone. Welded joint samples were cut out of different sections across the weld thickness ($t/4$ and $t/2$), and base metal samples — only from the plate mid-thickness ($t/2$). Two samples of each alloy were tested for the base metal, and six samples of each alloy for the welded joints (three with a notch in the weld, and three with a notch in the fusion zone). FCPR graphs plotted by averaged values of test results of all the samples are given in Figure 6.

Results of testing welded joints of alloy 2024 showed that with increase of the range of strength intensity factor up to values $\Delta K = 20$ MPa$\sqrt{\text{m}}$, the rate of crack propagation both in the weld metal and in the fusion zone is much lower than in the base material. With further increase of ΔK the values of fatigue crack propagation rates da/dN in the weld and the fusion zone are very close to those of the base metal.

Both in the weld metal and in the fusion zone of welded joints of alloy 7010 the fatigue cracks propagate slower compared to the base metal at values of

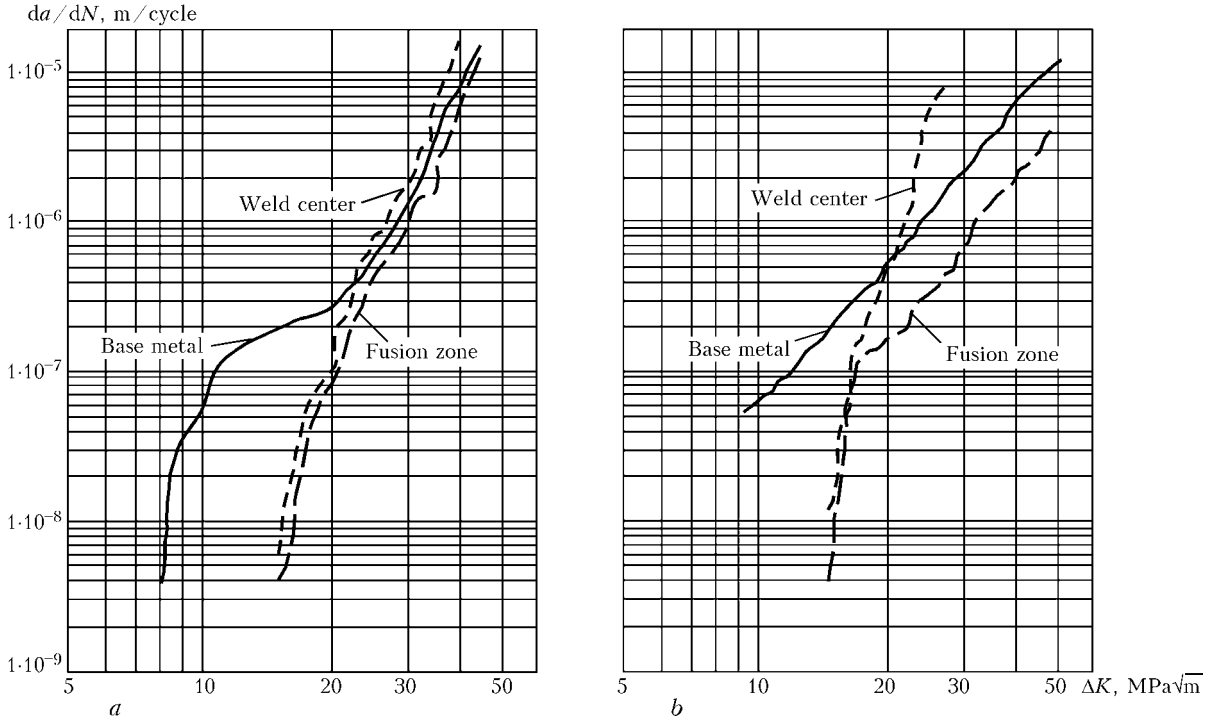

Figure 6. Variation of the rate of fatigue crack propagation in the base metal and welded joint of alloy 2024 (*a*) and 7010 (*b*) depending on the stress intensity factor

the stress intensity factor ΔK below 20 MPa$\sqrt{\text{m}}$. With ΔK increase the weld crack resistance decreases compared to the base metal. On the other hand, the rate of fatigue crack propagation in the fusion zone is still lower than the crack propagation rate in the base metal even in the case of ΔK rise. It should be noted that no significant differences in the results of testing samples cut out of different sections across the weld thickness were found for either of the alloys.

A number of additional studies were performed for welded joints of alloy 2024, which is rather widely used in different aircraft components, requiring higher fault tolerance and corrosion resistance. In this connection samples of welded joints of alloy 2024 were tested for fracture toughness under the conditions of a plane strain state, as well as for susceptibility to stress corrosion cracking in 3.5 % NaCl solution. For comparison similar testing was performed on base metal samples.

Fracture toughness. Testing was conducted in keeping with the requirements of ASTM E399 standard on compact samples of C(T) type 40 mm thick. Samples were cut out in such a way that the fracture under the notch propagated along the weld for welded joints and along the plate rolling direction for base metal. On welded joint samples the notch was oriented both along the weld center, and in the fusion zone. All the samples were cut out at mid-thickness of the weld/plate ($t/2$). It is established that fracture toughness of the weld and fusion zone of welded joints of alloy 2024 is close to that of the base metal (36.0–36.5, 32.5–37.5 and 38.0–39.5 MPa$\sqrt{\text{m}}$, respectively).

Corrosion cracking susceptibility. Testing procedure corresponded to the requirements of ASTM G44 standard. Variable one hour test cycle consisted of sample immersion in 3.5 % NaCl solution for 10 min with subsequent soaking for 50 min in air. This test cycle was repeated for 40 days up to sample fracture. Standard samples cut across the weld (rolling direction) from weld/plate mid-thickness ($t/2$) were tested by four-point bending. Welded joints and base metal were evaluated by two load levels. The first batch of samples were tested under load equal to 50 % of the material proof stress, and the second batch at 75 %. Level of applied load for each welded sample was controlled using strain gauges located in different zones of the welded joint, namely the weld, fusion zone, HAZ metal (Table 6). Testing showed that samples of EB welded joints of alloy 2024 100 mm thick are stable to corrosion cracking in 3.5 % NaCl solution at up to 210 MPa loads. Such a load level is equal to 75 % of the welded joint proof stress (see Table 3).

Table 6. Results of testing for susceptibility to stress corrosion cracking of base metal and welded joints of aluminium alloy 2024 100 mm thick for 40 days

Test object	*Load, MPa (% of proof stress)*	*Results*	*Test object*	*Load, MPa (% of proof stress)*	*Results*
Base metal	160 (50 %)	Without fracture	Welded joint	140 (50 %)	Without fracture
	240 (75 %)	Same		210 (75 %)	Same

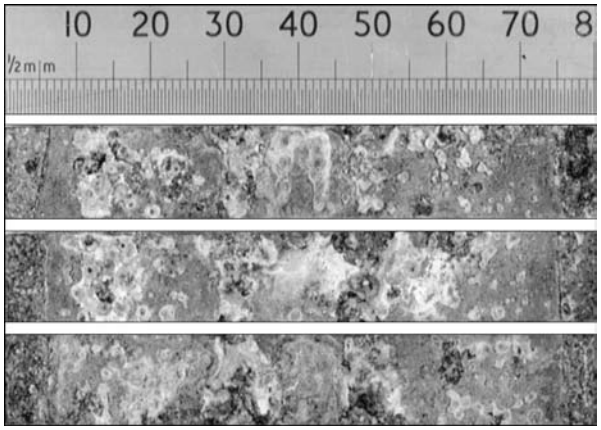

Figure 7. Appearance of samples of welded joints of alloy 2024 after corrosion testing at 210 MPa load for 40 days

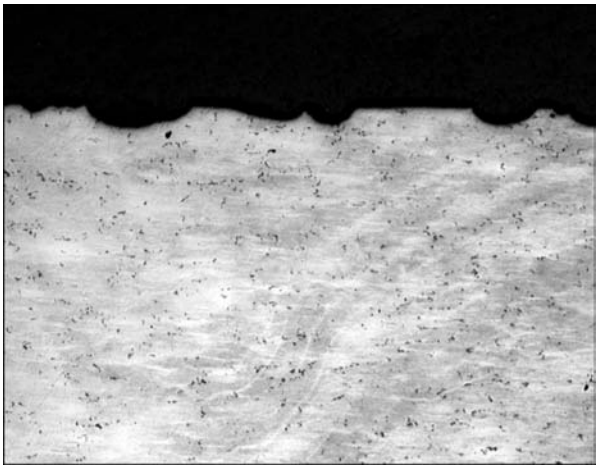

Figure 8. Transverse section of a welded sample of alloy 2024 with pitting corrosion in the HAZ metal after testing at 210 MPa load for 40 days (×150)

Subsequent analysis of welded samples after testing showed that corrosion processes were the most intensive in the HAZ metal regions located at approximately 3 to 4 mm from the fusion zone on both sides of the weld. The width of these regions was approximately 5 mm. The weld and some base metal regions were less prone to corrosion (Figure 7). Metallographic studies of the samples after removal of corrosion products from their surface revealed the pitting type of corrosion processes in all the zones of the welded joints which were susceptible to corrosion attack. In this case the maximum depth of corrosion penetration into the HAZ metal is 0.15 mm (Figure 8).

Investigation results demonstrate that EBW can be used with success for joining thick high-strength aluminium alloys 2024 and 7010 designed for use in aircraft structures. Welded joints are characterized by good quality, high static strength and quite reliable performance.

The authors hope that the results of this work will be of interest for designers and technologists of aircraft-making plants, and will promote further research in this field.

1. Nazarenko, O.K., Kajdalov, A.A., Kovbasenko, S.N. et al. (1987) *Electron beam welding*. Ed. by B.E. Paton. Kiev: Naukova Dumka.
2. Akopyants, K.S., Nazarenko, O.K., Gumovsky, V.V. et al. (2002) System of electron beam diagnostics in electron beam welding units. *The Paton Welding J.*, **10**, 27–30.
3. Zinchenko, N.S. (1961) *Course of lectures on electron optics*. Kharkov: KhGU.
4. Hermann, R., Birley, S.S., Holdway, P. (1996) Liquation cracking in aluminium alloy welds. *Materials Sci. and Eng.*, **212**, 247–255.

MIAB WELDING OF SOLID PARTS

S.I. KUCHUK-YATSENKO, V.S. KACHINSKY and **V.Yu. IGNATENKO**
E.O. Paton Electric Welding Institute, NASU, Kiev, Ukraine

A new method to control the arc motion over the entire cross-sectional area of solid parts in magnetically-impelled arc butt (MIAB) welding is considered. Features of welded joint formation in MIAB of solid parts have been studied. Technology has been developed of welding the above-mentioned parts of up to 32 mm diameter.

Keywords: *press welding, arc heating, magnetic field, solid parts, arc displacement, joint formation, welding technology*

Magnetically-impelled arc butt (MIAB) welding became widely accepted in industry for joining thin-walled pipes and cylindrical parts of up to 200 mm diameter and wall thickness of up to 5–6 mm. Limit wall thickness corresponds to the diameter of active spots in the arc column that may be produced, when using standard arc welding sources. Use of universally accepted MIAB technologies does not allow welding pipes with walls thicker than the diameter of the active spots of the arc column, as these technologies do not provide metal heating uniform across the thickness or formation of the melt on the edges needed to produce sound joints [1].

Study [2] shows the possibility of a considerable increase (up to 16 mm) of the thickness of MIAB welded pipes by finding the methods to control the arc motion in the gap between the parts, providing a uniform heating over the entire cross-sectional area. This is achieved by controlling the radial and axial components of the magnetic field induction during welding.

Figure 1. Formation of a crater on the end face of rods with a minimum value of the axial component of the magnetic field induction

The purpose of this study is finding the methods to control the arc motion in the gap between the solid parts and development of MIAB welding technology, in particular of R-bars of up to 32 mm diameter.

Investigations were performed on R-bar samples of 12–32 mm diameter, as well as rods of a similar cross-section of steels St3, steel 20, 35GS and 25G2S. Welded joints were subjected to rupture, bending and impact bending tests. Welding of solid parts was performed in MD101 and MD103 machines of PWI design, currently applied for welding pipes. Standard rectifier VDU-1201 was used as the power sources.

When developing the technology of MIAB welding of solid parts, investigations were performed without using any shielding gases, preventing oxidation of the heated surfaces, this greatly simplifying the welding technology.

Arc behaviour was studied in the gap between the solid samples of different diameter, when changing the radial and axial components of the magnetic field induction in a broad range. The size of the gap between the part edges was assumed to be $\delta = 2$ mm, i.e. the same as in pipe welding. Experiments have demonstrated that at minimum values of the axial component of the magnetic field induction, the arc shifts to the central part of the specimens and stays in a stable position there for a long time. This leads to local overheating of the edge surface with their melting and formation of a deep crater (Figure 1), which cannot always be pressed out during upsetting.

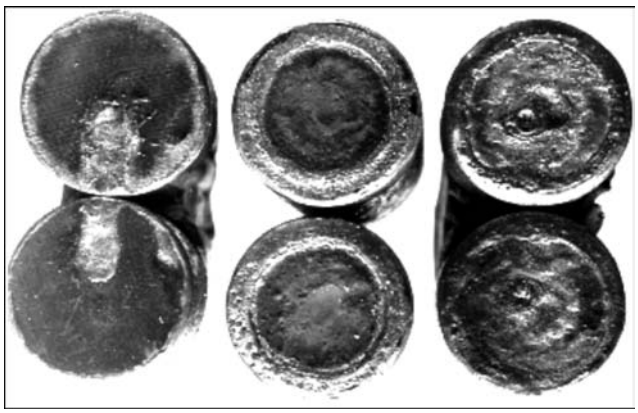

Figure 2. Appearance of the rod end faces with traces of the active spots of the arc column in different welding modes

Figure 3. Appearance of the rod end faces with traces left by the anode (A) and cathode (C) spots of the arc column after the arc shifting to the edges ($t = 0.015$ s)

At maximum values of the axial component of the magnetic field induction, the arc is driven to the peripheral sections of the rod end faces, where it can run for a long time with heating and melting of the edges surface (Figure 2).

Depending on selection of the ratio of the axial and radial components of the magnetic field induction [3], it is possible to maintain arcing for a short time (0.02–0.05 s) in different intermediate positions relative to the sample center. However, it is not possible to maintain stable arcing for a long time in these positions, as the arc is moving either to the central part or to the peripheral part of the part end faces. At a large enough size of the gap ($\delta > 2$ mm), a jump-like displacement of the active spots of the arc column is observed. In this case first a shifting of the cathode spot of the plasma flow is observed, which all the time tries to take up a new position with formation of a new anode spot (Figure 3).

The nature of the trace left by the arc varies, when the end faces have protrusions or roughness. Surface melted spots form on the rod end faces after the arc shifting. The trace left by the arc on the rod end faces can have different shapes, which is related to the magnitudes and directions of the axial and radial components of magnetic field induction, electric and thermal processes in the places of arcing, surface roughness of the rod end faces.

Such a process is the most typical for the initial period of welding, when the part end faces are cold. With heating of the part edges the cathode and anode spots are trying to take symmetrical positions. At a high frequency of rotation and frequent alternation of the magnetic field induction components in the gap, a practically continuous rejuvenation of all the sections of the end face can be ensured due to the impact of a rotating arc on them. The end face surface is covered by a thin layer of molten metal, which does not have enough time to solidify in the respective time intervals between the arc passing over them.

Metallographic investigations showed that in heating of a 23 mm diameter rod by a magnetically-impelled arc, the end face is covered by a layer of the melt, the thickness of which is 0.11 mm in the central part, 0.26 mm in the peripheral section and 0.01–0.05 mm in the intermediate section. With such a thickness of the melt, removal of the formed oxides

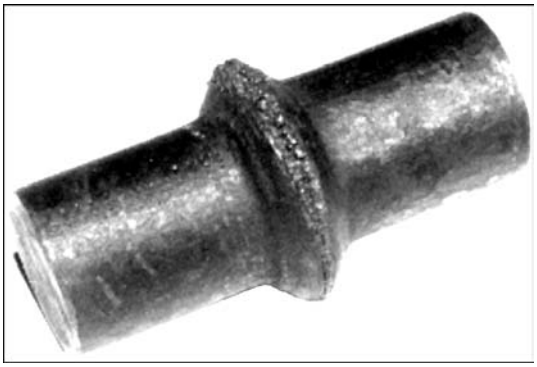

Figure 4. Welded joint of rods of 23 mm diameter produced by MIAB method

from the melt at upsetting is improbable. The fact that testing of welded joint samples (Figure 4) with a notch in the welding plane (Figure 5) did not reveal any defects, is indicative of formation of sound joints over the entire rod end faces.

A narrow HAZ in MIAB welding (for instance, in rods of 23 mm diameter, it is equal to 2.6–2.8 mm), allows upsetting to be performed without using the limitation of the travel of the welding machine moving plate. This is achieved by removing from the joint zone a layer of molten metal on the rod end faces and formation of joints without an overheated region in the HAZ in some cases.

These data suggest that in the above sections the joint formed in the solid phase under the conditions of intensive gas shielding from oxidation by air. Such a shielding is provided at repeated passage of the arc in a closed volume, accompanied by intensive evaporation of the metal. The effectiveness of the shielding depends on the intensity of the arc rotation in all the sections of the sample cross-sectional area in the pre-upsetting period.

If before upsetting an intensive rotation of the arc is ensured just in the peripheral section, a sound joint will only from in this section (Figure 6). In the central cross-sectional area defects are observed. Therefore, establishing a self-shielding gas environment just around the perimeter of the welded section turns out to be insufficient for oxidation protection of the central region of the cross-section.

The welded joint of AIII class R-bars of 32 mm diameter is given in Figure 7. Compared to a similar joint, made by other pressure welding processes (for

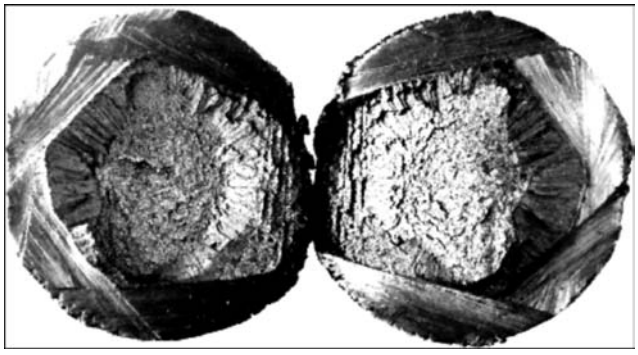

Figure 5. Appearance of rod MIAB welded joint fracture after mechanical testing with a notch in the welding plane

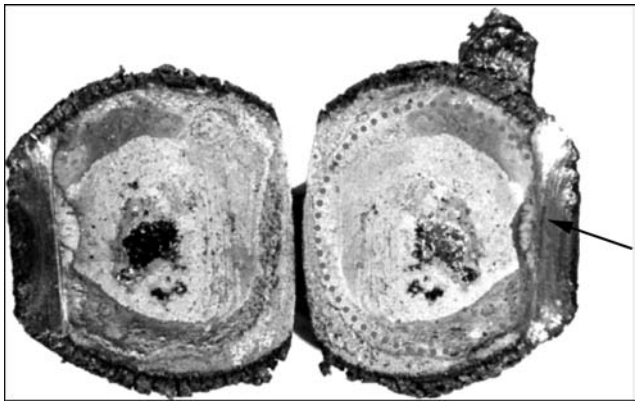

Figure 6. Appearance of the rod end faces with characteristic formation of the welded joint along the external edges (shown by an arrow)

instance flash-butt welding) MIAB welded joints are characterized by a more narrow HAZ and finer grains in the welded joint metal zone exposed to intensive heating.

Metallographic investigations were conducted on a specially made section of a welded joint on AIII class R-bar of 32 mm diameter (Figure 8). A sample was etched in 4 % solution of HNO_3 in alcohol. Hardness was measured in the LECO micro hardness meter M-40, at 50 g load. Grain point was measured to GOST 5639–82.

It was found that the fusion line is a fine lightly-etching strip, the width of which varies along the section height, becoming narrower closer to welded

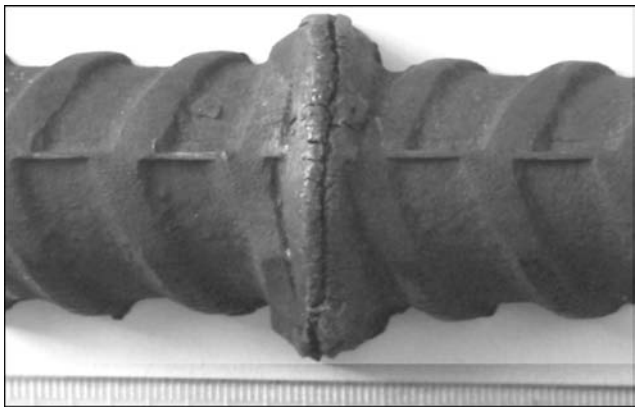

Figure 7. Welded joint of AIII class R-bar of 32 mm diameter

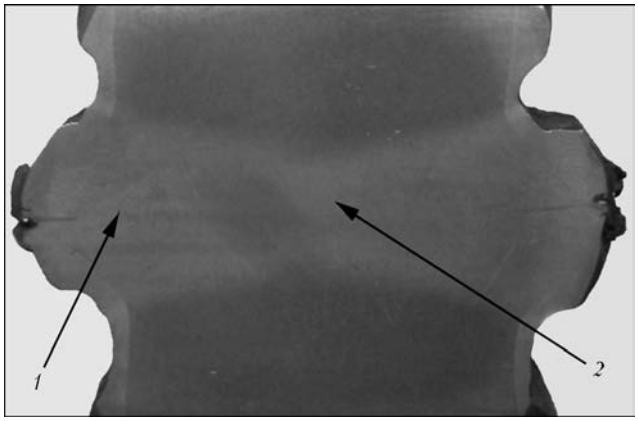

Figure 8. Macrosection of a welded joint of AIII class R-bar (*1, 2* — for explanation see the text)

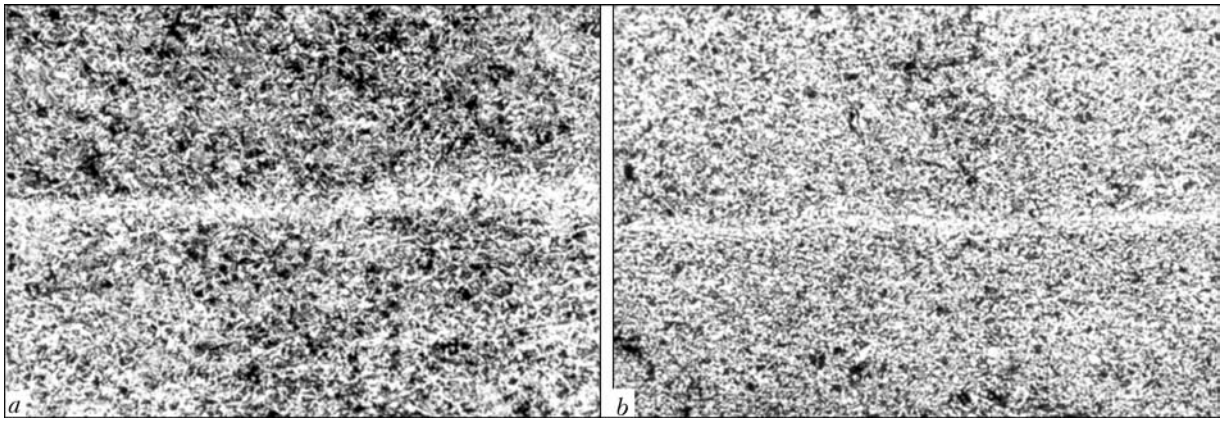

Figure 9. Microstructure of welded joint metal in sections *1* (*a*) and *2* (*b*) (see Figure 8) (×156)

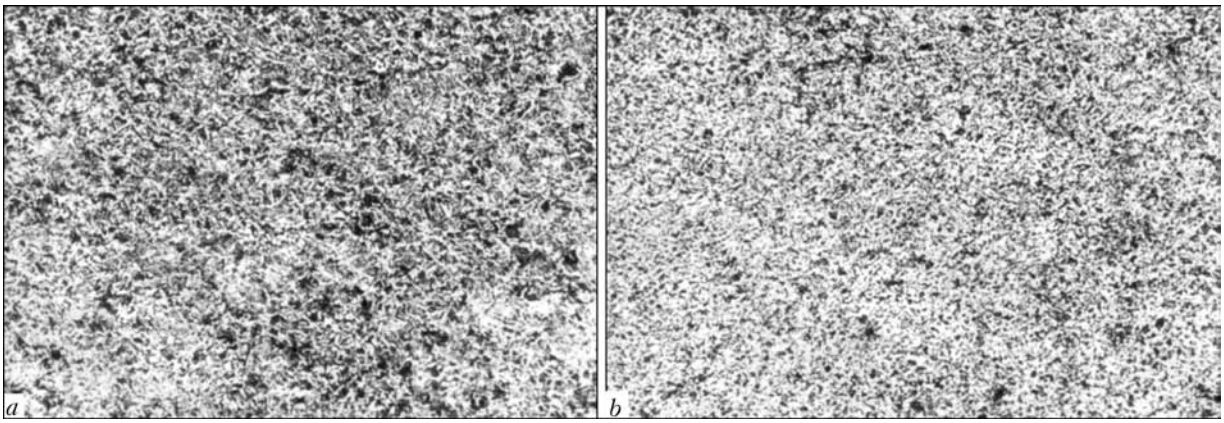

Figure 10. Microstructure of the HAZ metal of the welded joint in sections *1* (*a*) and *2* (*b*) (see Figure 8) (×156)

joint center. The strip width along the reinforcement edges was 0.36 and 0.32 mm. At 4.25 mm distance (Figure 8, *1*) on one side, and 5.43 mm on the other side, the strip width was 0.1 mm. In the central part *2* of the welded joint the strip width was 0.005 mm.

Microstructures of a welded joint and HAZ of a R-bar are shown in Figures 9 and 10.

The welded joint metal structure is that of ferrite-pearlite with prevailing of the ferrite component. In the section of the pressed-out metal and adjacent section the ferrite grain point is 7 with hardness *HV*0.05-97–232.

Microstructure of welded joint metal at 4.5–5.5 mm distance from the welded joint edge is shown in Figure 9, *a*. Ferrite grain point being 8–9 and hardness *HV*0.05-214–232.

In the central part of the welded joint the strip is hardly visible (Figure 9, *b*), the metal structure is finely dispersed with 9–10 grain point and hardness *HV*0.05-210.

Process parameters and mechanical properties of welded joints of rods and R-bars

Steel grade	*Machine type*	*R-bar diameter, mm*	*Welding time, s*	*Tensile strength, MPa*		*Impact toughness KCV, J/cm²*	
				Base metal	*Welded joint*	*Base metal*	*Welded joint*
35GS	MD101	10	7	598–610 / 604	591–611 / 602	–	–
	MD102	18	10	598–610 / 604	590–618 / 610	–	–
St3	MD102	25	14	390–398 / 388	378–401 / 391	37–43 / 40	31–38 / 35
20	MD101	14	9	487–510 / 504	480–522 / 506	91–102 / 96	82–96 / 87
	MD102	22	12	487–510 / 504	480–510 / 496	90–100 / 96	81–94 / 85
25G2S	MD103	32	33	603–616 / 607	601–626 / 610	–	–

Note. The numerator gives the minimum and maximum values, and the denominator — the average val ues.

HAZ metal structure is different along the welded joint height. In the section of the pressed out metal and adjacent section, the microstructure corresponds to a classical overheating section and consists of rather coarse grains (5–6 points, sometimes 4) with bainite-pearlite structure with ferrite fringes. Thickness of ferrite precipitates is approximately 0.0022 mm. Bainite hardness is *HV*0.05-257–286; pearlite — *HV*0.05-232–236.

The structure is gradually refined and changed (Figure 10, *a*) and at 4.5–5.5 mm distance it is a mixture of ferrite, pearlite and small amount of bainite. Grain point is 8–9, seldom 7, bainite hardness being *HV*0.05-262–265 and ferrite-pearlite mixture hardness *HV*0.05-236–244.

In the central part of the welded joint in the HAZ the structure is fine-grained ferrite-pearlite with prevalence of the ferrite component (Figure 10, *b*), grain point being 9–10, and hardness *HV*0.05-216–219.

Traces of rolling texture are visible in the middle part of the welded joint in the HAZ. In the complete recrystallization section of the HAZ the structure is fine-grained ferrite-pearlite (point is 10), hardness being *HV*0.05-221–227.

The base metal has a pronounced rolling texture and consists of ferrite and pearlite with ferrite hardness *HV*0.05-229–232, pearlite hardness *HV*0.05-257–286, grain point 8.

These studies led to development of a technology of MIAB welding of rods and R-bars of 8 to 32 mm diameter. Process parameters and mechanical properties of rod welded joints and R-bars are given in the Table.

The above-said suggests that the known methods of controlling the arc motion do not allow creating the required conditions of heating in welding of solid parts. The proposed welding process allows controlling the arc motion over the entire cross-sectional area of solid parts, and provides the required heating. The developed technology of MIAB welding of parts allows making of solid joints up to 8 to 32 mm diameter.

1. Kachinsky, V.S., Ignatenko, V.Yu., Golovchenko, S.I. (1997) Magnetically-impelled arc butt welding (equipment and technology). *Avtomatich. Svarka*, **7**, 39–41.
2. Kuchuk-Yatsenko, S.I., Kachinsky, V.S., Ignatenko, V.Yu. (2002) Magnetically-impelled arc butt welding of thick-walled pipes. *The Paton Welding J.*, **7**, 24–28.
3. Kachynsky, V.S., Kuchuk-Yatsenko, S.I., Ignatenko, V.Yu. et al. *Method of magnetically-impelled arc butt welding* Pat. 98020715 Ukraine. Int. Cl. B 23 K 9/08. Publ. 15.04.02.

EXPRESS CONTROL OF QUALITY AND STRESSED STATE OF WELDED STRUCTURES USING METHODS OF ELECTRON SHEAROGRAPHY AND SPECKLE-INTERFEROMETRY

L.M. LOBANOV, V.A. PIVTORAK, V.V. SAVITSKY, G.I. TKACHUK and **I.V. KIYANETS**
E.O. Paton Electric Welding Institute, NASU, Kiev, Ukraine

Technology and procedures of non-destructive quality control and study of stressed state using electron shearography and speckle-interferometry are presented. Examples of application of quality control and results of determination of residual stresses in structure elements are given.

Keywords: *welded structures, diagnostics, non-destructive testing, residual stresses, shearography, speckle-interferometry, measuring system*

The improvement of quality, reliability and serviceability of welded structures is connected indispensably with the development and progress of express methods and equipment of non-destructive quality control and determination of residual stresses.

In modern branches of industry the radiographic, ultrasonic, magnetic, acoustic-emission, eddy-current and many other methods of NDT are used [1, 2]. The method of a laser interferometry, such as electron shearography, finds the more and more wide application in different branches of industry.

Over the recent years, the electron shearography is the most intensively progressing coherent optical method of tests and measurements, which is realized by using simple optical devices and allows no-contact examination of the object surface without its damage. This method can be used in investigation of different materials and structures. It gives a feasibility to measure the first derivative from displacements along the selected direction of the shear. By this, the non-sensitivity of shearography to the rigid displacements of the object, caused by effect of the surrounding medium, is stipulated that predetermines its universality and effectiveness of application under industrial conditions [3, 4].

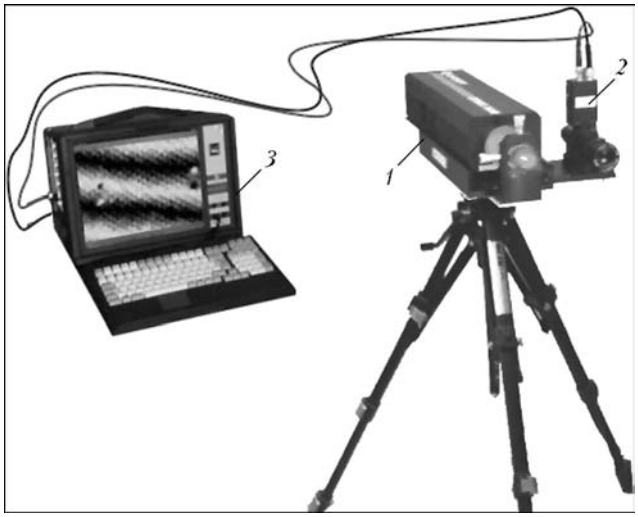

Figure 1. General view of a shearographic unit: *1* — laser; *2* — shearographic module; *3* — computer

The principle of the shearography method is as follows. The object being examined is illuminated partially or completely by a light wave, which after reflection from its surface is falling on a shear element, arranged in front of an objective of CCD-camera and dividing the aperture into two halves. In this case two displaced images of the object being examined are appeared in the plane of CCD-camera image.

When interfering the light waves, the chaotic microinterference speckle-pattern is formed and put into computer using CCD-camera. The obtained microinterference speckle-patterns, recorded for two states of the object (before and after its loading), are compared and processed to obtain the macrointerference fringes (shearograms).

In fulfillment of the non-destructive quality control of elements and assemblies of structures a compact shearographic equipment, composed of a single-mode laser with a wave length $\lambda = 532$ nm for the illumination of object surface being examined; a shearographic interferometer forming an object image; a CCD-camera for images recording; and a computer for obtaining and processing of interference fringes, was used (Figure 1).

The developed technology of the shearographic NDT allows realizing effectively the quality control of full-scale elements and assemblies of structures manufactured from different structural materials.

Experiments were made on non-destructive shearographic examination of quality of glass-reinforced plastic tubular elements of 300 mm length, 65 mm diameter and 2 mm wall thickness. The internal pressure of 300 kPa, which was created in a tubular element by a compressor, was used for loading. The general view of the tubular element examined and defects of about 10 mm, revealed as a result of experiments, are given in Figure 2.

The high efficiency of the method of electron shearography was confirmed in control of a three-layer $600 \times 500 \times 29$ mm welded panel, made of steel St3. The inner filler was a corrugated 2 mm thick sheet,

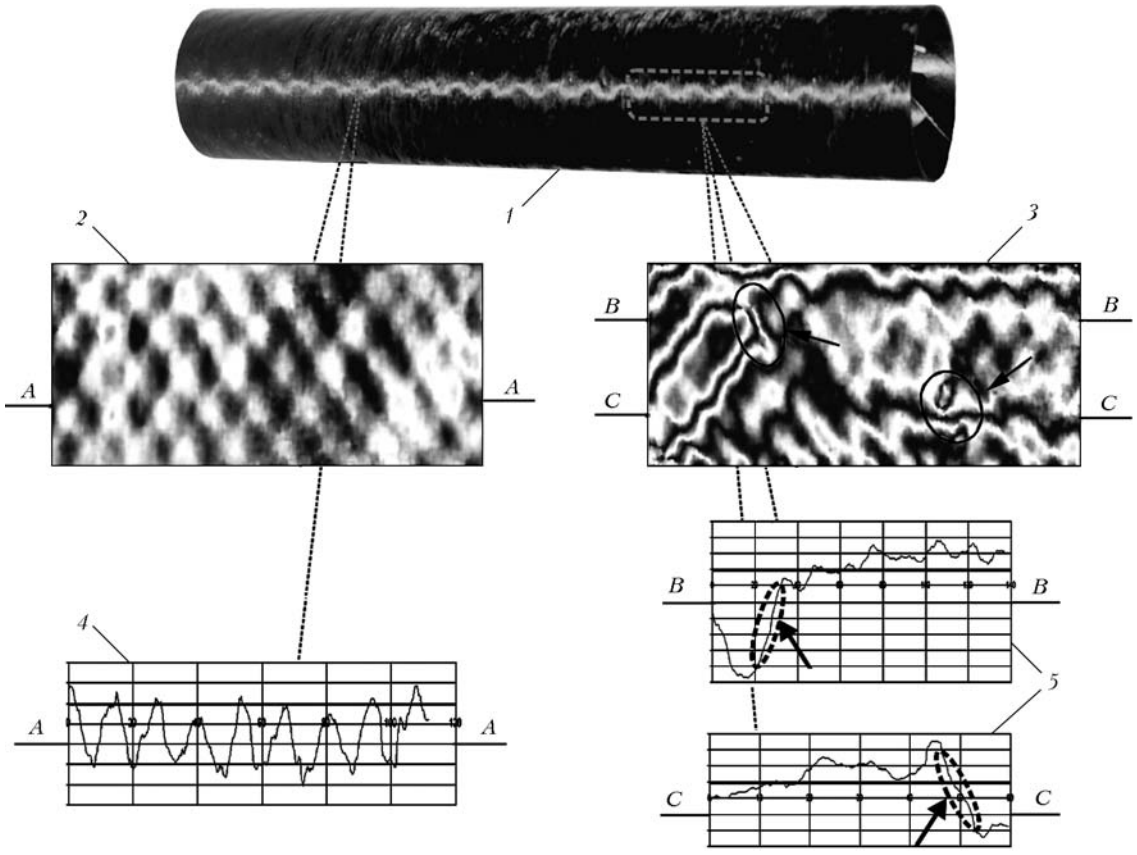

Figure 2. Results of quality control of glass-reinforced plastic tubular element: *1* — general view; *2, 3* — typical interference pattern obtained in testing areas, respectively, with and without defect; *4, 5* — change in derivative from out-of-plane displacements of structures along the selected sections (zones of defects are distinguished and shown by arrows)

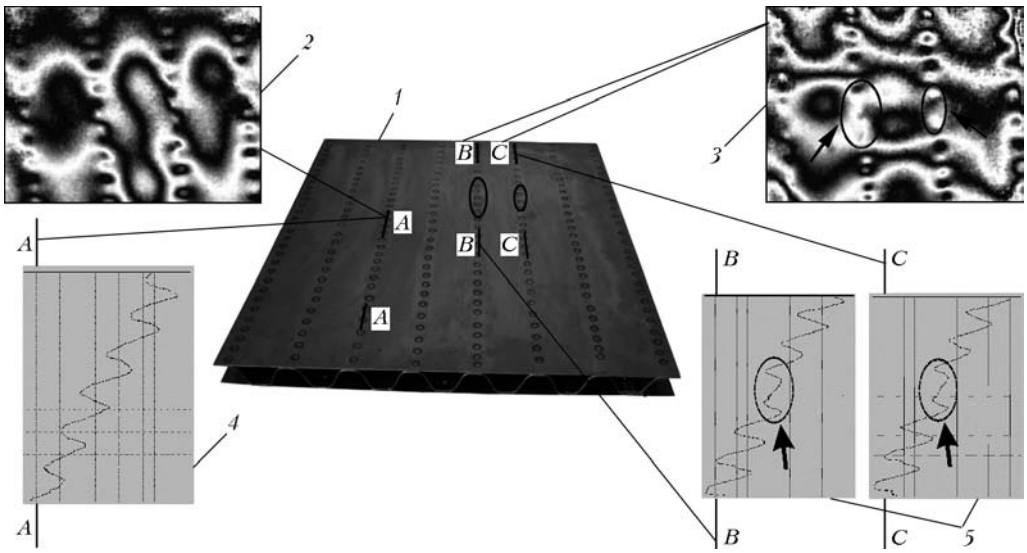

Figure 3. Results of quality control of a three-layer panel made by a spot resistance welding (for designations see Figure 2)

to which external sheets of the same thickness were welded by a resistance spot welding. To load the element examined, the heating of the area examined by a hot air (T = 70 °C) for 10 s was used. The general view of the welded panel and results of assessment of quality are given in Figure 3. The surface profiles of the object examined in section show the sites of visualization of defects of size of about 5 mm, whose occurrence was caused by a non-quality spot welding.

The important advantage of the electron shearography method is the fact that it makes possible to perform quality control of elements of 3D structures having an access only from one side. Figure 4 presents the general view of a thin-walled structure made from aluminium alloy AMg6. The internal side of its lining was strengthened by transverse and longitudinal stiffeners. Size of structure was 1580 × 680 × 420 mm, lining thickness was 1 mm.

In service of thin-walled structure a crack of 100 μm width and 5 mm depth was initiated at the area of crossing the transverse and longitudinal stiffeners in their vertical flange. Moreover, the thin-walled lining was not damaged. To load the structure, the heating of the examined area with a hot air (T = = 60 °C) for 5 s was used. The results of examination are presented in Figure 4.

The non-destructive quality control of elements and assemblies of structures using the electron shearography method showed that the created technology at a proper selection of the method of loading with account for a geometry of elements and materials examined (mechanical, thermal, etc.) allows revealing different types of defects (lack of penetration, cracks, lack of adhesion and other imperfections of materials), which create a local concentration of deformations under loading. The application of the above-mentioned technology of non-destructive quality control is the only possible variant in a number of cases for obtaining the valid information about the presence of defects in thin-walled structures made from metallic and non-metallic materials.

Residual stresses influence greatly the performance of welded structures. To determine them in elements and assemblies of structures, the methods of tensometry, X-ray and neutron diffraction, magnetic, ultrasonic, laser interferometry and others are used [5–7].

At the E.O. Paton Electric Welding Institute the technology has been created and compact equipment has been designed for the express determination of residual stresses using the method of electron speckle-interferometry in drilling of a blind hole. This method is based on using the optical scheme of the interferometer, in which an object area examined is illuminated by a laser beam under the same angle symmetrically in two directions that makes it possible to determine the components of vector of displacements which characterize the object deformation in its plane [8–10].

To determine the residual stresses in elements and assemblies of structures using this optical scheme, a small-sized unit has been developed, which is mounted directly on the object surface being examined (Figure 5).

The measurement is made in the following sequence. Speckle-interferometer is mounted on the object surface. The reflected light wave, characterizing the initial state of the area examined, is converted using CCD-camera into analog signal which enters the computer memory. After elastic unloading of stresses by drilling of a blind hole (diameter and its depth are 1.0–1.5 mm), the reflected light wave enters the computer memory in the similar way. After computer processing of data about these two light waves the interference pattern of fringes, arranged around the hole, is observed, containing the information about the values of residual stresses in the examined point of the object.

For the plate with a through hole, which is located in the field of stresses, the values of displacements of points at the object surface around the hole can be calculated analytically using relationships obtained in the work [6]. The similar problem for the plate with a blind hole has no analytical solution and, therefore, the empiric formulae from works [11, 12] are

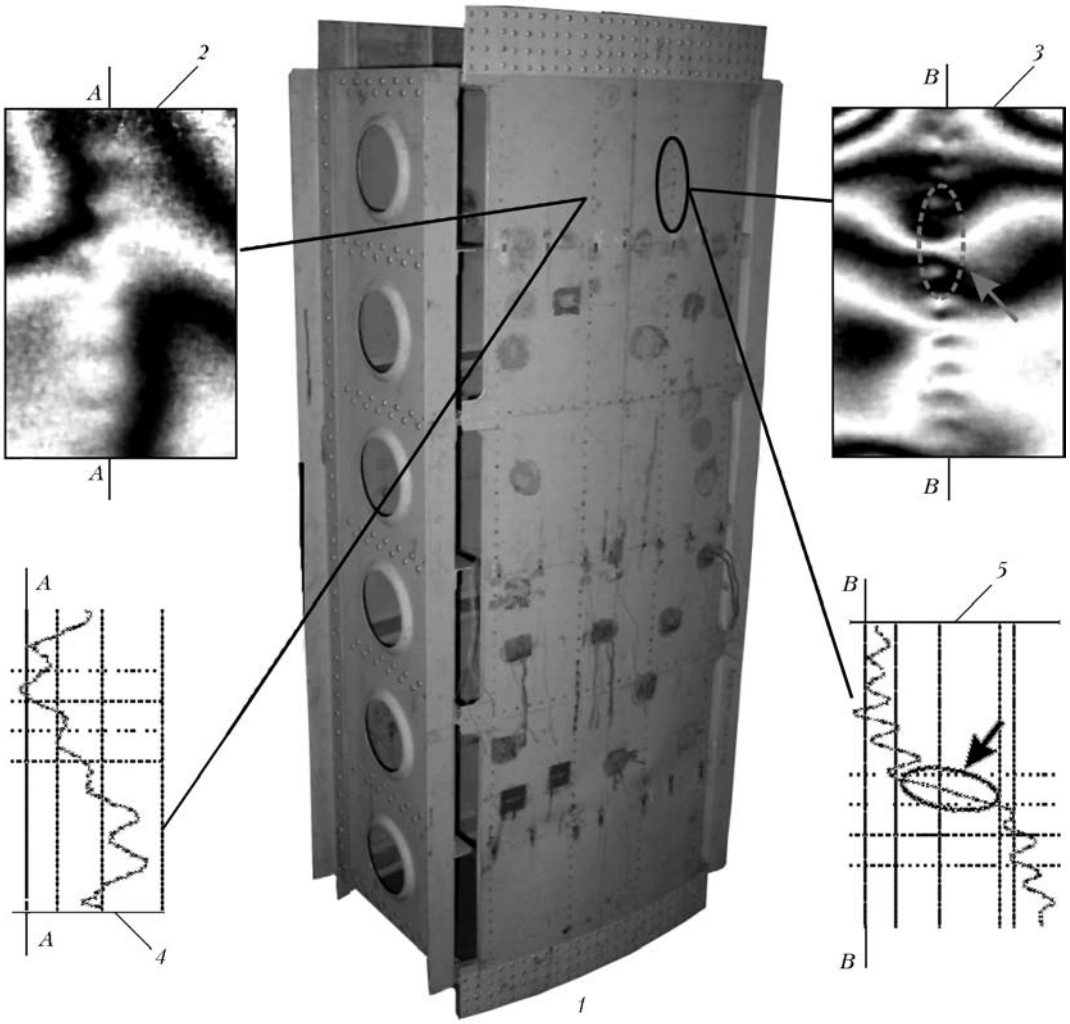

Figure 4. Results of quality control of thin-walled structure (for designations see Figure 2)

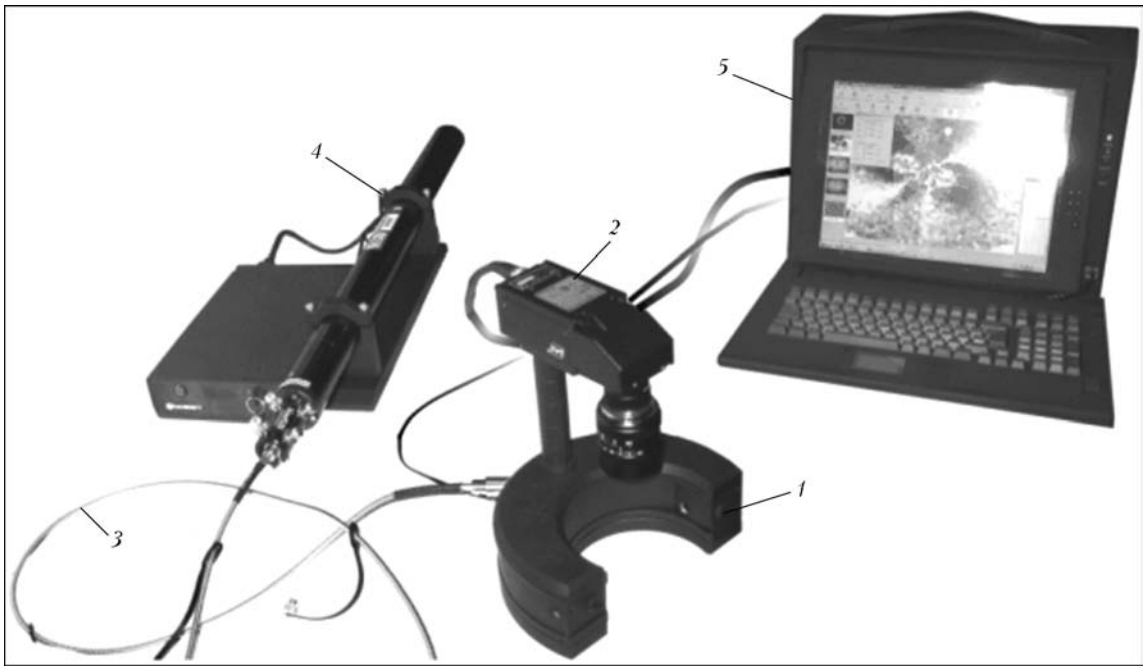

Figure 5. General view of speckle-interferometric measuring system: *1* — speckle-interferometer; *2* — CCD-camera; *3* — light guide; *4* — laser; *5* — computer

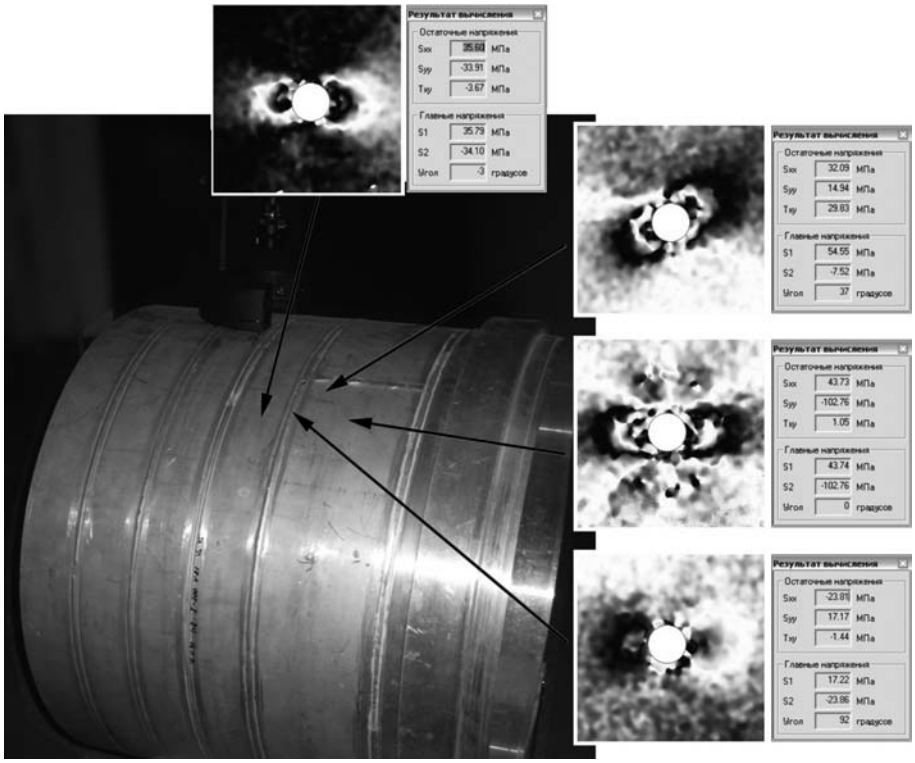

Figure 6. General view of welded aluminium shell and interference fringe pattern

used in this case. Dependence of displacements u_r and u_θ, occurring as a result of unloading of stresses σ_{xx}, σ_{yy} and τ_{xy} at some distance r from the hole center, on angle θ has the form [13]:

$$u_r(r, \theta) = A(\sigma_{xx} + \sigma_{yy}) + B\,[(\sigma_{xx} - \sigma_{yy})\cos 2\theta + 2\tau_{xy}\sin 2\theta], \quad (1)$$

$$u_\theta(r, \theta) = C\,[(\sigma_{xx} - \sigma_{yy})\sin 2\theta - 2\tau_{xy}\cos 2\theta], \quad (2)$$

where A, B and C are the empiric coefficients, depending on mechanical properties of the material, distance from the hole center to the point of measurement, its diameter and not depending on the kind of stressed state.

Procedure and equipment have been developed to determine experimentally the coefficients A, B and C. The procedure assumes to create a uniaxial stressed state in a special test sample with a known level of stresses. A hole is drilled in the loaded sample and the measurement of components of a vector of displacements was made using a speckle-interferometer in the hole zone. Values of empiric coefficients were calculated in the points examined from the data about displacements. To provide an additional check-out, they were also determined using a method of finite elements by a developed algorithm. The obtained results showed that data of a numerical determination of values of empiric coefficients A, B and C have a good correlation with experimental data.

The developed procedure assumes the measurement of a component of displacements $u_x(r, \theta)$ at a constant distance from the hole center (for example, $r = 2.5r_0$). Using equations (1) and (2), u_x can be presented in the form:

$$u_x(\theta)\,|_{r = 2.5r_0} = F(\theta)\sigma_{xx} + G(\theta)\sigma_{yy} + H(\theta)\tau_{xy}, \quad (3)$$

where $F(\theta)$, $G(\theta)$ and $H(\theta)$ are the functions depending on empiric coefficients A, B, C and angle θ.

Determination of residual stresses using the offered procedure is realized in the following sequence:

- at the $2.5r_0$ distance from the center of drilled hole of radius r_0, the points are selected at an optional angle with respect to the axis of illumination and their displacements in plane of surface of the object examined are measured using a speckle-interferometer;
- components σ_{xx}, σ_{yy} and τ_{xy} of tensor of stresses are calculated from data about displacements using (3) by a method of the least squares;
- values of principal stresses σ_1, σ_2 and angle η between the axis of illumination of speckle interferometer and direction σ_1 are determined.

To evaluate the accuracy of measurement of in-plane displacements using a small-sized speckle-interferometer and automated computer processing of interferograms, the solution of known problem about the bending of a console beam with a fixed end by a force applied to a free end was used. The experiments showed that the deviation of values of stresses, which were determined by a speckle-interferometric method, from estimated values does not exceed 5 % of yield strength of material examined [14].

Procedure of determination of residual stresses and equipment, designed for this purpose, were used for study of stressed state in 760 mm diameter AMg6 alloy welded shell, made by argon arc welding (Figure 6). Method of electron speckle-interferometry allowed determination of residual stresses in different areas of welds, in particular in the area of their intersection.

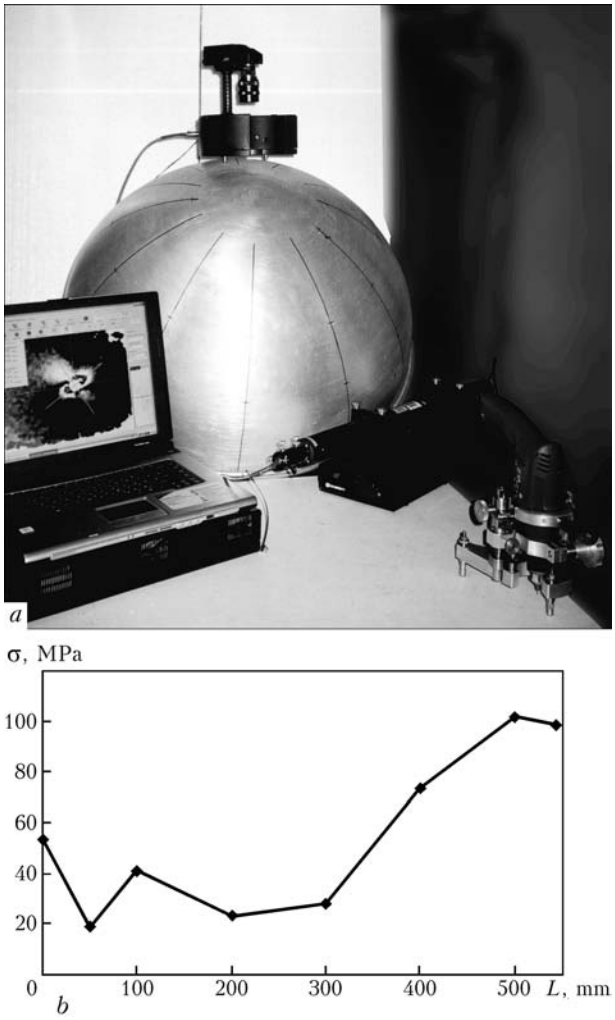

Figure 7. Appearance of semi-spherical shell of a variable thickness (*a*) and distribution of residual stresses along its generatrix *L* (*b*)

Using the designed compact equipment, the patterns of interference fringes were obtained, which contain information about residual stresses. This gives an opportunity to repeat the measurement of stressed state of elements of structures after a definite time interval and to compare them with results of prior measurements and to assess the effect of service conditions on residual stresses.

Technological stresses were also investigated, occurring in manufacture of 760 mm diameter semi-spherical shell of a variable thickness, used in machine building (Figure 7). The technology of manufacture of structures using similar semi-spherical shells with minimum stresses was updated on the basis of results of investigation of the above-mentioned stresses.

The procedure of determination of residual stresses, updated by authors using a method of electron speckle-interferometry, makes it possible to evaluate the gradient of stresses on the basis of drilling holes, to increase the accuracy and validity of their calculations. The presented procedure was used for evaluation of peculiarities of distribution of residual stresses in welded joints of dissimilar materials. Thus, the residual stresses in welded joint of aluminium alloy AMg6 and titanium alloy VT4 were studied. At the first

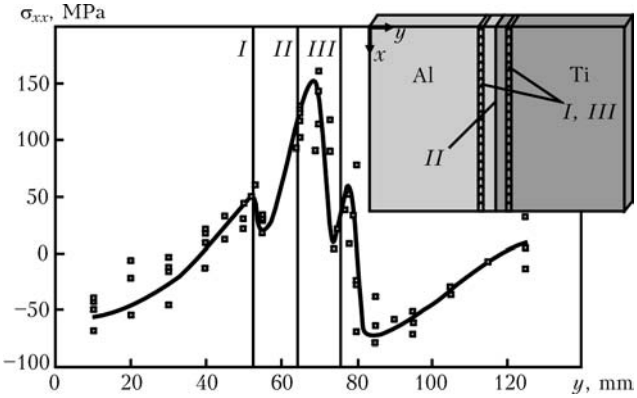

Figure 8. Diagram of residual stresses σ_{xx} in a central section across the welded joint of dissimilar materials: *I, III* — EBW; *II* — explosion welding

stage the Al–Ti joint was made by explosion welding, and then the joint Al–Al and Ti–Ti was made using EBW. It should be noted that the EBW is characterized by a high gradient of stresses and narrow weld. Figure 8 shows the diagram of residual stresses in a central section across the welded joint.

Thus, the developed procedure of determination of residual stresses, based on the method of electron speckle-interferometry in combination with a probing hole and realized using a designed small-sized speckle-interferometer, makes it possible to study the distribution of stresses at the surface of objects examined very quickly and at a high accuracy (about 5 % of material yield strength). This opens up wide opportunities for diagnostics of stressed state under laboratory and industrial conditions.

1. (2001) *Nondestructive testing and technical diagnostics*. Ed. by Z.T. Nazarchuk. Lvov: FMI.
2. Nedoseka, A.Ya. (2001) *Principles of calculation and diagnostics of welded structures*. Ed. by B.E. Paton. Kiev: Kniga.
3. Rastorgi, P.K. (2000) *Trends in optical nondestructive testing and inspection*. Amsterdam-Lausanne: Elsevier.
4. Lobanov, L.M., Pivtorak, V.A., Olejnik, E.M. et al. (2004) Procedure, technology and equipment for shearographic nondestructive testing of materials and elements of structures. *Tekhn. Diagnostika i Nerazrush. Kontrol*, **3**, 1–4.
5. (1990) *Experimental mechanics*. Book 2. Ed. by A. Kobayashi. Moscow.
6. Lobanov, L.M., Pivtorak, V.A. (1998) Development of holographic interferometry for investigation of stress-strain state and quality control of welded structures. In: *Advanced materials science of the 21st century*. Kiev: Naukova Dumka.
7. Bratukhin, A.G., Lobanov, L.M., Pivtorak, V.A. et al. (1995) Residual stresses in components of aircraft structures made of alloy 1420. *Avtomatich. Svarka*, **3**, 10–13.
8. Moore, A.J., Tyrer, J.R. (1996) Two-dimensional strain measurement with ESPI. *Opt. Lasers Eng.*, **24**, 381–402.
9. Zhang, J. (1998) Two-dimensional in-plane electronic speckle pattern interferometer and its application to residual stress determination. *Ibid.*, **37**, 2402–2409.
10. (1993) *Speckle metrology*. Ed. by R.S. Sirohi. New York: Marcel Dakker.
11. Makino, A., Nelson, D. (1994) Residual stresses determination by single-axis holographic interferometry and hole-drilling. Part 1: Theory. *Exp. Mech.*, **34**, 66–78.
12. Wu, Z., Lu, J., Joulaud, P. (1997) Study of residual stresses distribution by moire interferometry incremental hole drilling method. In: *Proc. of 5th Int. Conf. on Residual Stresses*. (Lin-Coping, Sweeden). Lin-Coping.
13. Schaer, G.S. (1981) Application of finite element calculations to residual stresses measurements. *J. Eng. Mater. Tech.*, 103(**4**), 157–163.
14. Lobanov, L.M., Pivtorak, V.A., Savitsky, V.V. et al. (2005) Express determination of residual stresses using the electron speckle-interferometry. *V Mire Nerazrush. Kontrolya*, **1**, 10–13.

METHODS FOR WELDING TITANIUM ALLOYS

V.N. ZAMKOV and V.P. PRILUTSKY
E.O. Paton Electric Welding Institute, NASU, Kiev, Ukraine

Ingenious methods for fusion welding of titanium alloys, developed by the E.O. Paton Electric Welding Institute, are described. Advantages of the application of halide fluxes developed by the Institute for electroslag, arc and electron beam welding are shown.

Keywords: *welding methods, titanium, halide flux, flux-cored wire, magnetically impelled arc, specialised semi-automatic device*

Being a reactive metal, titanium actively interacts with air during fusion welding. As a result, it becomes saturated with oxygen, nitrogen and hydrogen. Increase in the content of these impurities in titanium leads to increase in its strength and hardness, decrease in ductility, and to delayed fracture of parts and units during the operation process. The most common welding methods used for fabrication of structures of titanium alloys are TIG welding in argon atmosphere and electron beam welding. However, their commercial application involves a number of problems, the main of which are sensitivity of the weld metal to porosity, necessity to use multilayer welding and, hence, multiple heating in making of the TIG welds in titanium not more than 3 mm thick.

Research conducted by S.M. Gurevich at the E.O. Paton Electric Welding Institute as far back as the middle of the 1950s showed the feasibility of successful welding of titanium using fluxes. As a result, the metallurgical principles were formulated for designing fluxes based on halides of alkali and alkali-earth elements. The research served as a basis for the development of a number of welding methods, which were fundamentally new for titanium, i.e. automatic metal-electrode submerged-arc welding, electroslag welding (ESW), and argon-arc tungsten-electrode welding over the flux layer (TIG-F) and using flux-cored wire (TIG-FW)

The research proved the possibility of shielding molten titanium with a halide atmosphere in automatic metal-electrode submerged-arc welding using fluxes ANT-1, ANT-3 and ANT-7. The welding zone, molten titanium in the weld pool and fusion of wire in the arc — all of them are isolated from contact with air, molten halide flux and its vapours. This method can provide the welds of almost any type and size. The maximal penetration depth (without groove preparation) is 11–12 mm. Advantages of this welding method include a high welding speed (up to 50 m/h), reliable shielding and, what is most important, guaranteed absence of porosity in the weld metal.

Automatic metal-electrode submerged-arc welding provides the required level of properties of welded joints in commercially pure titanium, α- and $(\alpha + \beta)$-titanium alloys. This technology is commercially applied primarily in chemical engineering for fabrication of welded structures operating in aggressive environments (Figure 1).

Electroslag welding of titanium is based on the experience gained in ESW of ferrous metals and metallurgical peculiarities of halide titanium fluxes. Flux ANT-2 that meets all the requirements is used for ESW of titanium alloys. The main feature of ESW of titanium consists in argon shielding of the slag pool. It should be noted that the high quality of welded joints can be ensured only at the presence of the above extra gas shielding. Like in metal-electrode submerged-arc welding, the ES welds in titanium are characterised by the absence of porosity, which guarantees welded joints with a high fatigue strength. The ESW technology is applied for fabrication of large-size 3D structures with heavy-section members, as well as for enlargement of semi-finished products (Figure 2).

Halide flux performs fundamentally new functions in TIG welding in argon atmosphere. The use of fluoride fluxes in this case widens technological capabilities of the arc, increases the penetration depth in titanium (other conditions being equal), decreases heat input and prevents porosity in the weld metal. Allowing for these peculiarities, a new, more efficient method was developed for welding titanium, called TIG-F. Then this technology was adapted to other metals, steels in particular, and called A-TIG.

The TIG-F method allows welding of titanium alloys not 3 but 6 mm thick in one pass without groove preparation, making welds of any type both with and without a filler wire, in flat position and on a vertical

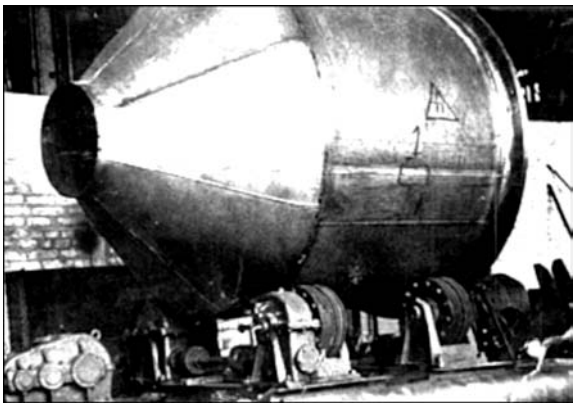

Figure 1. Shell of a filter made from commercial titanium VT1-0 (grade 2) using automatic metal-electrode submerged-arc welding

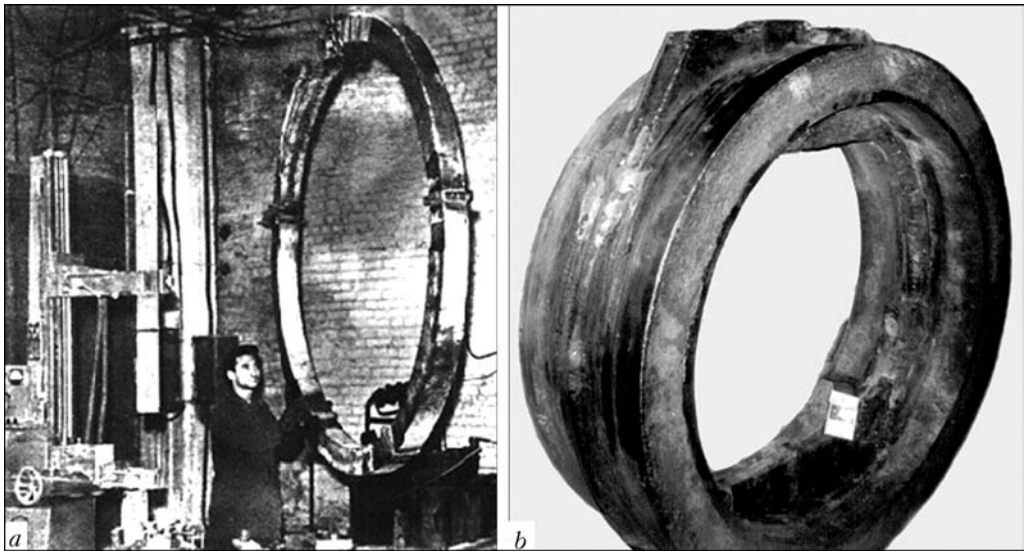

Figure 2. Flange of alloy PT3V (grade 9) with a cross section of 150 × 200 mm (*a*) and position butt joint in pipe 1000 mm in diameter with a wall thickness of 100 mm (grade 2) (*b*) made by ESW

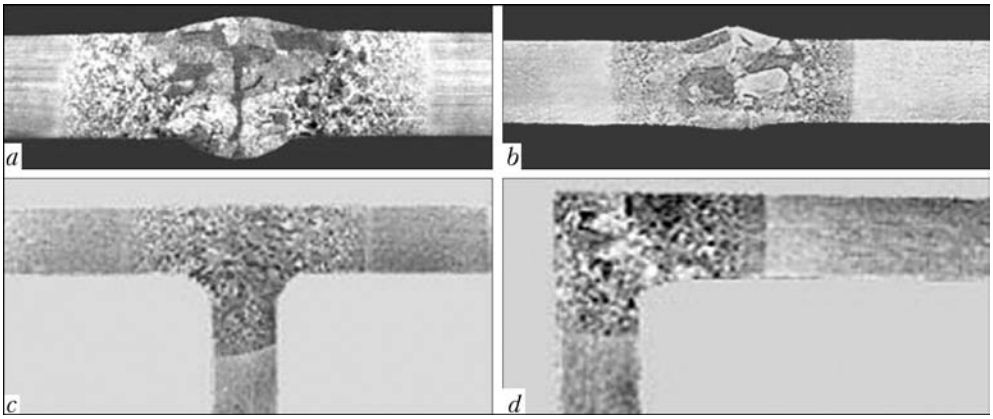

Figure 3. Macrostructure of TIG-F welded joints: *a, b* — butt joints 6 mm (flat position) and 3 mm (vertical plane) thick, respectively (alloy OT4); *c, d* — T- and fillet joints, respectively, with elements 3 mm thick (alloy VT6)

plane (Figure 3). The consumption of flux (irrespectively by of thickness of a metal welded) is no more than 10 g per metre of the weld.

TIG welding received a further development effort after a new welding consumable for titanium had been designed, i.e. flux-cored wire. Welding using a filler flux-cored wire (TIG-FW) allows the welds in titanium and its alloys 5–16 mm thick to be made in one pass without groove preparation (Figure 4). Like TIG-F welding, this method is applied for making any type of the welds. It should be noted that TIG-FW welding also provides the pore-free weld metal and welded joints with high values of fatigue strength. The consumption of filler flux-cored wire is no more than 1.5 m per metre of the weld. Standard equipment is used for welding by the TIG-F and TIG-FW methods.

Flux exerts a positive effect on metal of the welds in titanium alloys made also by EBW in vacuum.

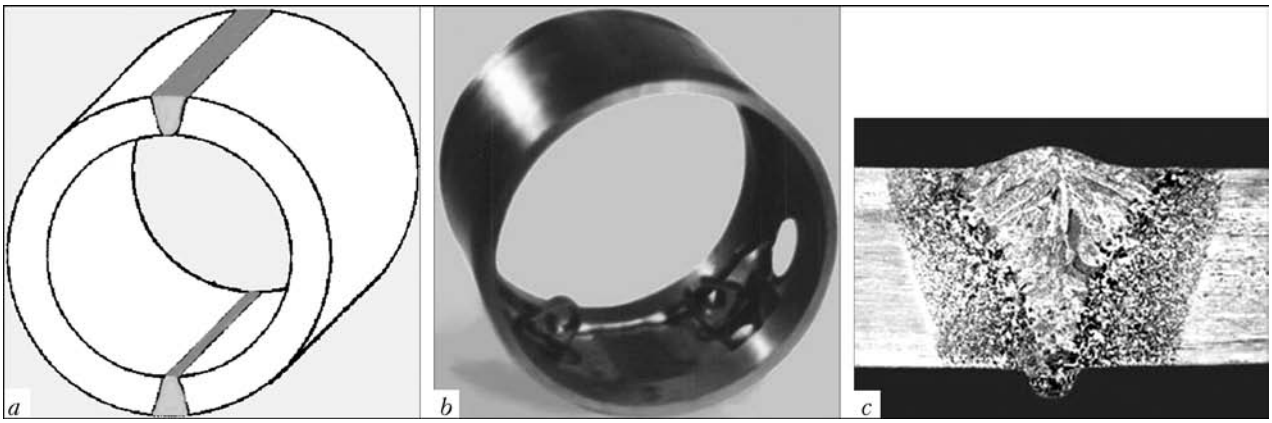

Figure 4. Cylindrical frame of alloy VT6 (Ti–6Al–4V) with a wall thickness of 14 mm made by the TIG-FW method: *a* — welded billet; *b* — part; *c* — macrostructure of welded joint 14 mm thick

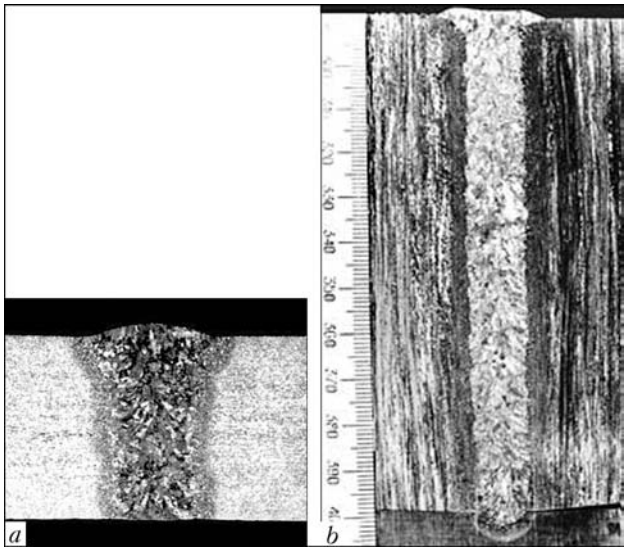

Figure 5. Macrostructure of different-thickness welded joints made by the narrow-gap magnetically-impelled arc welding method: *a* — 25 mm (VT1-0); *b* — 110 mm (Ti–6Al–4V)

EBW of titanium causes a large amount of micropores less than 0.1 mm in diameter formed in the cast metal, especially in the fading-out region of circumferential welds. In a number of cases this has a negative effect on performance of welded joints. To prevent this phenomenon, the use is made of flux of the ANT-23A grade, which provides a substantial (by an order of magnitude) decrease in the amount of micropores. In this case, the welding process involves no difficulties associated with either hardware or technology. The application of flux in EBW, e.g. of alloy Ti–6Al–4V, increases fracture toughness coefficient K_{1c} of the weld metal and stress corrosion resistance of welded joints.

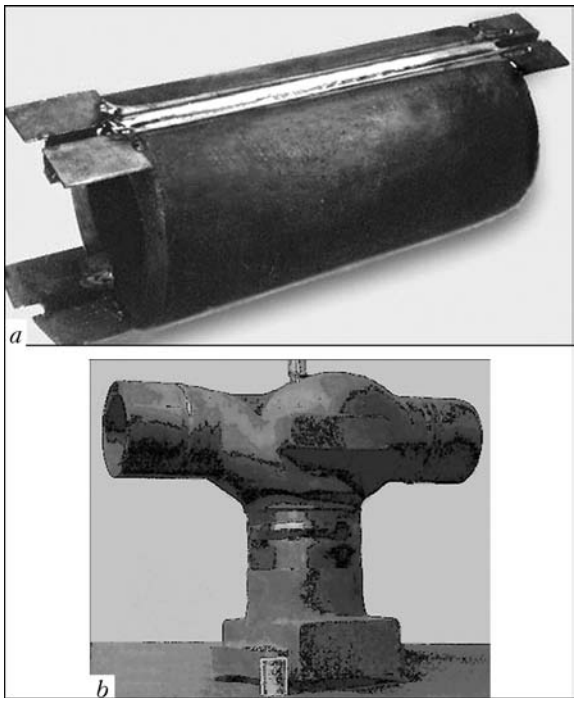

Figure 6. Examples of application of argon-arc narrow-gap magnetically-impelled arc welding: *a* — welded cylindrical cathode for production of copper foil (VT1-0, 50 mm thick); *b* — casing of a pump for transportation of aggressive fluid (alloy PT3V, grade 9, 50 mm thick)

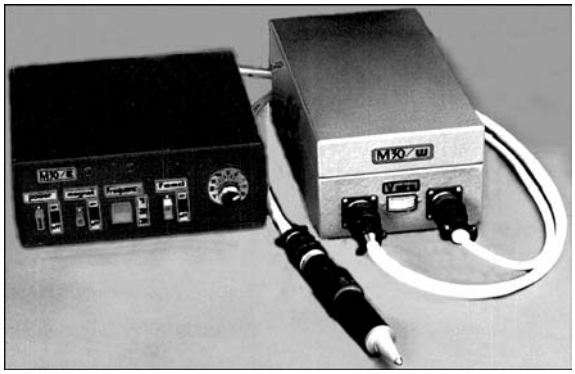

Figure 7. Semi-automatic TIG welding device M30

To join heavy sections of titanium alloys (20–100 mm), the E.O. Paton Electric Welding Institute developed equipment and technology for narrow-gap magnetically-impelled arc TIG welding in argon atmosphere. Movement of the arc over an assigned path provides the defect-free welds, reliable fusion of vertical edges of the gap with beads that fill the gap, and absence of pores in the cast weld metal (Figure 5). The welding head is equipped with a system for automatic maintaining of the arc length and TV system for viewing of the welding process. Figure 6 shows examples of application of this technology.

The commercial automatic arc welding processes developed by the E.O. Paton Electric Welding Institute offer a wide option of efficient technologies for manufacturers of different-purpose and different-size welded structures in titanium alloys.

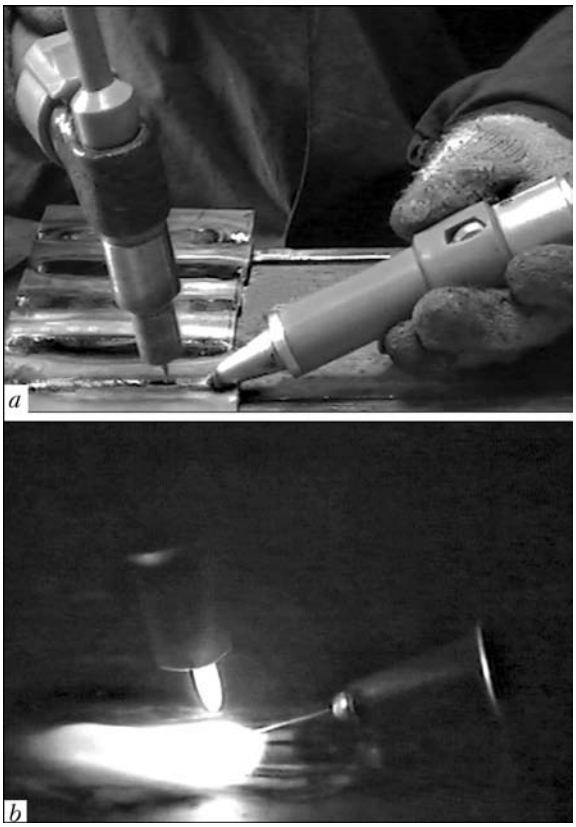

Figure 8. Welding procedure using semi-automatic welding device M30: *a* — position before welding; *b* — welding process

However, there are many parts and units, especially in piece work production and in erection of titanium structures, that are still manufactured by manual TIG welding. In this connection, the E.O. Paton Electric Welding Institute conducted a package of research on upgrading of this method, intended for improvement of reliability and quality of manual welded joints, as well as decrease in requirements for welders' skill. These efforts resulted in the development of the semi-automatic device M30 for mechanised TIG welding (Figure 7), allowing adjustment of the path of the anode arc spot relative to the weld axis and, hence, penetrating power of the arc. This provides substantial reduction of the risk of defects that may be formed due to errors in fit-up of pieces for welding. With this device, a welder, as usually, holds a torch in one hand, moving it along a joint, and nozzle in his other hand, via which a filler wire is fed and the arc is magnetically controlled (Figure 8).

In addition to the above commercial technologies intended for welding titanium alloys, development of automatic vertical TIG welding in argon atmosphere has been completed at a laboratory level. Titanium plates from 15 to 30 mm thick are uphill one-sided welded using no filler wire. The samples are assembled for welding without groove preparation and without a gap. Welding is performed using the 5 mm dia. tungsten electrode of the EVI-2 grade. To provide through penetration, the electrode is automatically moved in a welded joint plane following a special path. The welding current is kept unchanged.

LASER-ARC AND LASER-PLASMA WELDING AND COATING TECHNOLOGIES

V.D. SHELYAGIN, I.V. KRIVTSUN, Yu.S. BORISOV, V.Yu. KHASKIN, T.N. NABOK, A.V. SIORA, A.V. BERNATSKY, S.G. VOJNAROVICH, A.N. KISLITSA and **T.N. NEDEJ**
E.O. Paton Electric Welding Institute, NASU, Kiev, Ukraine

Peculiarities of processes occurring in the case of combined utilisation of laser beam and consumable-electrode arc or plasma jet are considered. Fundamentally new approaches have been developed for one- and multipass hybrid laser-arc welding, as well as combined and hybrid laser-microplasma deposition of coatings (including diamond and diamond-like thin coatings). Advantages of the new hybrid (combined) processes are shown in comparison with the available laser and arc ones.

Keywords: *laser welding, filler wire, arc, consumable electrode, hybrid process, steels, aluminium alloys, large thickness, multipass welding, conditions, heat input, microplasma, combined process, surface alloying, coating, diamond and diamond-like coatings, metallography, structures, properties*

There are cases where laser technologies fail to yield a positive result, unless some extra techniques are applied. In a case of butt welding, for example, it is often necessary to form the root and upper beads of weld reinforcement, which requires the use of a filler material [1]. In a case of coating, sometimes it is necessary to localise the heat effect, so that it becomes close to that exerted in microplasma spraying, but that the strength of adhesion of layers to the substrate corresponds to that achieved in cladding. In addition, it is advisable to maximise productivity of the laser processes and, at the same time, minimise consumption of the expensive laser radiation power. These problems can be handled using hybrid or combined laser-arc processes [2, 3].

The E.O. Paton Electric Welding Institute of the National Academy of Sciences of Ukraine is active in research conducted in the field of hybrid laser-arc welding and related technologies. Primary target of this research is to study interaction between the two heat energy sources (laser beam and consumable-electrode arc, plasma arc or microplasma jet) to reveal peculiarities of the hybrid process, their effect on weld formation or surface modification, and possibility of combining advantages and eliminating drawbacks of laser and arc components of the process.

Investigations were conducted to study methods of hybrid welding using laser beam and consumable-electrode arc, combined laser-plasma alloying and surface modification, as well as deposition of diamond and diamond-like coatings. The most promising methods were chosen on the basis of the results of analysis of the above methods, and the ingenious hybrid laser-arc methods were offered on their ground [2, 4], the experiments with which were then conducted.

Studied were technological peculiarities of hybrid welding of low-carbon, low-alloy and stainless steels up to 20 mm thick (steels 20, St3kp (rimming), 19G, 17G1S, 13G1S, 09G2S, 09M2SF, 10KhSND, 10G2FBYu, 38KhN3MFA, Kh18N10T, 08Kh17T), as well as aluminium alloys up to 6 mm thick (AMg5, AMg6, 1915) and commercial-purity aluminium. Filler (electrode) wires Sv-08G2S (0.8–1.6 mm di-

ameter), Sv-12Kh18N9T (0.9 and 1.0 mm diameter) and Sv-AMg6 (1.2 mm diameter) were used for welding. In the combined processes of laser-microplasma alloying and deposition of thin coatings, the spraying materials used were powders with a particle size of 0–40, 60–100, 50–160 and 100–300 μm, produced from alloys of the Ni–Cr–B–Si (PG-AN6, PG-AN9, PG-12N-01, PG-12N-02, PG-10N-04) and Ni–Fe–B–Si (PG-N1, PG-N3) systems, and from Fe-base alloys (PG-S27), as well as chromium, nickel, tungsten carbide and titanium nitride powders. Separate studies were carries out to produce diamond and diamond-like coatings, as well as silicon oxide coatings.

The experiments were conducted using the 10 kW technological lasers LT-104 [5] and 2 kW laser DF 020 HQ (ROFIN-SINAR). Power supplies VDU-601 and PSG-500 were employed for hybrid welding with the consumable-electrode arc, in-house 110 A current supply was used for hybrid welding with the plasma arc, power supplies MPU-4 were used for the combined coating process, and PWI inverter-type power supply was applied for deposition of diamond thin coatings and silicon oxide. The experiments were carried out using a test rig based on a two-axis manipulator with a working field of $X:Y$ = = 2000:1200 mm, positioning accuracy of up to 0.1 mm and travel speed of up to 600 m/h, test rigs based on screw-cutting lathes, as well as a process fixture of the in-house development.

The experiments on hybrid laser–consumable-electrode arc CO_2 welding of low-carbon low-alloy steels show that the resulting welds have mostly a ferritic-pearlitic structure of low hardness (HV1-200–250), and that the HAZ contains some quenching bainitic structures with hardness HV1-250–300. At the same time, quenching bainitic and martensitic structures are dominant in the laser welds made at the identical speed, both in the weld and HAZ. However, despite the presence of the quenching structures and high hardness (HV1-300–350), the laser welds have rather high values of strength and ductility. This is associated with the presence of fine-grained equiaxed martensite [6]. Nevertheless, as requirements to the welds and HAZ often limit their hardness to a level of HV1-260–280, the laser-arc welding process proves to be a better choice.

Another advantage of laser-arc welding is elimination of root defects in the laser welds, which are characteristic of welding using any highly concentrated energy source and lead to the risk of undercutting and porosity [7]. This is related to variations in hydrodynamics of the weld pool. In addition, periodic increases and decreases in the penetration depth are also related to the hydrodynamic processes occurring in the weld pool in hybrid welding, compared with laser welding at an identical process speed and laser radiation power [4]. Investigations into these processes allow adjustments to be made in the technological process to enhance the hybrid effect. It was established that 1 kW power of the consumable-electrode arc could replace 1 kW power of the laser beam in hybrid welding of steels up to 4–5 mm thick, while in welding thicker steels 1 kW power of the arc could replace 0.5 kW power of the laser beam (Figure 1).

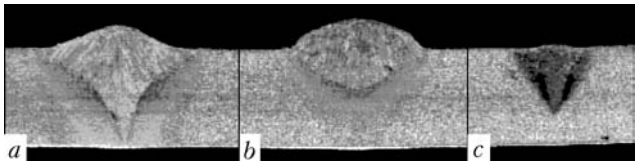

Figure 1. Macrosections of claddings on steel 09G2S (δ = 6 mm) made by hybrid (*a*), arc (*b*) and laser (*c*) methods: *a* — P = = 2.5 kW, I = 90 A, U = 24 V, v_w = 42 m/h; *b* — I = 200 A, U = = 19 V, v_w = 21 m/h; *c* — P = 2.5 kW, v_w = 42 m/h

It was proved that laser-arc welding with the laser and arc sources having a power of 3–4 kW is indicated for one-pass penetration of steel up to 10 mm thick. Larger thickness requires either an increased power (first of all of the laser component) or multipass welding. Trials were carried out to apply multipass laser and hybrid laser-arc welding processes for steels 10–20 mm thick. 6–8 passes were required for penetration of low-carbon steel 20 mm thick by the laser beam using the 1.2 mm dia. filler wire Sv-08G2S. Hybrid welding allowed the number of passes to be reduced to four.

In a case of hybrid welding, the laser beam stabilises the electric arc and makes it go down into a narrow (no more than 10°) gap of the V-groove to a depth of 20 mm. This effect was used as a basis for the development of the hybrid welding techniques for thick steels (Figure 2). In this case the weld pool is comparatively small in size (20–30 mm long). The rigid thermal cycle characteristic of one-pass laser welding is mitigated by the arc component, while the repeated passes provide lower sensitivity to formation of quenching structures. In a case of laser welding using a filler the heat input in one pass was 0.84 MJ/m at a welding speed of 12 m/h, while in a case of hybrid welding the heat input in one pass was 1.125 MJ/m at a welding speed of 24 m/h. Thus,

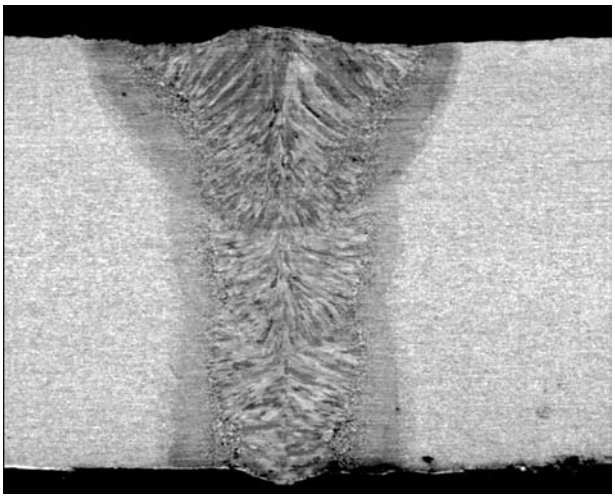

Figure 2. Macrosection of butt joint in steel 10G2FBYu (δ = = 18.7 mm) welded by the hybrid method in 4 passes using 1.2 mm dia. wire Sv-08G2S (P = 2.5 kW, v_w = 24 m/h, v_f = 400 m/h, I = 200 A, U = 26 V)

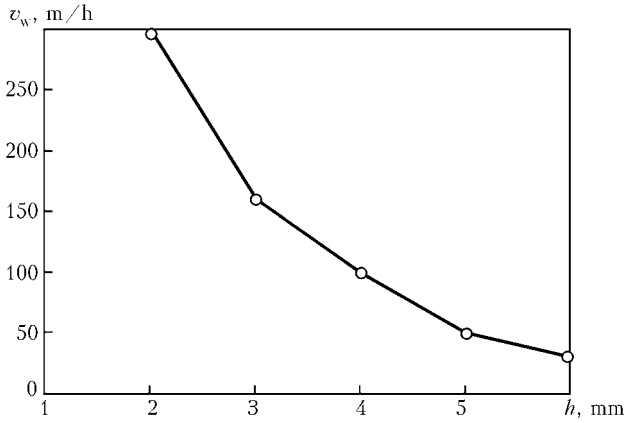

Figure 3. Dependence of speed of hybrid welding of aluminium alloys upon plate thickness (P = 2.8 kW, v_f = 400 m/h, I = 200 A, U = 20 V)

increase of about one third in the heat input allows the total productivity of the multipass welding process to be raised by a factor of four, providing that the hybrid laser-arc process is used instead of the laser one.

Studies were conducted to determine impact toughness of the welds and HAZ using standard U-notched specimens at a temperature of 20 °C. The specimens were cut from central part of laser and hybrid welded joints (three specimens of each type). In addition, two similar specimens of base metal were made and tested to compare results obtained for the welded joints with those for the base metal. Decrease in impact toughness was not in excess of 7–8 % in all the cases, which is a satisfactory indicator of ductility [8]. In a case of laser welding using a filler, the value of impact toughness of the welds exceeds that of the HAZ metal, in contrast to hybrid welding, where the picture is reverse.

For welding volumetric structures, it is important to know the behaviour of the weld pool and changes in the weld quality depending upon the spatial positions in which welding is performed. Therefore, the corresponding experiments were conducted, where laser and laser-arc welding was performed in flat, upper (overhead), uphill and downhill positions. It was found that downhill welding was characterised by an unsatisfactory quality (porosity) and decrease of 40–50 % in the penetration depth, compared with flat

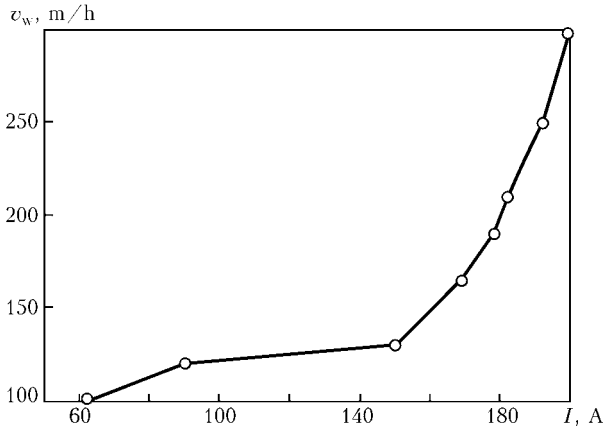

Figure 4. Dependence of speed of hybrid welding of aluminium alloy AMg6 (δ = 2 mm) upon welding current (P = 2.8 kW)

welding. This can be explained by the fact that molten metal from the tailing portion of the weld pool flows down to the keyhole, causing its collapse. In uphill welding, the penetration depth increases by about 20 %, compared with flat welding, while filler metal is often unnecessary in this case. The latter is caused by better conditions for molten metal to outflow from the keyhole to the tailing portion of the weld pool. Overhead welding is almost identical to welding in flat position.

Laser welding of aluminium alloys differs from welding of steels not only because of high thermal conductivity of aluminium. To achieve a stable process of welding aluminium alloys using the laser beam with wavelength λ = 10.6 μm, it is necessary to exceed a certain power threshold, otherwise the laser beam will be fully reflected from the sample surface, which may lead to fracture of the focusing lens, hitting a human by the beam, etc. For materials up to 4 mm thick this threshold is equal to 2 kW. In a case of using lower wavelengths (Nd:YAG laser with λ = 1.06 μm or diode laser with λ = 0.808/0.940 μm), this threshold is much lower. This is related to the dependence of the absorbing ability of the metal surface upon the laser beam wavelength.

Comparative experiment was conducted on welding alloy AMg5 (δ = 3 mm) using CO_2-laser in argon atmosphere. In all the cases the laser beam focused on a sample had a 2 kW power. In laser welding without a filler the process speed was 60 m/h. The use of the 1.2 mm dia. filler wire Sv-AMg6 caused a two times decrease in the welding speed. The hybrid process, where the consumable-electrode arc of the same wire at a welding current of 100 A and arc voltage of 20 V was used in addition to the laser beam, allowed the welding speed to be raised to 120 m/h. The experimental results on hybrid welding of aluminium alloys are shown in Figures 3 and 4. It can be seen from Figure 4 that in a case of hybrid welding of aluminium alloys there is a threshold value of the welding current, which is equal to 150 A for alloy AMg6 (δ = 2 mm). To exceed this threshold, increase of 3 A in the welding current will provide a not more than 1 m/h increase in the welding speed, and then increase of 1 A in the welding current will allow the welding speed to be raised by about 3 m/h. Hybrid welding of alloy AMg6 provided a satisfactory formation of the upper and lower beads of the weld reinforcement at a welding speed of 300 m/h (Figure 5). Residual strains in this case were much lower compared with consumable-electrode welding, and structure of the welds became more fine-grained and equiaxed.

One of the main drawbacks of CO_2-laser welding of aluminium alloys and stainless steels is underutilisation of laser radiation, which is attributable to its partial absorption by argon plasma. To avoid this drawback, the diode laser radiation (λ = = 0.808/0.940 μm) was used as a laser component of the hybrid process. However, the hybrid effect failed

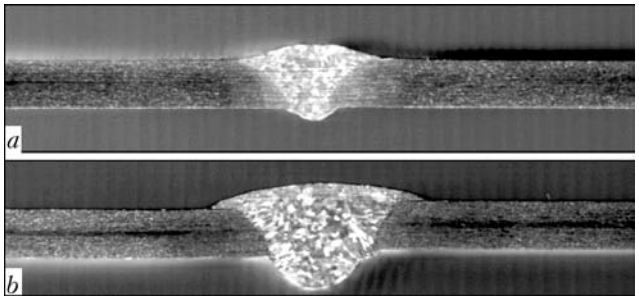

Figure 5. Macrosections of butt joints in AMg6 alloy (δ = 2 mm) made by the hybrid (*a*) and arc (*b*) methods

to show up on stainless steel because of an insufficient power density (focusing spot was 1.0–1.2 mm), in contrast to aluminium alloys (Figures 6 and 7). This can be explained as follows. The more intensive the evaporation of materials welded under the influence of laser radiation, i.e. the more intensive the formation of the laser plasma, which is a current-conducting channel for the arc, the stronger the hybrid effect. And the aluminium alloys contained volatile magnesium.

Investigations were also conducted to study the combined laser-microplasma coating and alloying processes. Companies LERMPS-IPSe and IREPA-Laser developed and patented the PROTAL technology, which provides the surface preparation effect through incomplete overlapping of the plasma spraying zone by the laser heating zone, thus eliminating the need to perform jet-abrasive blasting [9]. Unlike this technology, the coating and alloying processes we offer are close to laser cladding and laser alloying. Here, the presence of laser radiation allows avoidance of preliminary preparation of the sample surface, and the microplasma component makes it possible to eliminate microcracking of the deposited layers, which is characteristic of laser cladding.

Figure 8 shows the flow diagram of the combined process, with which the experiments were conducted, as well as basic parameters of the coating and alloying processes. The most significant of these parameters (linear speed of sample v, mass flow rate of powder G_{powd}, coefficient of overlapping of strips K_o, radiation

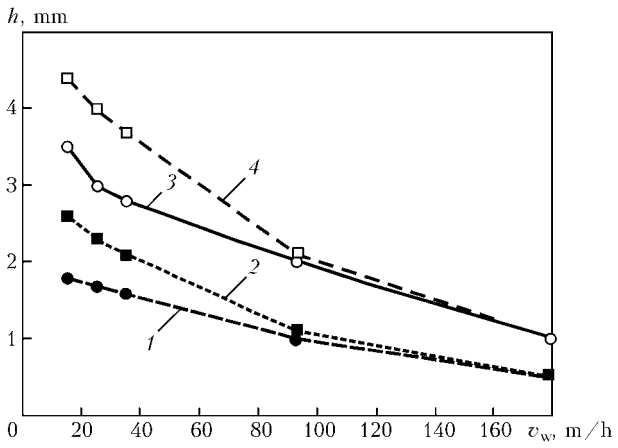

Figure 6. Dependence of the depths of laser (*1*), plasma (*2*) and hybrid (*3*) penetrations of stainless steel plates upon the welding speed at a 2 kW power of diode laser and 2 kW power of argon plasma: *4* — total depth of laser and plasma penetrations

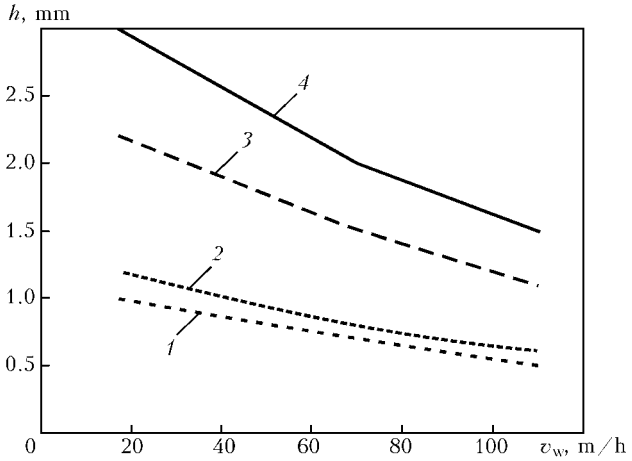

Figure 7. Dependence of the depths of laser (*1*), plasma (*2*) and hybrid (*4*) penetrations of AMg6 plates upon the welding speed at a 1.2 kW power of diode laser and 0.8 kW power of argon plasma: *3* — total depth of laser and plasma penetrations

power density W_p) are indicated in Figure 9. Metallography revealed the presence of a narrow transition zone (3–5 μm) and absence of the HAZ in a case of the coating process, as well as the presence of the HAZ (up to 0.2–0.3 mm) in a case of alloying. In both cases a fall of 20–30 % in hardness compared with hardness of a filler metal takes place in upper layers of the coatings (alloying strips). This is not critical, as size of these layers is comparable with that of finishing allowance. Thickness of the layers deposited in one pass is affected primarily by the mass flow rate of a powder and strip overlapping factor. The sample speed and power density of laser radiation affect to a lesser degree. No impact on the coating thickness by a change in angle between the laser radiation and microplasma jet axes was detected during the experiments.

Another surface modification method is the laser-plasma technology for deposition of thin diamond and diamond-like coatings. Formation of a highly reactive carbon and other radicals in the plasma jet with carbon-containing gases added to it resulted in expansion of efforts on utilisation of arc plasmatrons for depo-

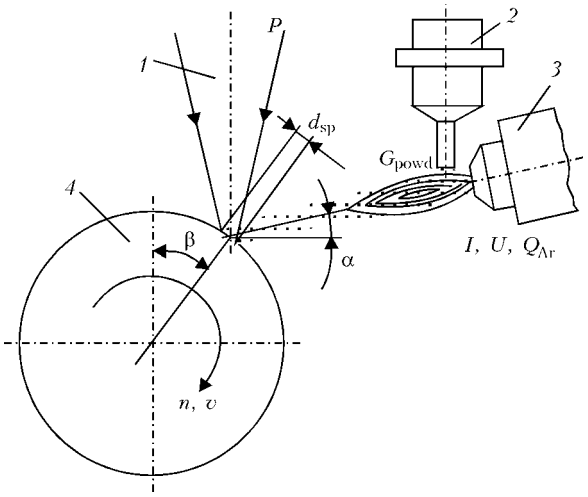

Figure 8. Flow diagram of the laser-microplasma coating and alloying processes: *1* — laser radiation; *2* — powder feeder; *3* — microplasmatron; *4* — sample

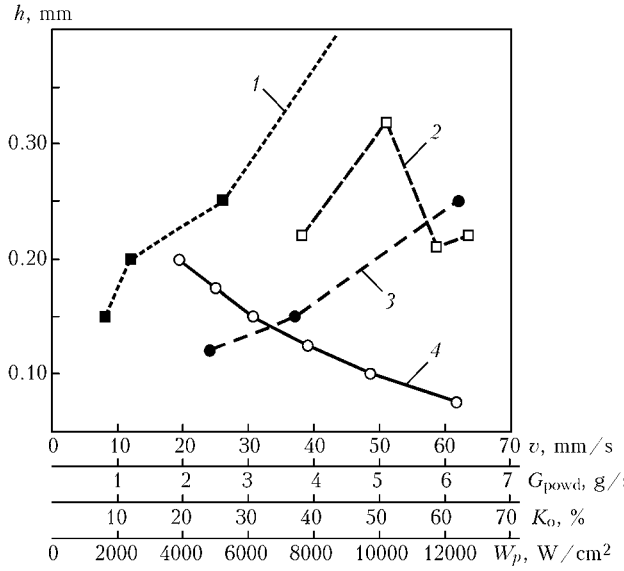

Figure 9. Dependencies of thickness of a deposited layer upon parameters of the combined coating process using powders PG-AN9 and PG-N1 produced under the following conditions: *1* — W_p = = 10.19 kW/cm^2, v = 30.6 mm/s, K_o = 24 %; *2* — v = 30.6 mm/s, G_{powd} = 0.26 g/s, K_o = 62 %; *3* — W_p = 10.19 kW/cm^2, v = = 30.6 mm/s, G_{powd} = 0.26 g/s; *4* — W_p = 10.19 kW/cm^2, G_{powd} = = 0.26 g/s, K_o = 37 %

sition of diamond and diamond-like coatings [10–12]. The possibility of intensification of this process by implementing the laser-plasma technology furthered the experimental work in this area.

The test rig for deposition of diamond coatings by the laser-plasma method consists of the MPN-004 microplasma spraying unit [13], CO_2-laser and chamber with a shielding gas (Ar), where a sample for spraying is placed. The laser beam intersects the arc plasma at an angle of 90°. The combined laser-arc discharge zone [2] is formed at the intersection point (Figure 10), and a gas mixture consisting of 95 % H_2 and 5 % CH_4 is blown into the chamber. Temperature of the substrate on which a coating is deposited ranges from 600 to 800 °C. The experiments proved the feasibility of using this method for production of diamond coatings. Figure 11 shows appearance of a layer consisting of diamond crystals 2–3 μm in size on a silicon plate after treating its surface for 15 min by the combined plasma containing reactive radicals.

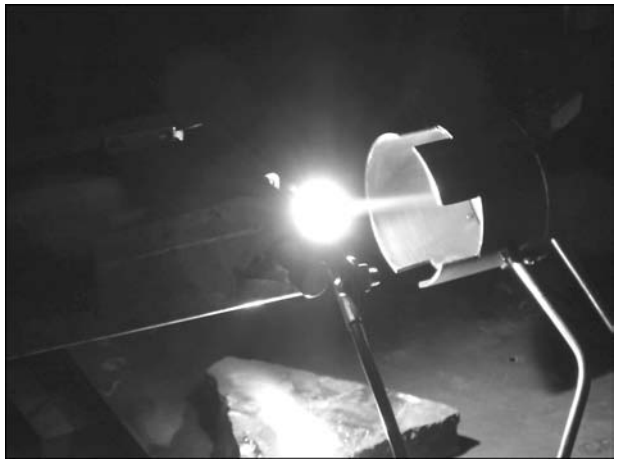

Figure 10. Region of the combined laser-arc discharge in deposition of diamond and diamond-like coatings

Furthermore, this laser-plasma spraying rig was employed for deposition of coatings using powders of self-fluxing nickel alloy PG-10N-01, zirconium oxide and glass-ceramics OK-93. As indicated by analysis of microstructure of the coatings, intensification of the process of heating of spraying particles takes place under these conditions, and the coatings have a denser structure consisting of thinner lamellae (Figure 12).

It can be noted in conclusion that the effect on the surface of the weld pool by electrode metal drops in hybrid welding leads to the resonance phenomena, which may enhance the penetrating power of the laser component. The hybrid effect is directly proportional to growth of power density of the laser component. Laser radiation forms an intensive, narrow and directed flow of metal vapours from the heating spot. This flow leads to contraction and stabilisation of the electric arc, and makes it go down into the keyhole or narrow gap in welding thick-plate steels. Extra heat effect of the electric arc allows a targeted control of the process thermal cycle to produce desirable structures of the weld and HAZ metal. In thermal cycle of the hybrid welding process the steep slope of the leading edge is close to that of the laser process, and flatness of the trailing edge can be adjusted so that no quenching structures are formed in the weld and HAZ metal. At a laser beam power of up to 3–4 kW,

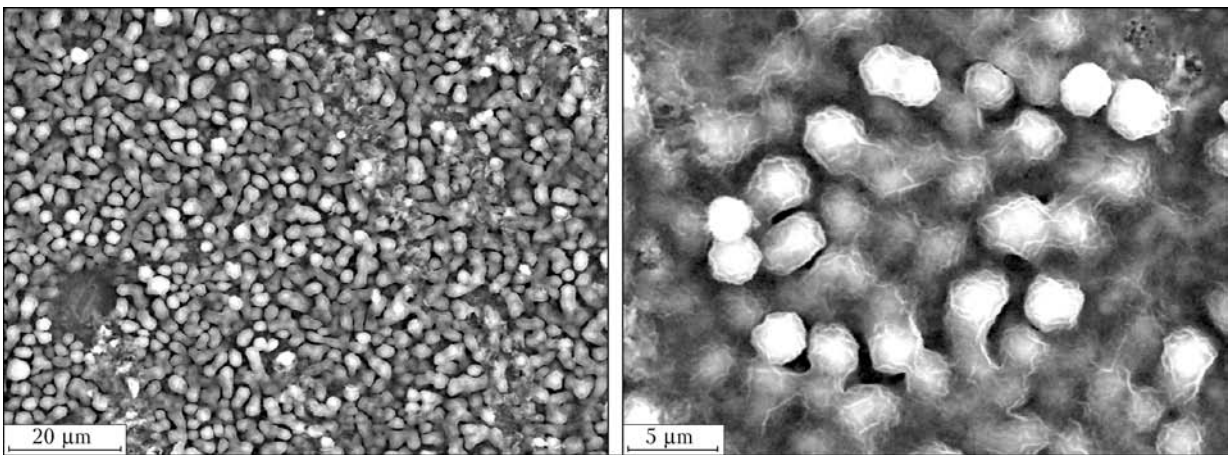

Figure 11. Morphology of the surface of a diamond coating produced by the hybrid laser-plasma method

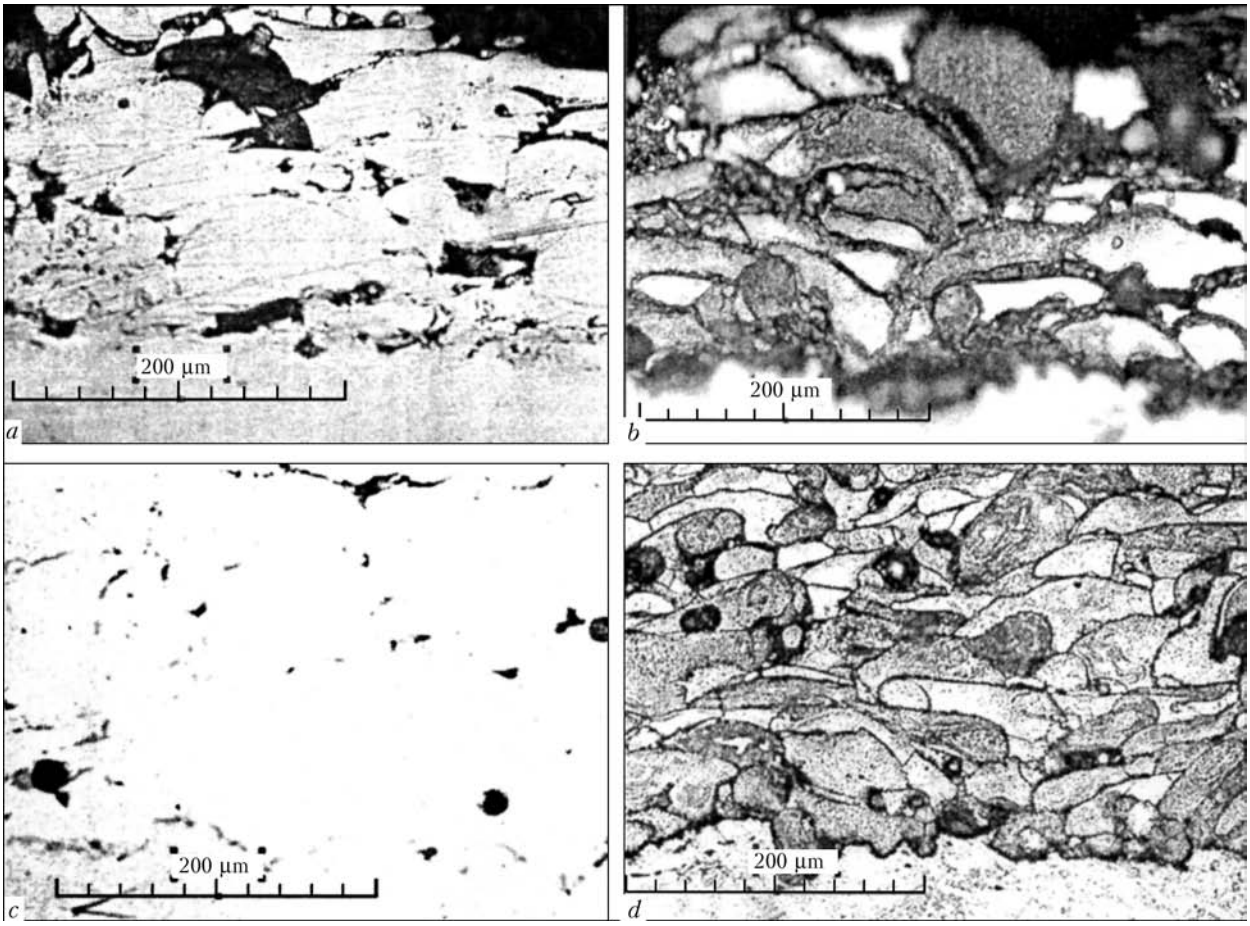

Figure 12. Microstructure of the PG-10N-01 powder coatings produced by the methods of microplasma (*a, b*) and hybrid laser-microplasma spraying (*c, d*) (*a, c* — non-etched; *b, d* — etched)

the use of the hybrid welding process is indicated for steel plates up to 10 mm thick. Above this thickness the penetration depth does not grow, irrespectively of decrease in the welding speed. Thicker metal can be welded by using the multipass laser or hybrid processes with no increase in the laser beam power. Investigation of hybrid welding in different spatial positions proved versatility of this method. The penetration depths in flat and overhead positions were found to be identical. In uphill welding the penetration depth increases by about 20 %, and in downhill welding it decreases by about 40 %, which is accompanied by formation of pores. This is caused by the hydrodynamic processes occurring in the weld pool. The combined processes of laser-microplasma alloying of steels and deposition of thin coatings (50–300 μm) on them allow avoidance of microcracking and necessity of jet-abrasive blasting for surface preparation, as well as decrease of 30–150 μm in finishing allowance.

1. (1974) *Technology of electric fusion welding of metals and alloys*. Ed. by B.E. Paton. Moscow: Mashinostroenie.
2. Seyffarth, P., Krivtsun, I.V. (2002) *Laser-arc processes and their applications in welding and material treatment*. Vol. 1. London: Taylor and Fransis Books.
3. Shelyagin, V.D., Khaskin, V.Yu. (2002) Tendencies in development of laser-arc welding (Review). *The Paton Welding J.*, **6**, 25–28.
4. Shelyagin, V.D., Khaskin, V.Yu., Garashchuk, V.P. et al. (2002) Hybrid CO_2-laser and CO_2 consumable-arc welding. *Ibid.*, **10**, 35–37.
5. Garashchuk, V.P., Shelyagin, V.D., Nazarenko, O.K. et al. (1997) Technological 10 kW CO_2-laser LT 104. *Avtomatich. Svarka*, **1**, 36–39.
6. Gulyaev, A.P. (1963) *Metals science*. Moscow: Oborongiz.
7. Nazarenko, O.K., Kajdalov, A.A., Kovbasenko, S.N. et al. (1987) *Electron beam welding*. Ed. by B.E. Paton. Kiev: Naukova Dumka.
8. Semyonov, S.E., Mandelberg, S.L., Goncharenko, L.V. (1989) The optimal level of impact toughness of gas pipe weld metal. *Avtomatich. Svarka*, **11**, 55–57.
9. Coddet, C., Montaron, G., Marchione, T. et al. (1998) Surface preparation and thermal spray in a single step: the PROTAL process. In: *Proc. of 15th ITSC* (Nice, France). Vol. 2.
10. Li, R., Shi, H., Yan, Z. et al. (1991) Deposition of diamond film by DC arc plasma CVD. In: *Proc. of 2nd Plasma-Technique Symposium* (Lucerne, Switzerland). Vol. 1.
11. Lugscheider, E., Muller, U., Deuerler, F. et al. (1993) Synthesis of crystalline diamond coatings by the DC-plasma jet CVD process. In: *Proc. of ITSC* (Duesseldorf, Germany).
12. Lugscheider, E., Weber, T., Schlump, W. (1991) General study associated with diamond synthesis by vacuum plasma spraying or DC arc plasma vapour deposition. In: *Proc. of ITSC* (Pittsburg, USA).
13. Borisov, Yu.S., Vojnarovich, S.G., Bobrik, V.G. et al. (2000) Microplasma spraying of bioceramic coatings. *Avtomatich. Svarka*, **12**, 63–67.

ELECTRODE MATERIALS FOR MECHANIZED ARC SURFACING

I.A. RYABTSEV
E.O. Paton Electric Welding Institute, NASU, Kiev, Ukraine

The paper describes the welding-technological characteristics of the main groups of surfacing materials for mechanized surfacing processes. The composition, hardness and purpose are given for the most widely used in industry solid and flux-cored wires, flux-cored, cold-rolled and sintered strips developed at the E.O. Paton Electric Welding Institute.

Keywords: *arc surfacing, surfacing materials, flux-cored wires, flux-cored, sintered, cold-rolled strips*

The E.O. Paton Electric Welding Institute has traditionally focused on development of electrode materials for mechanized arc welding processes, namely flux-cored and solid wires, and flux-cored, sintered and cold-rolled strips [1–3]. For the above surfacing processes the Institute has now developed more than 100 grades of Fe-based electrode materials [4] that may be classified by different indices, namely composition, purpose, structure, etc. The most successful is the classification by composition proposed by the International Institute of Welding, according to which the Fe-based surfacing materials can be divided into nine groups (Table 1).

Unalloyed or low-alloyed steels are used to restore shafts, axes, casing parts, etc. Cr–W, Cr–Mo high-temperature steels are applied for surfacing of hot rolling rolls, hot cutting shears, press and stamping tools and other parts, contacting the hot metal in service. W-, W–Mo high-speed steels are designed for surfacing metal-cutting tools. Low-carbon chromium stainless steels are recommended for restoration and strengthening of rolls for continuous casting machines, hydraulic press plungers and other parts, operating with metal–metal friction. Chromium steels with higher content of carbon alloyed with tungsten, vanadium, molybdenum and other elements have a high resistance to abrasive wear. High-manganese austenitic steels are recommended for surfacing parts, subjected to abrasive wear in combination with strong impacts, and are used for reconditioning the railway frogs, parts of crushing-milling equipment, as well as repairing defects of G13L steel castings. Depending on alloying, Cr–Ni and Cr–Mn stainless austenitic steels have a high resistance in different corroding

Table 1. Classification, composition and hardness of Fe-based deposited metal

Group No.	*Deposited metal type*	*Weight fraction of elements, %*									*Hardness* HRC_e
		C	*Mn*	*Si*	*Cr*	*Ni*	*W*	*V*	*Mo*	*Other*	
I	Unalloyed and low-alloyed steels with ≤ 0.4 % C	≤ 0.4	0.5–3.0	≤ 1.0	≤ 5.0	≤ 3.0	–	–	≤ 1.0	–	20–45
II	Unalloyed and low-alloyed steels with ≥ 0.4 % C	≥ 0.4	0.5–3.0	≤ 1.0	≤ 5.0	≤ 3.0	–	–	≤ 1.0	–	52–60
III	Cr–W, Cr–Mo and other high-temperature steels	0.2–0.5	≤ 2.0	≤ 1.0	1–5	≤ 5.0	1–10	0.2–1–5	≤ 4.0	–	52–60
IV	W-, W–Mo and other high-speed steels	0.6–1.5	≤ 0.5	≤ 0.4	4–6	–	1.5–18.0	≤ 3.0	≤ 10	≤ 15Co	52–60
V	Low-carbon chromium steels	≤ 0.3	≤ 0.8	≤ 2.0	12–30	≤ 5.0	–	–	≤ 2.0	–	35–50
VI	Chromium steels with higher carbon	0.3–2.0	0.3–1.5	≤ 3.0	5–18	≤ 5.0	≤ 1.5	–	≤ 2.0	≤ 5Ti	50–60
VII	High-manganese austenitic steels	0.5–1.2	11–18	≤ 4.0	≤ 5.0	≤ 4.0	–	–	≤ 1.0	–	25–35
VIII	Cr–Ni, Cr–Ni–Mn steels	≤ 0.3	1–8	≤ 5.0	12–20	8–25	–	–	≤ 5.0	≤ 1.5Nb ≤ 1Ti	18–25
IX	High-chromium special cast irons	2–5	0.5–8.0	≤ 5.0	18–35	≤ 4.0	≤ 5.0	≤ 10	≤ 8.0	≤ 8Nb ≤ 4Ti ≤ 3B ≤ 5Co	55–65

Table 2. Solid steel surfacing wires

Wire grade	Group No.	Weight fraction of elements, %					Hardness	Typical surfaced items
		C	Mn	Si	Cr	Other		
Np-35	I	0.32–0.40	0.5–0.8	0.2–0.4	≤ 0.25	–	*HB* 160–220	Axles, shafts
Np-45	I	0.42–0.50	0.5–0.8	0.2–0.4	≤ 0.25	–	*HB* 160–220	Same
Np-65G	I	0.6–0.7	0.7–1.0	0.2–0.4	≤ 0.3	–	*HB* 230–310	Crane wheels, support rollers
Np-30KhGSA	I	0.27–0.35	0.8–1.1	0.9–1.2	0.8–1.1	–	*HB* 220–300	Crane wheels, cogging rolls
Np-30Kh5	I	0.27–0.35	0.4–0.7	0.2–0.5	4.0–6.0	–	*HRC* 37–42	Section mill rolls
Np-40Kh2G2M	II	0.35–0.45	1.8–2.3	0.4–0.7	1.8–2.3	0.8–1.2 Mo	*HRC* 54–56	Crank shafts
Np-5KhNM	II	0.5–0.6	0.5–0.8	0.4–0.7	1.8–2.3	0.15–0.30 Mo	*HRC* 40–50	Hot stamping dies
Np-50Kh6FMS	III	0.45–0.55	0.3–0.6	0.8–1.2	1.8–2.3	0.35–0.55 V 1.2–1.6 Mo	*HRC* 42–48	Stamps, rolling mill rolls
Hp-30Kh13	V	0.25–0.35	≤ 0.8	≤ 0.8	12.0–14.0	–	*HRC* 32–38	Hydraulic press plungers
Np-40Kh13	VI	0.35–0.45	≤ 0.8	≤ 0.8	12.0–14.0	–	*HRC* 42–52	Different cutters, dies
Np-45Kh4V3F	III	0.4–0.5	0.8–1.2	0.7–1.0	3.6–4.6	0.1–0.2 W 0.3–0.5 V	*HRC* 38–45	Dies, rolling mill rolls
Np-65Kh3V10F	III	0.55–0.65	1.3–1.8	0.4–0.7	2.6–3.6	9.0–0.5 W 0.3–0.5 V	*HRC* 42–50	Rolling mill rolls

media. Materials of the type of high-chromium cast irons are recommended for surfacing parts operating under the conditions of abrasive, hydro- and gas-abrasive wear with impacts of different intensity.

Several specific compositions of surfacing materials in the form of stick electrodes, solid and flux-cored wires, cold-rolled, flux-cored and sintered strips can correspond to each type of deposited metal.

Solid wires. The standards and specifications envisage manufacture of solid steel surfacing wire of 0.3–6.0 mm diameter (2.0–4.0 mm diameter wires are mostly used), as well as rods of 6.5 and 8.0 mm diameter. In addition, solid steel welding wire is used for surfacing. Composition, hardness of the deposited metal and purpose of the most widely used solid surfacing and welding wires designed for submerged-arc or gas-shielded surfacing, are given in Tables 2 and 3.

Flux-cored wires The task of providing high-alloyed electrode materials for mechanized surfacing processes is rather easily solved by using flux-cored wire, which consists of a sheath of a soft strip (steel, nickel, etc.), and a core of alloying component powders (ferroalloys, pure metals, carbides, borides, etc.). Also added to the flux-cored wire core are gas- and slag-forming substances, deoxidizers and elements having a high chemical affinity to nitrogen. In this case, surfacing can be performed without flux or shielding gases, and such wire is called self-shielding. In industry flux-cored wires are applied for submerged-arc, gas-shielded and open-arc surfacing. Compared to solid wires, flux-cored wires provide a higher surfacing efficiency and greater possibilities for deposited metal surfacing.

Coefficient of filling (ratio of filling-powder weight to wire weight expressed in percent) of the surfacing flux-cored wire usually is not higher than 45 %, that to a certain extent limiting the possibilities of producing some types of highly alloyed deposited metal, using these consumables. Submerged-arc surfacing is most often performed using flux-cored wire of 3.6 mm (5.0 to 6.0 mm diameter for large-sized parts), and open-arc surfacing with wire of 1.6–3.0 mm diameter.

Drawing or rolling methods are used in flux-cored wire manufacture. The first method envisages drawing of the initial tube rolled up in the profile-iron bending machine fitted with charge metering device. In production mills for flux-cored wire manufacture drawing is performed in multistand drawing mills, mounted in one line with the profile-iron bending machine. Draw-

Table 3. Solid steel welding wires for surfacing

Wire grade	Group No.	Weight fraction of elements, %					Hardness	Typical surfaced items
		C	Mn	Si	Cr	Other		
Sv-08	I	≤ 0.1	0.35–0.60	≤ 0.03	≤ 0.15	–	*HB* 120–160	Axles, shafts
Sv-10G2	I	≤ 0.12	1.5–1.9	≤ 0.03	≤ 0.2	–	*HB* 180–210	Same
Sv-08GS	I	≤ 0.1	1.4–1.7	0.60–0.85	≤ 0.2	–	*HB* 180–200	»
Sv-12GS	I	≤ 0.14	0.8–1.1	0.6–0.9	≤ 0.2	–	*HB* 190–220	»
Sv-08G2S	I	0.05–0.11	1.8–2.1	0.70–0.95	≤ 0.2	–	*HB* 180–210	»
Sv-18KhGS	I	0.15–0.22	0.8–1.1	0.9–1.2	0.8–1.1	–	*HB* 240–300	»
Sv-20Kh13	V	0.16–0.24	≤ 0.3	≤ 0.3	12–14	–	*HRC* 42–48	Rolls for CCM, plungers
Sv-10Kh17T	V	≤ 0.12	≤ 0.8	≤ 0.7	16–18	0.2–0.5 Ti	*HRC* 30–38	Stop valves

Table 4. Flux-cored surfacing wires

Wire grade	Group No.	Element weight fraction in the deposited metal, %						Hardness	Typical surfaced items
		C	Mn	Si	Cr	Mo	Other		
PP-Np-14GST	I	0.14	0.5	0.6	–	–	0.4 Ti	*HB* 240–260	Axles, shafts
PP-AN198	I	0.15	0.5	0.5	0.4	–	0.3 Al 0.3 Ti	*HB* 220–310	Axles, shafts, crane wheels
PP-Np-18KhG1M	I	0.18	1.4	0.8	1.4	0.4	–	*HB* 320–380	Same
PP-Np-30Kh2N2G	I	0.30	1.5	0.6	1.8	–	1.4 Ni	*HRC* 42–48	Axles, shafts, crankshafts
PP-Np-15Kh4GSMF	I	0.15	1.1	0.9	3.7	1.1	0.4 V	*HRC* 42–48	Same
PP-Np-12Kh14N3	V	0.12	0.6	0.8	14.0	–	3.0 Ni	*HRC* 38–48	Hydraulic press plungers
PP-AN159	V	0.15	0.6	0.8	13.0	–	–	*HRC* 38–48	Rollers of roller conveyor, CCM
PP-AN174	V	0.12	0.8	0.6	13.0	0.8	1.6 Ni 0.2 V	*HRC* 38–48	Same
PP-Np-25Kh5FMS	III	0.25	0.6	1.0	5.0	1.1	0.4 V	*HRC* 48–52	Rolling rolls, dies
PP-Np-35V9Kh3SF	III	0.35	0.9	0.8	3.0	–	9.0 W 0.3 V	*HRC* 48–52	Same
PP-AN105	VII	0.80	13.0	0.4	–	–	3.0 Ni	*HB* 160–240	Railway frogs, G13L casting
PP-AN192	VI	1.50	0.4	0.4	5.0	–	3.5 Ti	*HRC* 50–56	Agricultural machinery tools

ing allows producing wire of the necessary diameter and compacting the core charge. Flux-cored wire is also manufactured by the method of rolling seamless tubes filled with charge. Initial tube filling with the charge is performed in special vibrating benches. Rolling method allows producing small-diameter flux-cored wire. More over, in this case there is no need for application of any special soapy drawing lubricants.

The first flux-cored surfacing wires were developed at the E.O. Paton Electric Welding Institute at the start of 1950s [5]. Table 4 gives the compositions and purpose of the most widely used flux-cored wires.

Cold-rolled, flux-cored and sintered strips. Electrode strip surfacing has several advantages over electrode wire surfacing, the main of which are high efficiency of the process, small depth of base metal penetration, and large width of the deposited bead. Shallow penetration in strip surfacing is attributable to relatively low arc pressure on the pool surface due to a low average density of current. In submerged-arc surfacing with a thin strip a stable process is ensured at current density of 10–15 A/mm^2, this being much less than in wire surfacing. On the other hand, strip surfacing has one essential drawback, namely this process cannot be used in surfacing small-sized parts or parts of a complex surface.

Cold-rolled steel strip used for submerged-arc surfacing is made of standard steels, namely structural, tool and spring (Table 5). The thickness of strip used for surfacing usually is 0.4 to 1.0 mm with 20 to 80 mm width. At large width of the strip measures should be taken to compensate for the adverse effect of the magnetic blow of the arc on deposited metal formation.

As the cold-rolled strips can only be made of ductile deformable alloys with comparatively low content of carbon, they not fully meet the diverse requirements made of surfacing. Flux-cored and sintered strips open up wide possibilities in this respect.

Flux-cored strips (Table 6) are made in special mills fitted with metering devices and rollers for their forming, roll forming of the sheath strip and charge compacting in the formed flux-cored strip [2, 6]. Flux-cored strip manufacture does not involve any drawing process. Flux-cored surfacing strips have the thickness of 3 to 4 mm and width of 14 to 30 mm. Coefficient of flux-cored strip filling is up to 70 %, i.e. they can yield deposited metal with a higher degree of alloying than in flux-cored wire surfacing. A feature of most

Table 5. Cold-rolled steel strips for submerged-arc surfacing

Wire grade	Group No.	Weight fraction of elements, %						Typical surfaced items
		C	Mn	Si	Cr	Ni	Other	
50G	I	0.45–0.56	0.7–1.0	0.17–0.37	0.3	0.3	–	Rollers, axles, shafts
25KhFMS	III	0.2–0.3	0.5–1.0	0.6–1.2	4.8–5.7	–	0.2–0.6 V	Rolling rolls, roller conveyor rollers
Sv-2Kh13	V	0.16–0.25	0.8	0.8	12.0–14.0	–	–	Hydraulic press plungers
Sv-04Kh19N11M3	VIII	0.06	1.0–2.8	0.06	18.0–20.0	10.0–12.0	2.0–3.0 Mo	Reactor casing parts, petrochemical equipment
Sv-03Kh22N11B	VIII	0.03	1.5–2.0	0.2–0.4	21.7–23.5	10.3–11.3	0.95–1.20 Nb	Same
Sv-07Kh25N13	VIII	0.09	1.0–2.0	0.5–1.0	23.0–26.0	12.0–14.0	–	»

Table 6. Flux-cored surfacing strips

Strip grade	Group No.	Element weight fraction in the deposited metal, %					Hardness HRC	Typical surfaced items
		C	Mn	Si	Cr	Other		
PL-Np-10G2ST	I	0.1	2.0	1.0	–	0.2Ti	20–26	Axles, shafts
PL-Np-20Kh2G2ST	I	0.2	2.0	1.0	2	0.4Mo 0.7Ti	38–45	Axles, shafts, rollers
PL-Np-300Kh25S3N2G2	IX	3.0	2.0	3.0	25	2Ni	50–56	Beaters, excavator bucket teeth
PL-Np-400Kh38G3RSTYu	IX	3.0	3.0	1.0	38	0.2Al 0.9B 0.3Ti	50–54	Same
PL-Np-120Kh22R3G2S	VI	1.2	2.0	1.0	22	3B 1Ti	54–60	»
PL-Np-450Kh20B7M6V2	IX	4.5	–	2.0	20	2W 7Nb 6Mo	55–62	»
PL-Np-500Kh40N40S2R	IX	5.0	1.0	2.0	40	40Ni 0.2B	50–56	Blast furnace cones
PL-Np-550Kh44N34GSR	IX	5.5	0.8	0.8	44	34Ni 0.3B	54–62	Same
PL-Np-12Kh16N8M6C5G4B	VIII	0.12	4.0	5.0	16	8Ni 6Mo 1Nb	38–50	Power generation, petrochemical fittings
PL-Np-12Kh18N9S5G2T	VIII	0.12	2.0	5.0	18	9Ni 0.2Ti	27–34	Same

Table 7. Sintered electrode strips

Strip grade	Group No.	Element weight fraction in the deposited metal, %						Hardness HRC	Typical surfaced items
		C	Mn	Si	Cr	Mo	Other		
LS-18KhGSA	I	0.3	0.7	0.9	1.4	–	–	24–32	Axles, shafts
LS-70Kh3MN	II	1.0	0.4	0.7	4.5	0.9	1Ni	54–60	Parts of car chassi
LS-25Kh5FMS	III	0.4	0.4	0.7	6.2	1.5	0.8V	38–44	Rolling rolls
LS-50Kh4V3FS	III	0.7	0.4	0.5	5.0	1.5	0.7V 4W	42–46	Same
LS-15Kh13	V	0.2	0.5	0.5	16.5	–	–	38–42	Rollers for CCM
LS-12Kh14N3	V	0.2	1.1	0.5	16.0	–	3.5Ni	38–42	Same
LS-02Kh20N11G	VIII	0.02	2.0	0.4	20.0	–	11Ni	–	Petrochemical equipment

of the flux-cored strips is their versatility — they are designed both for submerged- and open-arc surfacing.

Sintered strips (Table 7). Technologies of manufacturing and application of sintered (metal-ceramic) strips as electrode materials for submerged-arc surfacing were developed at the E.O. Paton Electric Welding Institute and I.N. Frantsevich Institute for Materials Science Problems of the NAS of Ukraine [3, 7]. Fe-base sintered strips are made by powder metallurgy method by cold rolling and subsequent sintering in a protective atmosphere at the temperature of 1200–1300 °C of a mixture of metal powders, ferroalloys, graphite and other materials with particle sizes of 70 to 200 μm. Sintered strip of 1 mm thickness and 30 to 100 mm width is produced.

Due to its porosity the sintered strip has a higher electric resistance, which leads to a more intensive heating of the electrode stick-out during surfacing, thus providing a 20 to 30 % higher surfacing efficiency, compared to the cold-rolled strip of a similar cross-section and composition. A uniform distribution of the charge components across the sintered strip section promotes producing a more uniform deposited metal as to composition than when using a flux-cored strip, and this, in its turn, leads to its higher performance. Another advantage of the sintered strip is the ability to make it of super pure powders and to produce a high-quality deposited metal, respectively.

Thus, the developed materials for mechanized arc surfacing allow solving the problems of reconditioning and strengthening various parts exposed to different types of wear, ensuring a high quality and efficiency.

1. Ryabtsev, I.A. (2004) *Surfacing of machinery parts and mechanisms*. Kiev: Ekotekhnologiya.
2. Yuzvenko, Yu.A. (1970) Flux-cored strip. *Avtomatich. Svarka*, **2**, 23–26.
3. Oparin, L.I., Frumin, I.I., Otrok, A.I. (1968) Mechanized metal-ceramic strip surfacing of tool steel layer. *Ibid*., **12**, 58–61.
4. (1979) *Surfacing consumables of SMEA countries-members* Catalogue. Ed. by I.I. Frumin, V.B. Eremeev. Kiev-Moscow: VINITI.
5. Frumin, I.I. (1961) *Automatic electric arc surfacing* Kharkov: Metallurgizdat.
6. Yuzvenko, Yu.A. (1976) *Surfacing*. Kiev: Naukova Dumka.
7. Oparin, L.I. (1981) Some results and prospects of application of surfacing with sintered electrode strips. *Ibid*., **8**, 61–64.

NOVELTIES IN EXPLOSION CUTTING OF METALWORK

V.G. PETUSHKOV, L.D. DOBRUSHIN, L.A. VOLGIN, S.Yu. ILLARIONOV and **P.S. SHLENSKY**
E.O. Paton Electric Welding Institute, NASU, Kiev, Ukraine

New designs of extended cumulative charges resistant to electrochemical corrosion and with high cutting ability applicable for ground and underwater operations are developed. Efficiency of a number of shielding media providing suppression of a harmful side effect of the explosion is experimentally studied. Application of EC technology under water is presented.

Keywords: *explosion cutting, explosive, shock wave, extended cumulative charge, protection screen*

Explosion cutting (EC) finds extensive application in the industry due to its unique possibilities. Theoretical views on the cumulation both for a classical case of axial symmetry and for the plane one have been further developed [1]. Specialists of the E.O. Paton Electric Welding Institute created equipment and technology for production of a wide range of special explosive charges for extended cumulative charges (ECC) to carry out the process in different conditions including under water [2]. Alongside, the EC technologies require improvement of ECC structures for increasing of their efficiency, expanding of their applications and solving a number of ecological problems.

New ECC structures. ECC developed at the E.O. Paton Electric Welding Institute is a shaped copper tube filled with explosive (hexogen). A scheme of such charge with a half-cylindrical cumulative recess is presented in Figure 1, *a*, while structural parameters of the ECC are given in Table 1. Optimal efficiency of EC is provided under the following correlations of parameters:

$$d_{CR} = (0.42–0.44)D, \quad \delta_{CR} = (0.06–0.07)D, \quad \delta_1 \cong 0.1D,$$

where D, δ_1 is the diameter and thickness of shell of cumulative charge, respectively; δ_{CR}, d_{CR} is the thickness of the lining and diameter of the cumulative recess cylinder.

Hexogen density is about 1.7 g/cm^3, mass of hexogen sample per unit of the charge length is $\omega = 1.35[D - 2\delta_1)^2 - d_{CR}^2]$ (for example, for ECC 10 ω = 60 g/m). The experience has shown that ECC with half-cylindrical recess is distinguished with an increased consumption of explosive in cutting steel barriers. Correlations of the ECC structural parameters are optimized by experimental developments when correlations of structural elements under which a

Table 1. Structural parameters, their correlation and efficiency of the ECC action

ECC code (by D)	*Initial round billet d × δ₁, mm*	*Cumulative recess, mm*		*Height of charge h, mm*	$\frac{d_{CR}}{D}$	$\frac{\delta_{CR}}{D}$	*Mass of hexogen sample per length of charge ω, g/m*	*Depth of steel cutting l_{cut}, mm*	$\frac{d_{CR}}{\delta_{CR}}$
		d_{CR}	δ_{CR}						
Standard (half-cylindrical) ECC									
ECC 3	5.0 × 0.5	1.30	0.18	2.4	0.44	0.06	6	3.0	–
ECC 4	6.0 × 0.5	1.75	0.24	3.2	0.44	0.06	11	4.0	–
ECC 6	9.0 × 1.0	2.70	0.36	4.7	0.45	0.06	20	6.0	–
ECC 10	15.0 × 1.5	4.40	0.60	8.0	0.44	0.06	60	10.0	–
ECC 14.5	22.0 × 2.0	6.30	0.87	11.5	0.44	0.06	165	14.5	–
ECC 19	30.0 × 3.0	8.30	1.15	15.0	0.44	0.06	210	19.0	–
Sickle-shaped ECC									
ECC 4	6.0 × 0.5	2.50	0.20	3.2	0.63	0.050	6	4.0	12.5
ECC 8	12.0 × 0.5	5.00	0.40	6.6	0.63	0.050	20	8.0	12.5
ECC 10	15.0 × 1.0	6.30	0.50	8.0	0.63	0.050	33	10.0	12.5
ECC 16	24.0 × 1.5	10.00	0.80	13.0	0.63	0.050	100	16.0	12.5
ECC 25	38.0 × 2.0	15.50	1.10	20.0	0.63	0.044	200	25.0	14.0
ECC 30	52.0 × 3.0	18.50	1.20	24.0	0.63	0.040	400	30.0	15.0

Note. $l_{cut}/D = 0.8$; $h/D = 0.8$.

Table 2. Efficiency indices of optimal AECC using the barriers of aluminium alloy AMg6

No. of test	*D, mm*	ω, *g/m*	l_{cut}/ω
1	3.0	3.21	1.25
2	3.5	4.45	1.01
3	4.0	4.64	1.19
4	4.5	5.15	1.17
5	5.0	6.49	1.16
6	7.0	18.90	0.61
7	9.0	30.10	0.47
8	10.0	35.00	0.46

specified mass of the explosive produced the maximal cumulative effect were determined. A form of a cross-section of the ECC developed by these elaborations resembles a sickle. An additional correlation $d_{CR}\delta_{CR}^{-1}$ is introduced for sickle-shaped ECC (Figure 1, *b*). A dependence determining a maximal cutting ability of the charge has a form $\delta_{CR} \cong 1.55$ arc sin $0.033 d_{CR}$ (at $d_{CR} \le 30$ mm, $d_{CR}D^{-1} \cong 0.60$–0.65).

Copper shell of ECC finds a wider application due to high ductility and deformability of copper and also due to its high density. As a result, such systems have high efficiency and reasonable price. However, these charges have one essential disadvantage: they cannot be installed in corrosive media on structures of aluminum alloys for a long operational period since a galvanic couple, which causes metal corrosion, is formed between the charge and the aluminium barrier. A series of the ECC in aluminium shell named AECC were developed to remove the galvanic couple.

If cumulative jet and barrier have different density, then the depth of punching is determined by the formula $L = l(\rho_1\rho_2^{-1})^{0.5}$, where ρ_1 and ρ_2 are the densities of the metal jet and the barrier, respectively; l is the length of the jet. This dependence is true if the pressure under collision of the jet with the barrier exceeds ~20 GPa [3]. It is evident that with similar structural parameters the ECC in copper shell has a higher efficiency than the charges in the aluminium one because density of copper 3 times higher than the density of aluminium. Therefore, the development of aluminium ECC with optimal parameters was underlain by the technology for production of a sickle-shaped ECC

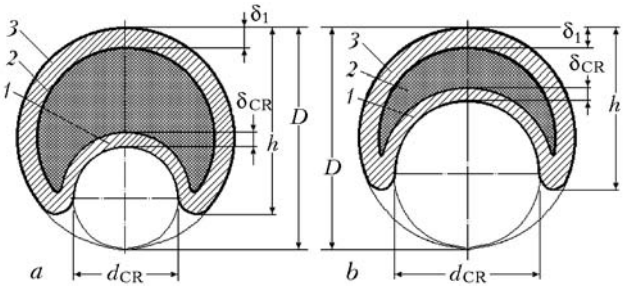

Figure 1. Structural parameters of ECC with half-cylindrical (*a*) and sickle-shaped (*b*) cumulative recess: *1* — shell of the cumulative recess; *2* — high explosive; *3* — shell of the charge (h — heigh of cumulative charge)

whose efficiency is by 50 % higher than that of the standard charges (Table 2, No.3).

By changing a shape and parameters of the cumulative charge (charge diameter and cumulative recess, thickness of its lining and a layer of explosive) it becomes possible to receive a shape with which the efficiency of the AECC action approaches the efficiency of the standard ECC in a copper shell. For example, ECC 6 in the copper shell of the standard shape with explosive sample 20.0 g/m provides a 12 mm depth of cut by alloy AMg6 and ECC 7 in aluminium shell with explosive sample 18.9 g/m — 11.5 mm. Data on the elaborations of AECC are given in Table 3 (Nos. 4–7).

The main parameters of AECC from Tables 2 and 3 optimized empirically assume the following values: $d_{CR}D^{-1} = 0.60$–0.64; $\delta_{CR}D^{-1} = 0.033$–$0.042$. It is note worthy that an optimal value of the correlation of cumulative recess thickness to the diameter is essentially smaller for aluminium charges than for copper ones ($\delta_{CR}D^{-1} \cong 0.06$).

The accelerated corrosion tests of charges were carried out on the AECC 5 (Table 2, No.5) located on the screens of titanium alloy VT-14 with a barrier of AMg6. Tests were performed in the chamber salt-spray by spraying 3 % solution of sodium chloride at the temperature 45 °C during 240 days, which corresponds to 7 years of operation. No signs of corrosion in AECC were observed during tests.

Let us consider the main peculiarities in the design of the underwater charges with steel cumulative recess and possibilities of their practical application. Technology of the layer-by-layer underwater EC of multilayer pipe bases marine stationary platforms (MSP) by underwater ECC in the foam plastic shell provides

Table 3. Results of elaboration of optimal geometry of AECC 4 mm in diameter

No. of test	δ_{CR}, *mm*	ω, *g/m*	l_{cut}, *mm*	*D, mm*	*Materials of charge shell*	l_{cut}/ω
1	1.75	0.24	11.0	8.0	Copper	0.72 (standard)
2	1.75	0.18	8.20	5.2	Aluminium	0.63 (standard)
3	2.50	0.20	6.00	7.5	Copper	1.25 (sickle-shaped)
4	2.40	0.16	4.67	5.0	Aluminium	1.07 (sickle-shaped)
5	2.50	0.14	4.64	5.0	Same	1.19 (sickle-shaped)
6	2.50	0.13	3.96	4.5	»	1.14 (sickle-shaped)
7	2.50	0.12	4.77	5.2	»	1.10 (sickle-shaped)

Table 4. Dependence of cut depth on angle at the vertex of cumulative recess

α, deg	Cut depth, mm	Explosive mass, kg/m
80	50–58	6.3
70	63–64	5.7
60	63–64	5.0
50	36–44	4.3

the use of specifically ECC in the copper shell 19–41 mm in diameter with explosive mass 200–750 g/r. m. In this case a thickness of the pipe–cement barriers to be cut is 10–60 mm. When using underwater charges in the foam plastic shell for cutting pipe bases of the platform the depth should not exceed 50 m since its increase leads to compression of the shell, thus resulting in a sharp decrease of the efficiency of the underwater charge.

The MSP base at the level of the sea bottom consists, as a rule, of five pipes 426, 377, 325, 273 and 219 mm in diameter, so the diver when assembling underwater charges has to descent up to nine times for layer-by-layer separation of one base of the platform. Hence there was need to develop such design of the underwater charge that allows cutting five-layer pipe base by one explosion, i.e. it was necessary to cut the pipe–cement–pipe barrier up to 112 mm thick.

It is established that a maximal diameter of ECC in the copper shell cannot exceed 40–41 mm because when it increases it is impossible to bend ECC by radius equal to half of the diameter of the pipe platform base because of deformation of the copper shell of the charge. Therefore, large-size ECC with steel cumulative recess and a shell was created allowing separation of pipe barriers up to 122 m thick and even

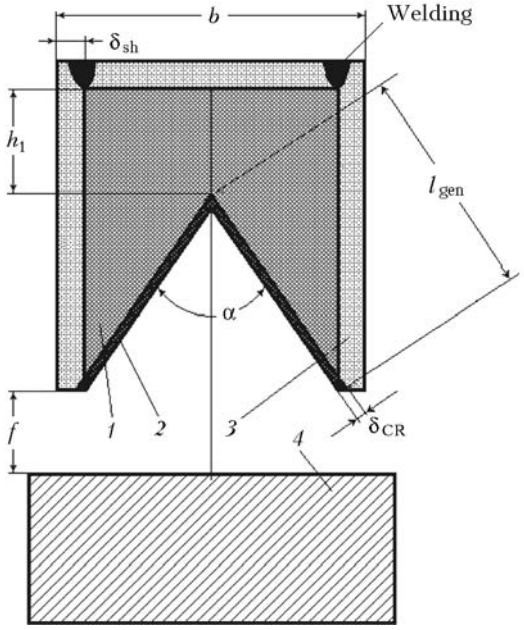

Figure 2. Diagram of large-size ECC in a steel shell: *1* — explosive (TH 35/65); *2* — lining of cumulative recess; *3* — external shell of ECC; *4* — barrier (δ_{sh} — thickness of shell wall; *b* — width of charge)

Table 5. Dependence of depth of the ECC cut on length of generatrix and thickness of shell of cumulative recess

Thickness of lining, mm	Length of generatrix, mm	Depth of cut, mm
2.0	50	60–65
	70	90–100
	100	110
2.5	50	70–75
3.5	50	80–85
5.0	50	100

thicker by one explosion. Experiments were carried out to determine the efficiency of cutting of steel barriers up to 120 mm thick depending on the angle α at the vertex of the cumulative recess, thickness of the cumulative recess lining δ_{CR}, length of the cumulative recess generatrix l_{gen} and a focal distance f between the cumulative charge and the barrier (Figure 2). The experiments were carried out on the straight-line segments of the lining of cumulative recess with explosive up to 200 mm long without external metallic shell of the charge. A mixture of TNT with not-retarded hexogen in proportion 1:2 was used as explosive. Lining of cumulative recess and shell of the charge was made of St3 steel plates. The results of these studies (geometrical parameters of the charges: $\alpha = 50–70°$, $\delta_{CR} = 2.5–5.0$ mm, $f = 70$ mm, $h_1 = 40$ mm) are presented in Tables 4 and 5.

Analysis of the given data supports a conclusion that optimal angles in the vertex of the cumulative recess are $\alpha = 70$ and 60° (charge with $\alpha = 70°$ is more effective since length of the initial section of the cut of the steel plate in the site where the explosive charge is initiated and where the maximal effect of the cumulative jet is achieved is about 2 times smaller) while thickness and length of the cumulative recess lining are 3.5 and 70 mm, respectively. It is established that optimal focal distance in EC of steel barriers is equal to the length of cumulative recess generatrix ($f \cong l_{gen}$). The use of steel shell in the cumulative charge allows increasing the depth of the cut by 15–25 mm.

Design and technology for production of underwater ECC in a steel shell with inner diameter 426 mm (Figure 3) were developed. It is appropriate to produce this charge from separated elements joint by welding. Thickness of the wall of the shell protecting the area of cumulative jet formation from water may be different depending on the depth of the MSP location. In this case the ECC protection shell 1.5 mm thick is able to stand the water pressure up to 3 MPa without losing the leak-proofness [4]. To make assembling on the pipe base of the platform easier the underwater charge is produced in the form of two half-rings joint by the diver in the water.

Experiments on cutting pipe base 3 m long consisting of five pipes 426, 377, 325, 273 and 219 mm in diameter with cement layer in the space between pipes were conducted at a depth of 2 m. The main

characteristics of the ECC: $\alpha = 70^{\circ}$, $\delta_{CR} = 3.5$ mm, $h_1 = 70$ mm; mass of explosive (alloy of TNT with hexogen in proportion 1:2) per the unit of the charge length was 1.2 kg/m. It was established that explosion of the underwater charge caused separation of the five-layer pipe base, a distinct cut by the cumulative jet being observed only on the first pipe 426 mm in diameter. On the other pipe one could detect only plastic deformation and rapture of the metal of pipes, i.e. separation of a multiplayer pipe–cement–pipe barrier by the cumulative charge has a breaking mechanism of a different nature. After separation of the first pipe by the cumulative jet when it enters the barrier with a lower density (cement) the jet destroys, and rapture of the next inner pipes is caused by the swelling deformations appearing by the circle of the pipe due to penetration of sprayed cumulative jet and the products of the explosive detonation into the rapture zone. After separation a section of a five-layer pipe base about 1 m long was kicked away at a distance of up to 100 m testifying about a great power of the underwater cumulative charge. Considering this circumstance it is possible to separate a five-layer base by one half-ring of the charge.

Shell of the underwater ECC. Since 1960s a method of explosion cutting of metalwork came into use along with other technologies of underwater cutting. Now it is applied for different underwater operations at a depth of down to 300 m [5–7]. EC with ECC favorably differs from thermal methods of underwater cutting by simplicity of the employed equipment and installation of the underwater charge, remoteness of the process and thus a relatively short period of time the diver stays under water. Besides, a possibility to use the EC does not depend on the depth of the immersion and the highly qualified experts are not necessarily needed for its performance. In some cases the EC is simply irreplaceable, for example, when working on objects with combustible or gaseous explosive mixtures, as well as when there is a danger of a shift and collapse of the parts of cut structures.

Metallic or rigid rubber shells as well as rubber chambers additionally filled with air up to the pressure equal to the one of the external water column are used to protect the areas of jet formation from water. It is also possible to the foam plastic shells (an area of cumulative jet formation cal also be filled with foam plastic) [4, 6–9]. The depth of punching of steel barrier in this case decreases by 2–3 mm as compared to a rubber shell.

Table 6. Permissible water pressure for protection shell tubes made of different materials

Material	*Size of tubes, mm*	*Water pressure, MPa*
Technical aluminium	34 × 2	1.5
Aluminium alloy AMg2M	63 × 1.5	1.3
	70 × 1.5	1.2
Copper of MT grade	60 × 2.5	1.4
	45 × 2.5	3.0
Aluminium alloy D16	85 × 2.5	≥ 3.0
Stainless steel	75 × 1.5	≥ 3.0

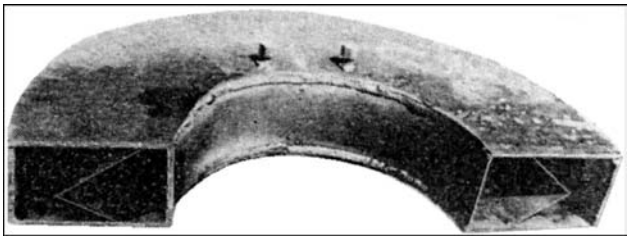

Figure 3. Appearance of half-ring of cumulative charge in a steel shell with inner diameter 426 mm

It is established that the efficiency of punching of metallic barriers sharply decreases if there is a layer of water more than 5 mm thick between the cut pipe and a protection shell. Therefore, it is necessary to take into consideration configuration and thickness of the barrier to be cut and a possibility to achieve a dense contact between them.

Let us consider the main advantages and disadvantages of different protection shells (metallic, rubber and foam plastic) used for underwater EC.

Metallic shell. Metallic tube of different materials (Table 6) is used as a protection shell (Figure 4). Tube of stainless steel and aluminium alloys endures water pressure (without residual deformation) up to 3 MPa. However, it is not always possible to bend a shell of these materials into the half-ring corresponding to the diameter of the pipe to be cut. Therefore, it is necessary to use plastic metals, such as technical aluminium and copper. It is possible to use tubes with wall thickness at least 2.0–2.5 mm at a depth down to 150 m and more then 2.5 mm at a depth down to 300 m. In EC of barriers it is necessary to consider the thickness of the wall in the protection shell.

The main disadvantages of the technology for production metallic protection shell of ECC for EC of pipe include:

• complexity of assembling and adjustment of ECC half-rings connected to the difficulty of their accurate

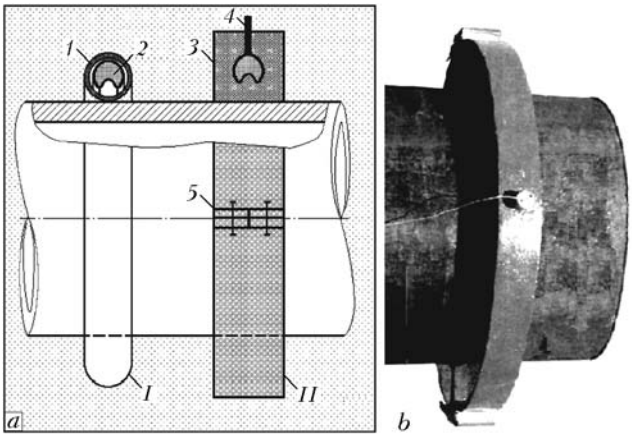

Figure 4. Diagram of arrangement for cutting pipes under water using ECC with insulation of a zone of jet formation with the help of metallic *I* and foam plastic *II* shell (*a*) and appearance of the charge (*b*): *1* — ECC; *2* — metallic (sometimes rubber) tube; *3* — foam plastic shell; *4* — electric detonator; *5* — connector

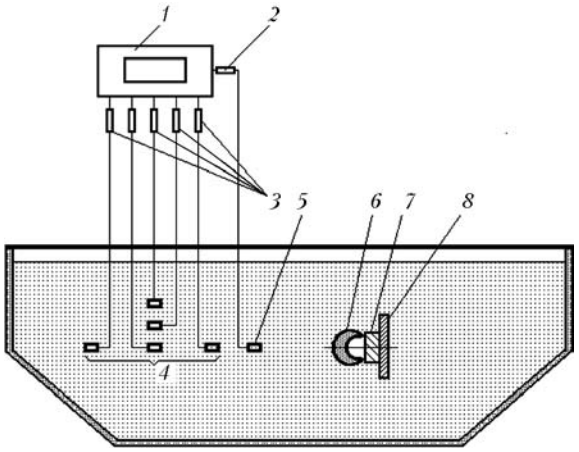

Figure 5. Scheme of measuring pressure during ECC explosion under water: 1 — oscillograph; *2, 3* — cathode and emitter followers, respectively; *4* — pressure sensor; *5* — trigger; *6* — ECC section; *7* — fixing arm (distance insert); *8* — barrier

placement into the inner space of the protection shell at a certain focal distance;

• complexity of accurate production of the shell because the pipes exposed to EC have different ovality and allowances for diameter, which inevitably leads to the appearance of clearances between the shell and the pipe to be cut as well as between joints of half-rings, thus lowering the efficiency of EC of these sections under water.

The mentioned disadvantages can be removed by using more powerful ECC providing a reliable cutting of the pipe. Production of straight protection shells involves almost no technological difficulties. The protection shell are insulated at the ends by the copper caps of corresponding thickness using a suitable adhesive (for example, «Sprut»).

Rubber shell. Bicycle or moto-cycle inner tubes insulated at the ends by metallic caps are the simplest method of this type of protection. Assembling of these shells on the pipe is carried out by special wire bindings. Before immersing into water they are preliminary filled with air through a nipple to check the leak-proofness. They are filled with air completely after installation on the pipe to be cut. In this case the rubber inner tube tightly fits the barrier and completely expels the water from the space between the shell and the pipe. Protection shells of this type are successfully applied for underwater ECC cutting of pipe multi-layer bases of a drilling platform at a depth of 33 m [6–10]. The rubber inner tubes are very sensitive to cuts and punctures therefore it is advisable

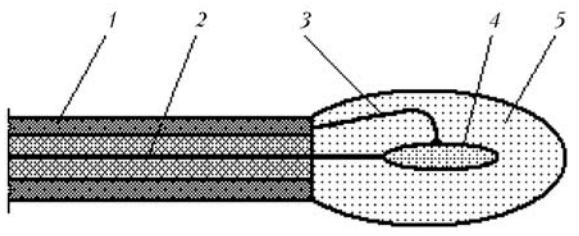

Figure 6. Diagram of pressure sensor: *1* — coaxial cable; *2, 3* — central and connecting wire, respectively; *4* — plate of piezoelectric ceramics; *5* — rubber head

to protect them additionally with dense material of tarpaulin type or to use half-rigid multiplayer rubber shell. Shells of such type can be used at the depths of more than 50 m.

Foam plastic shell (see Figure 4). It is rather simple to produce this shell. For this a mould is needed to where the charge is installed and then the mould is filled with foam polyurethane granules. The subsequent blow of the mould with steam (with pressure about 0.1 MPa) allows obtaining a dense shell. Before, the parts of equipment for fastening underwater charges are installed in the same mould. The main advantage of this shell is that the area of cumulative jet formation is filled with foam plastic, therefore its decompression is practically excluded. The foal plastic shell is also used for EC of the bases of drilling platforms [4, 5, 11]. Tests in the high-pressure chamber allowed establishing that such shell can endure pressure to 0.5 MPa without decreasing a depth of the barrier punching.

Shock waves during underwater EC and their dampening. Let us consider the results of pressure measurements in the shock wave propagating in the water under explosion of ECC section 19 mm in diameter and 250 mm long (mass of hexogen in ECC is 53 g) and effect of different types of protection screens for damping of shock waves. Simple technological methods and certain materials were used for production of protection screens: dry sand, foam plastic (LS-1-200 grade), expanded clay aggregate gravel, combine screens composed of sand and foal plastic layers as well as screens of air bubbles. Experiments were conducted in the pool 6 m in diameter and 3 m deep (Figure 6). Charge installed using fixing arm on the steel plate ($12 \times 400 \times 600$ mm) with 20 mm clearance was immersed into the pool with water at a depth of 1.5–1.7 m and then by the electric detonator was initiated. Pressure of the shock wave in different points of the pool were measured by a five-beam oscillograph S1-33 using special pressure sensors produced on the basis of piezoelectric ceramics TsTS -19 with a sensing element $1.5 \times 1.5 \times 0.7$ mm in size. TsTS-19 plates 0.3 mm thick after determination of the polarization direction were brazed together by the Wood alloy so that the silver-plated surfaces of identical polarity were in reliable electric and acoustic contact with each other and with three or four thin copper conductors. Free ends of conductors were brazed to the central conductor *2* (see Figure 5) of the radio-frequency coaxial cable *1* of RK-50-2-II type. External silver-plated surfaces of piezoelectric elements were brazed with thin copper conductors *3* to the cable braiding *1*. A layer of raw rubber about 0.7 mm thin was glued to the side surface of the piezoelectric element. Crystals prepared in such a way were covered with a cold hardening compound on the basis of epoxy resin with a fine corundum powder filler. The compound right before application to the piezoelectric element was treated in vacuum during 5 min to remove the air bubbles. After polymerization of the compound the

pressure sensor was completely sealed and protected against action of the shock wave on its side surfaces owing to the rubber ring *5*. Time resolution of sensors is about 10^{-6} s, inner resistance of the ready sensors is at least 100 mOhm. Capacitance 10^{-5} pF was determined, mainly, by the length of the cable. High sensitivity of sensors allowed providing a signal without preamplifiers directly to the input of the oscillograph through the emitter followers to insure matching by resistances. A scheme of measurement was calibrated by a reference signal as a shock wave created by the explosion of the electric detonator. Pressure in the shock wave in the point of the sensor location was determined by the Coal formula $P = 1470R^{-1.13}$ (MPa) [12], where R is the distance from the charge to the point of measurement in the charge radii. Total error of the measurement did not exceed 20 %.

Results of the measurements of attenuation of the shock wave with its propagation are presented in Figure 7. Distance from the charge to the measurement point is shown on the X-axis and a peak value of pressure in the wave — in the Y-axis. The wave of pressure from explosion of a single charge as well as the wave from electric detonator has a sharp front with subsequent slow fading approximately by the exponent.

The bubble protection was studied according to the following scheme. A rubber hose with holes in its upper part (about 1 mm in diameter) was wrapped into a plane spiral and placed on the bottom of the pool right under the studied charge. Diameter of the largest wrap was 0.6 m. Air bubbles fed by the compressor were passing through the holes and rising up to the water surface, thus forming a bubble area with a charge fastened to the steel plate in the center. Comparison of the pressure oscillogram with such protection with the oscillogram of the shock wave from ECC without protection showed that the form of pulse practically did not change, the wave front remained rather steep. However, approximately three-fold decrease of the amplitude level of load is observed in this case. For the whole measurement area the maximal pressures in the wave passed through the layer of water saturated with air bubbles are much lower than the amplitude loads in the same points where the ECC operates without protection. For example, a peak pressure at a distance of 2 m from the charge dropped down to 1.5 MPa as against 15 MPa without using any protection.

Experiments with the above mentioned protection means were carried out according to the scheme presented in Figure 8. Thickness of the protection screens was 200 mm, i.e. about ten diameters of the charge. Screens of such materials as sand and expanded clay aggregate gravel were made of parts of automobile rubber tubes filled with materials. The ends of the tubes were cramped to insulate the inner space from the water. The screen consisted of three layers of foam plastic each 50 mm thick and layers of sand 20 mm thick located between the plates of the foam plastic.

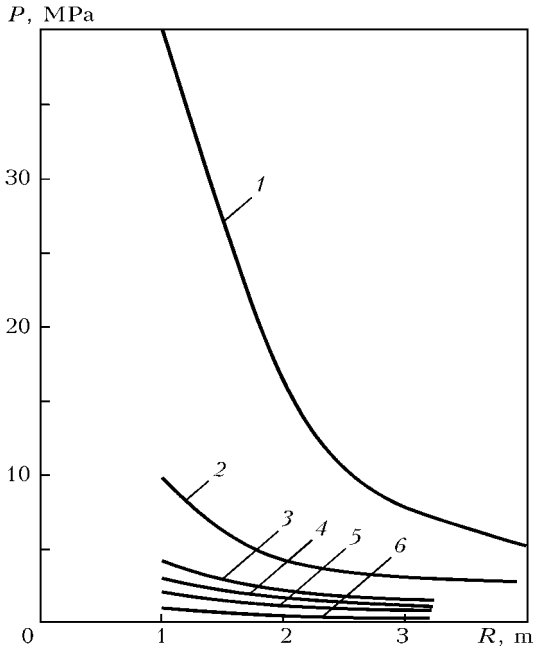

Figure 7. Curves of shock wave amplitude attenuation: *1* — explosion of ECC section without protection; *2* — bubble protection; *3–6* — screen of dry sand, expanded clay aggregate, foam plastic and laminar, respectively

As against bubble protection the screens of expanded clay aggregate gravel, dry sand and foam plastic qualitatively change the load making the front sloping, the wave longer with simultaneous essential decrease of pressure in the peak. Amplitude pressures of the shock wave under explosion of ECC 19 section without protection and with different screens are presented in Figure 9.

The use of expanded clay aggregate gravel of grade 500 is most advisable from technological standpoint. Facility on its basis with practically zero buoyancy does not require immersion of additional ballast as in the case of using foam plastic.

The measurement results show that at a distance from 1 to 3.5 m the bubble protection decreases pressure 5 times, sand screen — 10 times, expanded clay aggregate gravel — 20 times, foam plastic — 30 times,

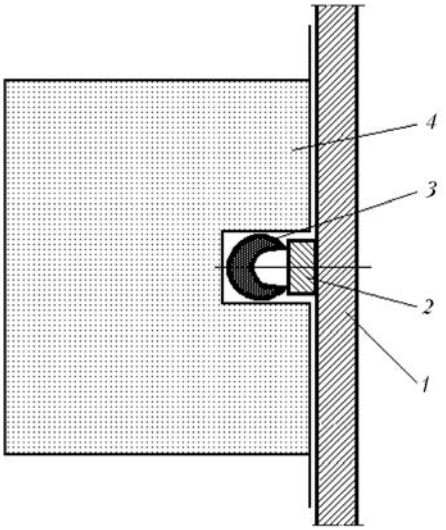

Figure 8. Scheme of protection device: *1* — steel plate; *2* — focal distance catch; *3* — ECC; *4* — protection screen

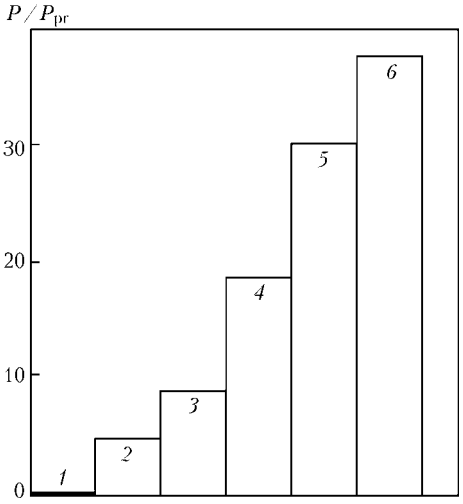

Figure 9. Efficiency of different protection media during ECC explosion in the water at a distance of 3.5 m from the charge (for designations see Figure 7 and the text)

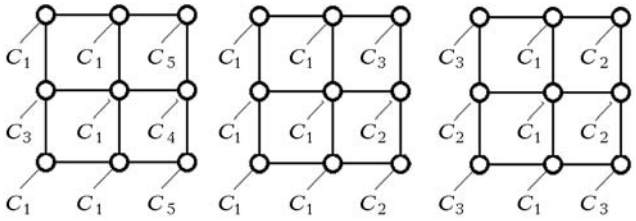

Figure 10. Location of piles in the base of drilling platform

alternating layers of sand and foam plastic — 40 times. Foam plastic screen, which at the same time is the ECC protection shell and may play a role of the bubble protection, is most appropriate by technological and economical indices. If need be a safety area for marine fauna may be expanded by scaring fish with acoustic methods from the ECC explosion zone in the radius up to 3–5 m [4, 13].

Examples of pilot-industrial application of underwater EC. Let us consider dismounting with the help of charges TrKKP (circular cumulative underwater pipe cutter) the base of the drilling platform

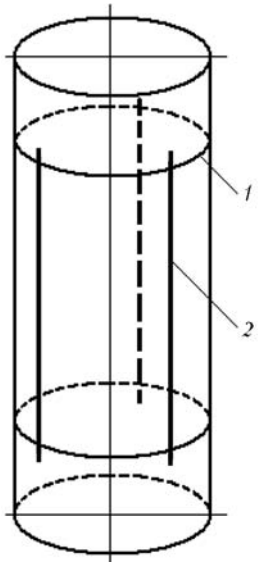

Figure 11. Scheme of EC pile of ECC multiplayer MSP base: *1* — circular cut; *2* — cross-section cut

Table 7. Sizes of piles of the platform bases

Platform	*Pipe sizes, mm*				
	Ø426 × 11	*Ø377 × 11*	*Ø325 × 11*	*Ø273 × 10*	*Ø219 × 8*
C_1	+				+
C_2	+		+	+	
C_3	+		+		+
C_4	+	+	+	+	+
C_5	+	+	+	+	

Note. «+» sign marks the presence of this pipe size in the pile of platform base.

located in the Black Sea in the region of Golitsin elevation at a distance of about 75 km from town Evpatoriya. The base of the drilling platform consisted of three similar strakes each installed on nine piles (Figure 10, Table 7). Each pile presented a structure consisting of coaxially located pipes 219–426 mm in diameter, wall thickness of which was 8–11 mm, with a cement layer in the space between the pipes. EC was performed by two divers at a depth of 33 m. Preparation operations and additional control of the cutting results were performed by a diver in a metal diving armor. A layered cutting was carried out by the scheme presented in Figure 11. Initially two TrKKP were installed on the pipe at a distance of 700 mm. After cutting three liner charges were placed uniformly by the pipe perimeter. Their explosion led to separation of the «coil» and destruction of the solid cement layer. Subsequent cutting of pipes of a smaller diameter was carried out in a similar way, in this case a length of linear charges and a distance between circular cuts were accordingly decreased. EC of pipes was carried out by charges of TrKKP type 19 and 41 mm and by linear ECC 19. For TrKKP a protection shell of foam plastic and rubber tubes filled with air and sealed with metallic caps by the ends were used. Protection shell for linear charges was produced of aluminium tube 34 × 2 mm in diameter sealed by the ends with copper foil caps 0.3 mm thick and with adhesive «Sprut».

Every diver for one descent installed four circular or six linear charges. Electric detonators with power

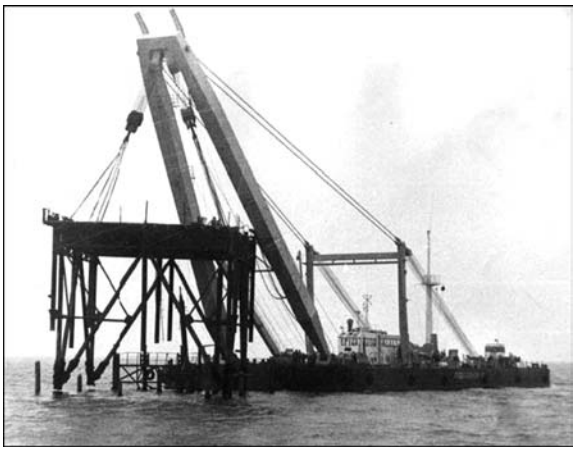

Figure 12. Lifting of the drilling platform base dismounted by EC

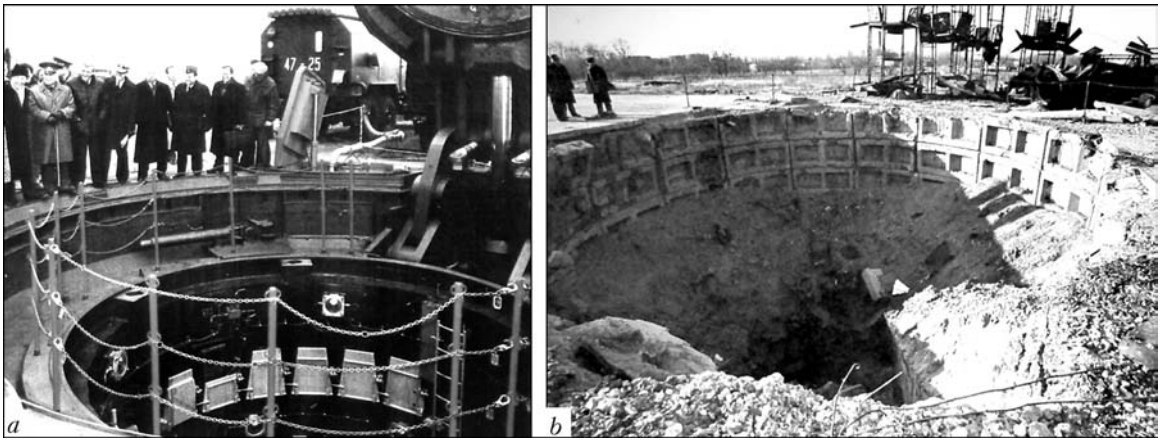

Figure 13. Appearance of pit launchers before (*a*) and after (*b*) EC

network were installed after installation of charges on the pipes to provide safety of underwater explosion works.

The electric detonators were placed into a special device with detonation conductors (extended charge in the aluminium shell) excluding a direct connection of the detonator with metallic structures. When divers were under water external ends of the power network were thoroughly sealed. Work of divers was terminated at seaway of more than three magnitudes. The last 3–4 pipes of the block base were cut simultaneously. The underwater device on the basis of ECC 41 on piles of C_2, C_4 and C_5 (see Figure 10) cut simultaneously two pipes, i.e. the total thickness of the cut barrier of cement and pipes was 35–36 mm.

While dismounting of the drilling platform bases 96 pipes were cut by explosion. Total time of direct underwater explosion works was 15 days. After cutting of pipe bases three blocks of the platform were lifted by a vessel-lifting crane (Figure 12), loaded on the barge and sent to the sea experimental testing ground (settlement Katsiveli, Crymea). Then they were installed at a distance of 100 m from the sea shore. This platform was then used for special hydrophysical studies.

The explosion technology was used in 1985 for dismounting of the prospecting platform located in the Azov Sea at a depth of 11 m. In 1986 similar works were done for dismounting blocks of MSP located in the Black Sea at a depth of 30 and 33 m. Also EC was performed for 30 pipe supports of water-development projects located in the Caspian Sea at a depth of 6 m. As a result a section of the overpass 300 m long was dismounted. In 1990–1991 the works were done on EC of pontoons of MSP after their dismounting on the shelf.

In 1996–1998 the E.O. Paton Electric Welding Institute participated in liquidation of the pit launchers (PL) of intercontinental ballistic missiles SS-19 and SS-24 in the frame of the works on liquidation of strategic offensive arms. The operation was reduced to destruction of the upper parts of PL about 6 m height (Figure 13). 37 PL were liquidated in total.

The works were done by two different technologies. The first one developed in 1992 for liquidation of the training PL (town Pervomajsk) provided using only EC. The second technology developed together with the company ALBA (Germany) is based on joint use of hydro-abrasive cutting and EC. It allowed carrying out explosive operations in the vicinity of housing area (radius of the dangerous zone is 50 m), which was achieved by cutting steel plates by hydro-cutting method before explosion. The ECC developed by the E.O. Paton Electric Welding Institute were used for both technologies. Axially symmetric cumulative charges for formation of blast-holes in metallic reinforced concrete construction were used for the first time.

Now axially symmetric cumulative charges are at the stage of acceptance tests for liquidation of a body of large crushing machine at the Open Joint-Stock Company «Poltavsky GOK» (construction in its size and complexity of works more than ten times exceeds the works for liquidation of PL).

1. Petushkov, V.G., Volgin, L.A., Dobrushin, L.D. (2003) Explosion cutting and its application. *The Paton Welding J.*, **7**, 25–31.
2. (2002) *Physics of explosion*. Ed. by L.P. Orlenko. Vol. 1. Moscow: Fizmatlit.
3. Lavrentiev, M.A. (1957) Cumulative charge and principles of its operation. *Uspekhi Matematich. Nauk*, **4**, 41–56.
4. Grechka, Yu.V., Kucherenko, V.F. (1981) Selection of protective coverings of ECC for underwater cutting of tubular structures. In: *Explosion welding and cutting*. Kiev: PWI.
5. Kudinov, V.M., Palamarchuk, B.I., Vakhnenko, V.A. et al. (1963) Relaxation phenomena in a foamy structure. *Shock Waves, Explosion and Detonation*, **87**, 96–118.
6. (1978) Submersible-operated pipeline preparation. *Pipes and Pipelines Int.*, 23(**4**), 7–8.
7. Korolyov, I.V., Pasynskaya, L.L. (1984) Development of marine oil- and gas fields in Norway. In: *Inf. Rev. of VNIIgazprom*. Issue 4. Moscow.
8. Stalker, A.W. (1976) Survey of underwater cutting techniques. *Metal Construction*, **6**, 261–264.
9. Schafstall, H.G., Schalfer, R. (1979) Schneiden unter Wasser Entwicklungsaktiviteten fuer die Meerestechnik. *Schweissen und Schneiden*, 31(**2**), 516–524.
10. Galkin, V.V., Gilmanov, R.A., Drogovejko, I.Z. (1987) *Explosion operations under water*. Moscow: Nedra.
11. Kudinov, V.M., Palamarchuk, B.I., Lebed, S.G. et al. *Cumulative charge for cutting of obstructions in liquid medium*. USSR author's cert. 917598. Int. Cl. B 23 K 20/08, B 23 K 26/06. Priority on 25.08.80.
12. Coul, R. (1960) *Underwater shots*. Moscow: Inostr. Literatura.
13. Aliev, A.N., Bogatyryov, P.B., Vakhnenko, V.A. et al. *Method of extinction of shock waves in liquid* USSR author's cert. 1062966. Priority on 22.08.83.

MATERIALS AND TECHNOLOGY FOR FLUX BRAZING AND SOLDERING OF ALUMINIUM AND ALUMINIUM TO STEEL

O.M. SABADASH and **V.F. KHORUNOV**
E.O. Paton Electric Welding Institute, NASU, Kiev, Ukraine

Peculiarities of brazing of aluminium using high-temperature fluxes of the K–Al–Si/F system, as well as soldering using low-temperature fluxes, containing a new class of activators, i.e. complex tetrafluoborates (TFB) of metals Pb(II), Zn(II) and Cd(II) with nitrogen-containing bases, such as benzatriazole and morpholine, characterised by high reactivity, have been studied. Chemical interaction of aluminium with salt melts of the K–Al–Si/F ternary system results in formation of liquid alloy Al–Si at the interface. This alloy greatly improves spreading and filling of capillary gaps with brazing filler alloys, and it can independently perform the function of a brazing filler alloy. Reactive flux FAF540 is successfully applied for joining aluminium alloys containing up to 0.7 % Mg, as well as aluminium to stainless steel. In low-temperature soldering, the metal coatings are deposited from a composition of complex TFB on the surface of aluminium parts being soldered. The coatings can be readily wetted and dissolved by low-melting point solders and improve formation and properties of the aluminium joints.

Keywords: *brazing, soldering, aluminium, steel-aluminium joints, non-corrosive fluxes, brazing filler alloys, solders, brazed joint, soldered joint, salt melts, potassium hexafluosilicate, low-temperature fluxes, activators, complex tetrafluoborates*

Reduction in weight of structures and units with a simultaneous improvement in their technical characteristics and operational reliability under the effect of different kinds of loads is one of the most important engineering tasks, which can be partially addressed through using joints of light alloys based on aluminium and its combinations with other metals. Aluminium and its alloys are extensively applied in different-purpose structures, particularly heat exchangers for cars, aircraft and products of electronic industry. Structures of the ther type that are widely applied in industry are those that include aluminium to steel joints. They are used in pipe adapters of cryogenic plants, cars and bimetal utensils. Brazing and soldering are the main joining methods for products of all of the above types.

High-temperature brazing of aluminium. Current trends to improvement of high-temperature brazing of aluminium and its alloys are based on refusal from the use of corrosive fluxes, and in a number of cases from vacuum technologies, by fully replacing such processes with advanced processes of brazing in shielding gases (argon, nitrogen, helium) involving non-corrosive fluxes.

Optimal conditions for wetting the aluminium surface with brazing filler alloys in flux brazing can be provided through complete destruction of a refractory and strong surface film of aluminium oxide formed on workpieces and filler alloys during the brazing process. Brazed joints can be made using a filler alloy preliminarily placed into a gap, or an aluminium-containing metal alloy formed as a result of chemical interaction of the reactive flux components with aluminium.

As reported, destruction of an oxide film in high-temperature flux brazing takes place due to chemical interaction with gas atmospheres, e.g. phosphorus or boron trifluoride [1], or salt melts of chlorides of the Li–K–Na–Ba/Cl system containing active additions of aluminium, potassium and zinc fluorides [2]. However, high toxicity of such gas atmospheres and substantial corrosive activity of chloride fluxes and their remainders with respect to aluminium limits commercial application of these environmentally hazardous brazing processes.

Non-corrosive fluxes of the $KF–AlF_3$ system were used as a basis for the development of modern environmentally safe processes of gas-shielded brazing of parts of aluminium alloys containing up to 0.6 wt.% Mg [3–5]. An example is flux NOCOLOK, which is eutectic (45.8 % KF–54.2 % AlF_3) with a melting point of 560–570 °C [6]. For instance, the high-productivity technology for furnace brazing of car heat radiators in nitrogen (T_{dew} = –40 °C) using the NOCOLOK flux has substantial advantages as to productivity and cost effectiveness over the fluxless processes of abrasive and vacuum brazing [7].

One of the promising areas of development of flux brazing is the use of minor additions of complex fluorides for activation of wetting processes and capillary properties of brazing filler alloys at interfaces in the heterogeneous solid metal (aluminium)–ion melt (flux)–filler alloy system. When in contact with the salt melts, aluminium reduces elements in a composition of complex fluorides, which may form binary or multicomponent alloys with it. Therefore, thin layers of metal melts are formed on the mating surfaces during the brazing process, and these layers provide substantial improvement in the conditions of formation of brazed joints with or without a brazing filler alloy (they can independently function as brazing filler alloys).

Our research on fusibility and chemical interaction in the K–Al–Si/F system shows that thermally stable

salt mixtures are limited to a concentration triangle of $KF–K_3AlF_6–K_3SiF_7$ [8]. Salt melts that are beyond the above concentration triangle are characterised by chemical interaction between aluminium fluoride and complex fluoride with transition of silicon to the gas phase in the form of SiF_4, and subsequent formation of binary mixtures $K_3AlF_6–K_3SiF_7$ or $K_3AlF_6–AlF_3$ (depending upon the initial composition). This fact should be taken into account when using the salt melts as fluxes of this system for brazing aluminium.

Calculations of thermodynamics of interaction in the $K–Al–Si/F–Al_2O_3$ and $K–Al–Si/F–Al$ systems, made at a condition that $\Delta C = \Delta C_{298} = \text{const}$, and that variations in the reaction enthalpies with temperature are not large:

$$\Delta G_1(T) = \Delta H_{298} - T\Delta S_{298} + \\ + \Delta C_{298}[(T - 298) - T \ln (T/298)],$$

where $\Delta G_1(T)$ is the variation in free energy of the interaction reaction with temperature T; ΔH_{298}, ΔS_{298} and ΔC_{298} are the differences in enthalpies, entropies and heat capacities of the reaction products and initial reagents under standard conditions

$$2Al_2O_3 + 3K_2SiF_6 = 2K_3AlF_6 + 2AlF_3 + 3SiO_2,$$
$$\Delta G_1(T) = -437 - 0.0404T - 0.0318[(T - 298) - \\ - T \ln (T/298)]; \quad (1)$$

$$4Al + 3K_2SiF_6 = 2K_3AlF_6 + 2AlF_3 + 3Si$$
$$\Delta G_2(T) = -1207 - 0.0418T - 0.0449[(T - 298) - \\ - T \ln (T/298)] \quad (2)$$

show that potassium hexafluosilicate performs two functions: it furthers destruction of oxide Al_2O_3 (1), and in interaction with aluminium it reduces (aluminothermic reaction) silicon in a composition of complex fluoride (2). Equilibrium of both processes is almost completely shifted to the interaction products.

Thermography of salt melts of the $KF–AlF_3–K_2SiF_6$ ternary system, containing 0–50 wt. % K_2SiF_6, was conducted. Compositions of the salt melts of this ternary system with melting point ranges of 560–585 °C, which can be used for brazing aluminium, were identified.

In this study we conducted investigations of spreading of brazing filler alloy Al–12.5 % Si (volume of weight — 63 mm^3) using salt melts of the $KF–AlF_3–K_2SiF_6$ ternary system on samples of aluminium AD1 (99.3 wt.% Al, GOST 4784–97) in the form of a horizontal plate $40 \times 40 \times 1$ mm in size, as well as formation of a joint between the horizontal ($40 \times 40 \times 1$ mm) and vertical ($40 \times 50 \times 1$ mm) plates of a T-sample with a brazing filler alloy (volume of filler alloy weight — 150 % of size of the gap) and without it. The ratio of brazing filler alloy (A) and flux (F) during the experiments was (vol.%) A:F = 1:1 in spreading and A:F = 1:0.75 in gap filling, respectively. Reactivity of salt melts of the $KF–AlF_3–K_2SiF_6$ system in aluminium brazing was evaluated on the basis of the area of spreading of aluminium filler alloy.

Video filming of the processes of spreading of Al–Si filler alloys and filling of the capillary gaps between the plates with them allowed peculiarities of these processes to be revealed at a brazing temperature of 570–630 °C:

(1) melting, spreading over aluminium and rapid filling of the brazing gaps with fluid salt melts (T_b = = 575–595 °C);

(2) active destruction of the surface oxide film as a result of chemical interaction with a salt melt (T_b = = 585–630 °C);

(3) formation of a thin layer of liquid metal melt Al–Si at the interface in interaction with aluminium (T_b = 585–630 °C);

(4) melting and distribution of a brazing filler alloy over the surface and in the gaps in a case of using a filler alloy weight (T_b = 595–605 °C);

(5) formation of a liquid metal layer (filler alloy) and filling of a gap with it in the case of using only flux (T_b = 595–615 °C).

Metallography of brazed joints shows that thickness of this layer is 1–20 μm and depends upon the amount of the reacted silicon hexafluosilicate. Comparative tests of aluminium specimens made by brazing using the NOCOLOK flux show that processes (3) and (5) do not occur, because this type of flux interacts only with aluminium oxide. The area of spreading of the filler alloy over aluminium AD1 was found to strongly depend upon the content of potassium hexafluosilicate in a salt melt and reactivity of the gas atmosphere in which the brazing is performed (Figure 1).

Analysis of microstructure of brazed joints in aluminium made under non-equilibrium solidification conditions revealed the following peculiarities of the eutectic structure (Figure 2). A large amount of the eutectic phase is formed in the seams made with a brazing filler alloy (Figure 2, *a*). The eutectic phase is located between dendrites of the aluminium-based α-solid solution, and the seam has relatively smooth boundaries. In a seam made without a filler alloy (Figure 2, *b*) the volume of the eutectic phase is much smaller, and the eutectic component penetrates to a substantial depth (approximately 150–300 μm) in the aluminium base metal. X-ray microanalysis of the seams made with a reactive flux showed substantial variations in a concentration of silicon from 0.4 to 13 wt.% in microvolumes.

Flux FAF540 was developed as a result of the investigations performed. It possesses high reactivity, compared with the NOCOLOK flux, and improves spreading of filler alloys over aluminium in air and helium atmospheres (spreading area is larger by a factor of 1.5 and 1.7, respectively). This flux can be applied for brazing aluminium and its alloys (with a magnesium content of up to 0.7 wt.%) both with and without a brazing filler alloy, and for joining structures having different thickness (differing more than by 3 orders of magnitude).

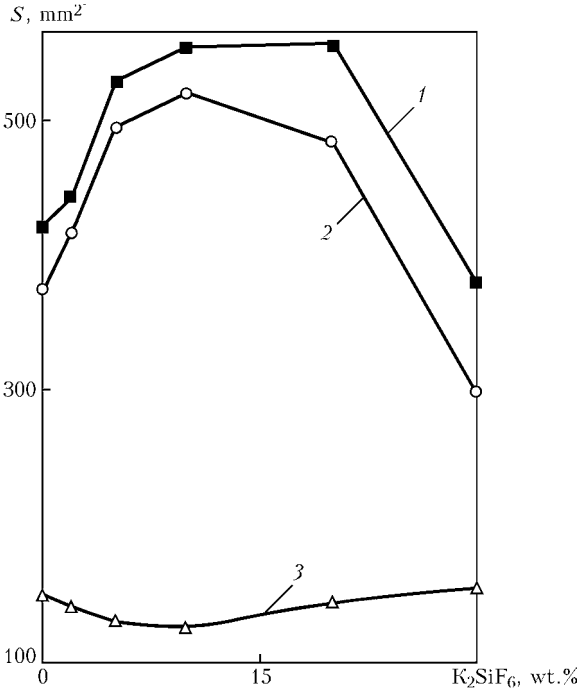

Figure 1. Variations in area of spreading S of brazing filler alloy Al–12 % Si over aluminium AD1 (*1, 2*) and steel 12Kh18N10T (*3*) depending upon the K_2SiF_6 content of salt melts of binary eutectic of the $KF–AlF_3$ system at T_b = 595–600 °C: *1* — gas atmosphere — helium; *2, 3* — air

Butt and overlap joints in aluminium AD1 and A5 have strength equal to that of the base metal, and strength of joints in alloy AMts in shear tests is (0.85–0.90)τ_{sh} of that of the base metal. Flux and its remainders after brazing cause no corrosion of the materials being brazed.

Flux FAF540 was applied, e.g. in the processes of high-temperature brazing of experimental batches of complex-design members of thermoelectric module radiators made from aluminium AD1 and A5 (Figure 3, *a*), and flat antennas for mobile communication (Figure 3, *b*) made from alloy AMts (Al–1.6 % Mn) in nitrogen with and without a filler alloy.

Brazing of aluminium AD1 to corrosion-resistant steel 12Kh18N10T. Production of sound joints between these materials by the brazing methods is hampered by substantial differences in their physical-mechanical properties. Transition layer consisting of intermetallic phases $FeAl_3$ and Fe_2Al_5 [9], which inhibits its spreading of a melt and leads to its interruption [10], is formed at the interface in interaction of solid iron with Al–Si melts. Therefore, different metallic coatings 5–25 μm thick are often deposited on the steel surface to improve conditions for production of brazed joints in dissimilar materials. These could be galvanic coatings of copper, nickel or silver [11], or coatings produced by dipping into metallic melts of aluminium, zinc or tin [12, 13], which perform the function of a diffusion barrier. In addition, rapid cooling is used for parts of a simple shape to limit growth in thickness and width of a brittle transition layer. Formation of solid metallic interlayers on the surfaces of dissimilar metals favours improvement in strength properties of the joints, despite some apparent drawbacks.

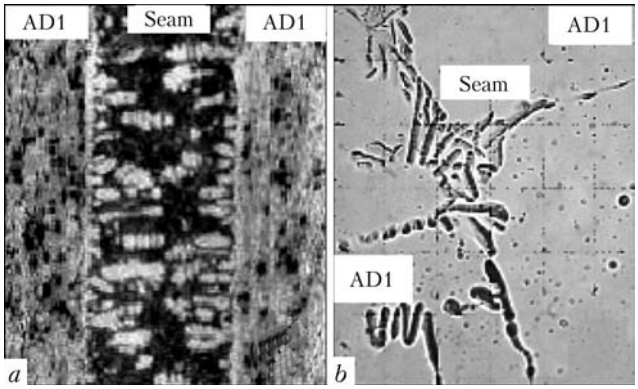

Figure 2. Microstructure of metal of brazed joints in aluminium AD1 made by using brazing filler alloy Al–12 % Si and flux FAF540 (*a* — ×200), and using only flux FAF540 (*b* — ×600)

One of the promising directions for improving quality of the aluminium to steel joints can be the use of reactive fluxes based on the K–Al–Si/F system (or their mixtures with brazing filler alloys), the salt melts of which, when interacting with aluminium, form liquid metallic (Al–Si) layers several microns thick on its surface. Flux brazing of such dissimilar materials can provide optimal capillary properties of brazing filler alloys and induce a modifying effect on structure of the brazed joints. As reported in [14], silicon improves properties of permanent joints between aluminium and steel by affecting the character of interaction at the interface between the condensed phases.

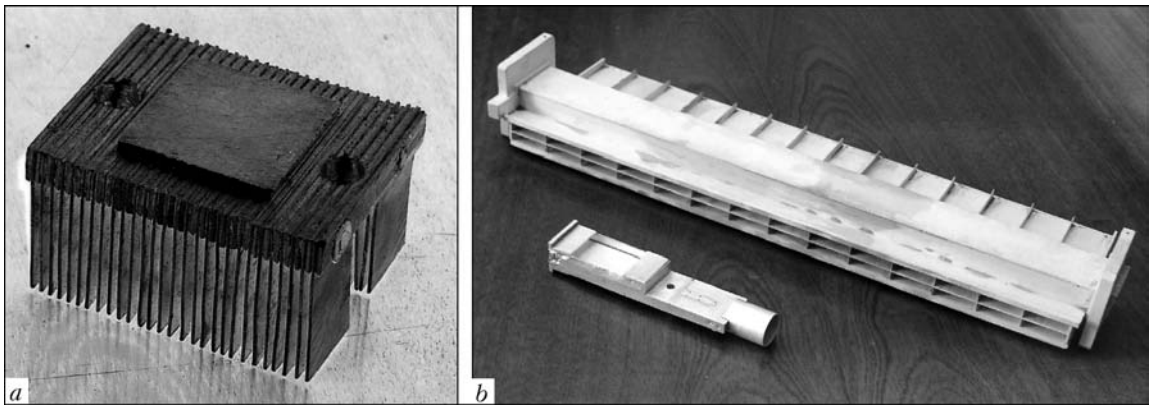

Figure 3. Appearance of aluminium parts brazed with flux FAF540 (using no brazing filler alloy): *a* — plate radiator consists of a set of plates of different height made from alloy A5 (99.7 wt.% Al); *b* — elements of flat antenna of alloy AMts

Reactive fluxes of the K–Al–Si/F ternary system and flux FAF540 were selected as the investigation objects. Brazing of standard samples of aluminium AD1 and steel 12Kh18N10T (analogue of steel SUS340) was performed in air atmosphere using induction heating from the VChG-1 generator with a working frequency of 66 kHz. Technological properties of brazing consumables and quality of brazed joints were evaluated as follows: from area of spreading of compact filler alloy (volume of weight — 63 mm^3) over the steel surface on samples 40 × 40 × × 1 mm in size; from the degree of filling of horizontal gaps with a mixture of powders (particle size — 0.05–0.16 mm) of silumin AKD12 (Al–12 % Si) and flux FAF540 on aluminium and steel samples (40 × 40 × × 1 mm — lower plate, and 20 × 20 × 1 mm — upper plate); and from tensile strength of overlap samples of type IV according to GOST 28830–90 (ISO 5187–85) after thermal cycling. Reportedly [15], heating in air atmosphere leads to decomposition of base of fluxes of the KF–AlF_3 system, in particular to reaction $2AlF_3 + 3H_2O = 6HF + Al_2O_3$. Optimisation of the rate of heating of workpieces, temperature and time of brazing allowed the effect of moisture and air oxygen on the reactivity of fluxed to be decreased and, thus, the amount of defects in brazed seams to be reduced.

In brazing using salt mixtures of the KF–AlF_3–K_2SiF_6 system a transition intermetallic layer of complex composition (basic phase is Fe_2Al_5) several microns thick is formed at the interface as a result of interaction of steel 12Kh18N10T with liquid Al–Si alloy (brazing filler alloy). For this reason, under the identical brazing conditions the area of spreading of filler alloy over the surface of steel 12Kh18N10T is several times (approximately by a factor of 4–6) smaller than on aluminium (see Figure 1). The use of flux FAF540 improves spreading of the aluminium filler alloy over the steel surface (spreading area is larger by 40 %), compared with salt mixtures of the KF–AlF_3–K_2SiF_6 system. As found experimentally, good filling of capillary gaps and formation of brazed joints in aluminium AD1 with filler alloy powders were achieved at a heating rate of 5–10 °C/s. For the aluminium-steel joints this value is 3–8 °C/s. The ratio of weight percent of flux to brazing filler alloy should range from 40:60 to 60:40. In this case particles of a brazing filler alloy are fused during brazing to form a homogeneous metallic alloy that fills the capillary gap.

Analysis of the results of electron metallography of the aluminium to steel brazed joints allows the following conclusion. These brazed joints are heterogeneous in structure and composition (Figure 4). The seam consists of a transition layer 8–10 μm thick of a variable composition, wt.%: 12–20Fe, 3–6Si, 3–6Cr, 0.1–0.3Ni, 0.05–0.2Ti, and Al — balance, and an adjoining layer 20–26 μm thick of the aluminium-based α-solid solution with interlayers of skeleton-like eutectic Al–12 % Si.

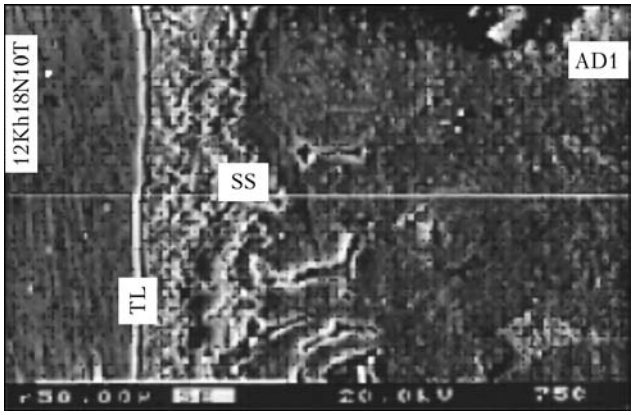

Figure 4. Microstructure of metal of brazed joint between aluminium AD1 and steel 12Kh18N10T made by using a brazing filler alloy (mixture of flux AlF_3–KF–$10K_2SiF_6$ and powder AKD12 — 50:50 wt.%) at T_b = 605 °C: TL — transition layer; SS — layer of Al-based α-solid solution with eutectic Al–12 % Si (×750)

Brazing of standard samples for mechanical tests was conducted using a flux powder (flux + brazing filler alloy — 50:50 wt.%) at T_b = 605–610 °C. Strength of such joints after thermal cycling was found to be within ±10 % of the initial one (Figure 5). Variations in strength of the brazed joints are attributable to an insignificant variation in thickness (increase of about 3–5 %) of the transition intermetallic layer as a result of a long-time temperature effect during thermal cycling.

The test results were used to develop the technology for brazing bimetal utensils of corrosion-resistant steel with an aluminium heat-distributing layer. Also, the technology was developed for brazing pipe steel-aluminium adapters up to 57 mm in diameter using induction heating. After 10-fold thermal cycling (cooling in liquid nitrogen at –196 °C and heating to 30 °C) the samples of the brazed pipe adapters provide air tightness at a pressure of 30 MPa.

Soldering. Strength of aluminium joints soldered using low-melting point solders of the Sn–Pb, Sn–Zn, Pb–Cd–Zn, Cd–Zn and Zn–Al–Cu systems depends to a substantial degree upon the corrosion resistance of the solders, when tested under conditions of in-

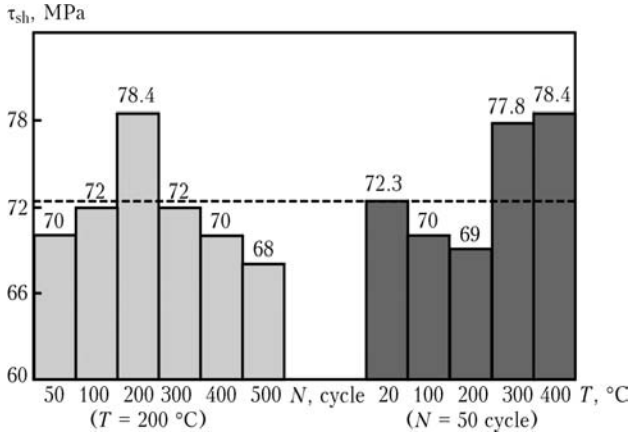

Figure 5. Variations in shear strength τ_{sh} of overlap brazed joints between alloy AD1 and steel 12Kh18N10T made by using a brazing filler alloy (mixture of flux FAF540 with powder AKD12 — 50:50 wt.%) at T_b = 600–610 °C, after thermal cycling (heating-cooling in water)

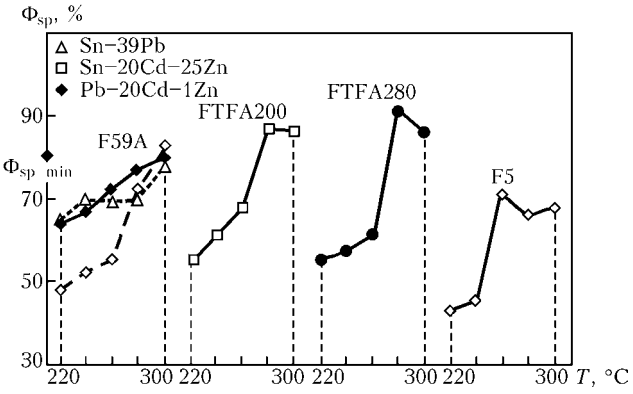

Figure 6. Factor of spreading, Φ_{sp}, of solders over aluminium A5 and copper M1

creased humidity and in sea water. Sn-base solders have low corrosion resistance compared with solders of other systems. Sensitivity of tin solders to corrosion can be decreased through increasing the zinc content (≤ 50 wt.%) [10]. Aluminium joints soldered with the Zn-based solders are most corrosion-resistant under these conditions. However, this replacement of the solder base leads to a substantial increase in soldering temperature (from 250 to 430 °C). Within a temperature range of 180–350 °C, it is impossible to provide their optimal technological compatibility with the Pb-Cd- and Zn-base solders because of low activation of the processes of wetting with the aluminium solders and insufficient reactivity of fluxes. In addition, insufficient thermal stability of a number of activators (amines, halides [16] and salts of tetrafluoboric (TFB) acid [17]) leads to contamination of air atmosphere with toxic thermolysis products [1, 18].

One of the ways of improving compositions of low-temperature fluxes is the use of a new class of compounds, which are more reactive and thermally stable than simple salts, i.e. complex TFB of metals with organic nitrogen-containing bases, as activators of fluxes.

We investigated efficiency of the activators, i.e. complex TFB of Pb(II), Zn(II) and Cd(II) with nitrogen-containing bases, such as benzatriazole (BTA) and morpholine (Mr), in a composition of low-temperature fluxes based on triethanolamine and glycerine, as well as their technological compatibility with Sn- and Pb-base solders in brazing of aluminium. Such materials produced by the preparative synthesis are white powders that are hard to hydrolyse in air and have a limited solubility in solvents of different nature. Synthesised complex compounds are characterised by sufficiently complicated thermochemical processes occurring in heating within a temperature range of 80–500 °C, such as melting, sublimation of boron trifluoride and destruction [19, 20].

Soldering of flat samples 25 × 25 × 0.5 mm in size of aluminium A5 (99.7 % Al) was conducted using a heating unit within a temperature range of 240–340 °C. Weights of a solder and flux with volume of 25 mm^2 (equal portions) were placed at the centre of a sample. The use was made of solders Sn–39 % Pb, Sn–20 % Cd–25 % Zn and Pb–20 % Cd–1 % Zn, as well as of low-temperature fluxes based on triethanolamine with different activators: zinc and cadmium fluoborates (F59A), amine fluoborates (F5), complex of lead TFB with BTA (FTFA200), and based on glycerine: complexes of cadmium and zinc TFB with Mr (FTFA280). Reactivity of fluxes was evaluated by the spreading factor (Standard QQ-58-3715, USA) and ability to form sound joints in T-samples:

$$\Phi_{sp} = (D - H)/D \cdot 100\ \%,$$

where D is the diameter of the solder drop in the form of an equivalent sphere of the volume equal to that of the solder sample tested, mm; and H is the height of a segment of the spread solder, mm.

The lowest reactivity was exhibited by fluxes containing amine fluoborates (F5), and the highest reactivity — by fluxes with synthesised complex TFB of metals — Pb, Zn, Cd (Figure 6). It was found that increase in the soldering temperature to 300 °C and heating rate to more than 50 °C/s provides a substantial improvement in spreading of solders of all the systems over the aluminium surface.

As found in [21], at temperatures above 220 °C the process of spreading of solders using flux F59A is accompanied by intensive decomposition of salts of zinc and cadmium tetrafluoborates, as well as evolution of gaseous products of reaction between boron trifluoride and triethanolamine vapours.

Evolution of gaseous reaction products from fluxes with complex TFB, i.e. mixtures of vapours of the base (triethanolamine or glycerine) with boron trifluoride, also takes place in soldering within a temperature range of 240–320 °C. The temperature limits of thermochemical interactions of aluminium with fluxes FTFA200 and FTFA280 are wider by about 20–60 °C and shifted to higher temperatures, in contrast to fluxes F59A and F5. X-ray microanalysis revealed substantial concentrations of lead reduced by aluminium from flux FTFA200 at solder–aluminium interfaces (2.41 wt.% at the surface and 15.8 wt.% in a soldered joint) (Figure 7).

The results obtained allowed evaluation of peculiarities of chemical interaction in the aluminium–solder–flux system containing complex TFB in soldering: boron trifluoride destroys the oxide film on the aluminium surface (at T = 200–280 °C), metal that is part of complex TFB is deposited on the aluminium surfaces in the form of a metal coating as a result of aluminothermic reduction (at T = 260–300 °C), and molten solder wets the coating, spreads over it under a flux layer and fills the soldering gap.

Replacement of organic ligand or metal in a composition of synthesised complex TFB makes it possible to vary over a wide range the melting temperatures, destruction and fluxing activity, which allows optimisation of both flux composition and technological compatibility of different solder–flux–base metal systems. The optimal compatibility in the aluminium–solder–flux system containing complex TFB of metals was selected, which enabled improvement of the qual-

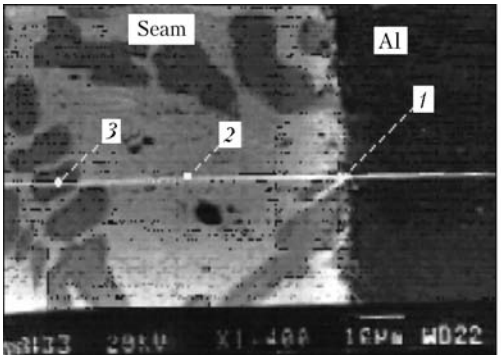

Point number	Content of elements, wt.%, in microvolumes				
	Sn	Cd	Zn	Al	Pb
1	39.2	43.3	1.3	0.3	15.8
2	77.0	19.0	3.9	0.1	0
3	77.0	0.74	99.2	0	0

Figure 7. Microstructure (×1400) of metal of soldered joint in aluminium A5, made by using solder Sn–20 % Cd–25 % Zn, flux FTFA200 at T_b = 280 °C (for *1–3* see the Table)

ity of soldered joints, i.e. strength of the aluminium joints was increased by about 8–10 % for all types of the solders, compared with that for flux F59A. Moreover, this makes it possible to reduce toxicity and, in a number of cases, cost of fluxes.

The investigation results were used for the development of the technology for soldering of aluminium wires 0.1–2.5 mm in diameter, foils 0.065–0.100 mm thick, and pressure seals of thin-walled tubes and casings. In all the cases the use was made of a soldering iron, gas torch or fan heater. The time of soldering using the Sn- and Pb-base solders is a few seconds. Fluxes FTFA200 and FTFA280, as well as their remainders after soldering, are of low corrosiveness and can be easily removed by water.

CONCLUSIONS

1. Salt mixtures of the K–Al–Si/F ternary system are a good base for development of reactive fluxes and processes of reactive flux brazing of aluminium and its alloys, as well as aluminium to steel. Contact of salt melts with aluminium results in formation of an Al–Si alloy that can function as a brazing filler alloy, which is especially important for quality brazing of multiple-element spatial structures.

2. The developed fluxes with synthesised activators, i.e. complex lead, cadmium and zinc tetrafluoborates with nitrogen-containing bases, are highly efficient for soldering aluminium using low-melting point tin- and lead-base solders.

1. (2003) *Refer. book on brazing*. Ed. by I.E. Petrunin. Moscow: Mashonostroenie.
2. Nikitinsky, A.M. (1983) *Brazing of aluminium and its alloys*. Moscow: Mashinostroenie.
3. *Satt att framstaella en loedskary mellan aluminium-eller aluminium-legeringskomponenter*. Pat. 7310586-8 Sweden. Int. Cl. B 23 K 35/36. Publ. 17.08.81.
4. *Method of brazing aluminium*. Pat. 3971501 USA. Int. Cl. B 23 K 35/12. Publ. 27.07.76.
5. Timsit, R.S., Janeway, B.J. (1994) A novel brazing technique for aluminium. *Welding J.*, 73(**10**), 119–128.
6. Philips, B., Warschaw, C.H., Mockrin, I. (1966) Equilibria in $KAlF_4$-containing system. *J. Amer. Ceram. Soc.*, 49(**12**), 631.
7. (1997) *Brazing technology: NOCOLOK flux*. Advertising brochure. Gannover: SOLVAY.
8. Andrijko, A.A., Panov, E.V., Yakovlev, B.V. et al. (1997) Fusibility and chemical interaction in salt system K–Al–Si/F. *Ukr. Khim. Zhurnal*, 63(**10**), 121–124.
9. Mondolfo, L.F. (1979) *Structure and properties of aluminium alloys*. Moscow: Metallurgiya.
10. Eryomenko, V.N., Lesnik, N.D., Pestun, T.S. et al. (1972) About kinetics of spreading of aluminium-silicon melts over iron. In: *Wetting and surface properties of melts and solids*. Kiev: Naukova Dumka.
11. Lashko, S.V., Lashko, N.F. (1988) *Brazing of metals*. Moscow: Metallurgiya.
12. Lashko, S.V., Lashko, N.F., Nagapetyan, I.G. et al. (1983) *Development of brazing technology of metallic products*. Moscow: Metallurgiya.
13. Vitkin, A.I., Tejdl, I.I. (1971) *Metallic coatings of sheet and strip steels*. Moscow: Metallurgiya.
14. Ryabov, V.R. (1973) *Aluminizing of steel*. Moscow: Metallurgiya.
15. Takemoto, T., Matsunawa, A., Kitagawa, A. (1996) Decomposition of non-corrosive aluminum brazing flux during heating. *J. Mater. Sci. Lett.*, 15(**4**), 301–303.
16. Khorunov, V.F., Samojlenko, V.G., Chebotaryov, A.N. et al. (1990) Tetrafluorborate fluxes for soldering. *Avtomatich. Svarka*, **6**, 64–66.
17. Ostrovskaya, T.V., Amirova, S.A. (1970) Chemical transformations of magnesium, calcium, strontium, zinc and cadmium tetrafluorborates in heating. *Zhurnal Neorganich. Khimii*, 15(**3**), 657–660.
18. Chebotaryov, A.N., Shestakova, M.V., Khorunov, V.F. et al. (2002) Special features of thermal transformations of tetrafluoborate salts of nitrogen-containing organic bases as the promising constituents of soldering fluxes. In: *Proc. of 1st Int. Sci.-Practical Conf. on Protection of Environment, Health, Safety in Welding Production* (Odessa, Sept. 11–13, 2002). Odessa.
19. Chebotaryov, A.N., Shestakova, M.V., Khorunov, V.F. et al. (2000) Complex tetrafluoborates of lead (II) with nitrogen-containing organic bases. *Ukr. Khimich. Zhurnal*, 66(**6**) 26–30.
20. Chebotaryov, A.N., Shestakova, M.V., Khorunov, V.F. et al. (2000) Synthesis and physico-chemical properties of complex tetrafluoborates of lead (II) and cadmium (II) with nitrogen-containing organic bases. *Ibid.*, 66(**8**), 81–86.
21. Khorunov, V.F., Sabadash, O.M., Chebotarev, A.N. (1999) Soldering of aluminium using low-temperature fluxes containing tetrafluorborate activators. In: *Proc. of 3rd Int. Seminar in Precision and Electronic Technology INSEL* (Warsaw, Nov. 22–24, 1999). Warsaw.

MATERIALS WELDABILITY CRITERIA

K.A. YUSHCHENKO and **V.V. DERLOMENKO**
E.O. Paton Electric Welding Institute, NASU, Kiev, Ukraine

The new definition of weldability implies that it is a property of material, which is determined by the degree of degradation and can be evaluated as an integrated indicator. Examples of degradation of some materials characterising their weldability are given. Premises for development of a modern concept of weldability in terms of its control are considered.

Keywords: *weldability, evaluation of weldability, joinability, weldability criterion, control, degradation*

The E.O. Paton Electric Welding Institute is active in fundamental research on investigation of weldability (joinability) of materials. A new approach to definition of the concept of weldability of materials and a possible method for its evaluation have been suggested in the last years [1, 2, 3]. The main point of the approach is [3, 4] that weldability (joinability) is a physical property of material. Weldability is defined as follows.

Weldability (joinability) is the property of material to form a permanent joint of the required quality and level of physical-mechanical and functional properties exhibited both during the process of its production and during operation of a product. Weldability is determined by the degree of degradation of properties of the joint as a whole and its different zones, and should be estimated as an integrated indicator.

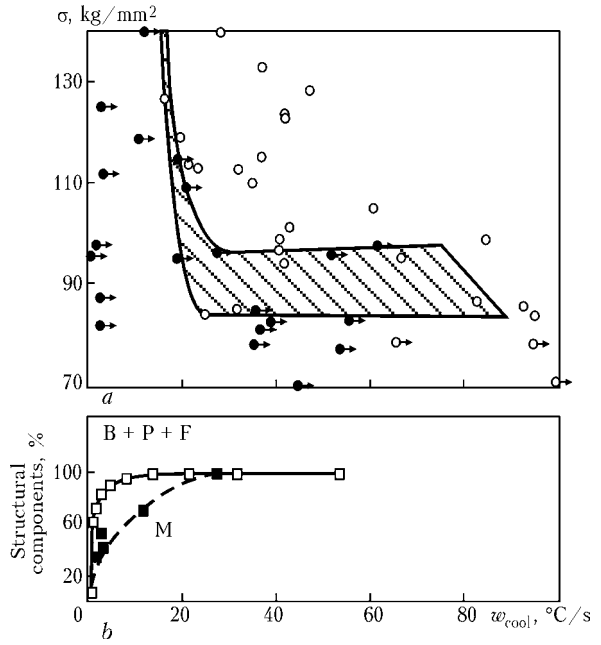

Figure 1. Effect of the cooling rate on resistance of HAZ on steel 35KhGSA to delayed fracture (*a*) and on proportion of its structural components (*b*). Dark circles in (*a*) show the specimens that did not fracture during a test time of 4 days, and light circles show the fractured specimens. Solid curve in (*b*) indicates cooling conditions without deformation, and dashed curve — with a 5–12 % deformation of austenite within a cooling temperature range of 550–400 °C [5]

This property is evaluated by the degree of degradation of physical, electrochemical, service, functional and other characteristics with respect to the initial material, depending upon the joining technology and operational conditions. It is necessary to determine peculiarities of the degradation to control weldability (joinability) as a property of material. Knowing these peculiarities, it is possible to use the principle of variation of thermal, force, physical or electrochemical methods to affect the material in order to achieve a specified (permissible) degradation level.

Consider some examples showing the character of degradation of materials in a joint and its level.

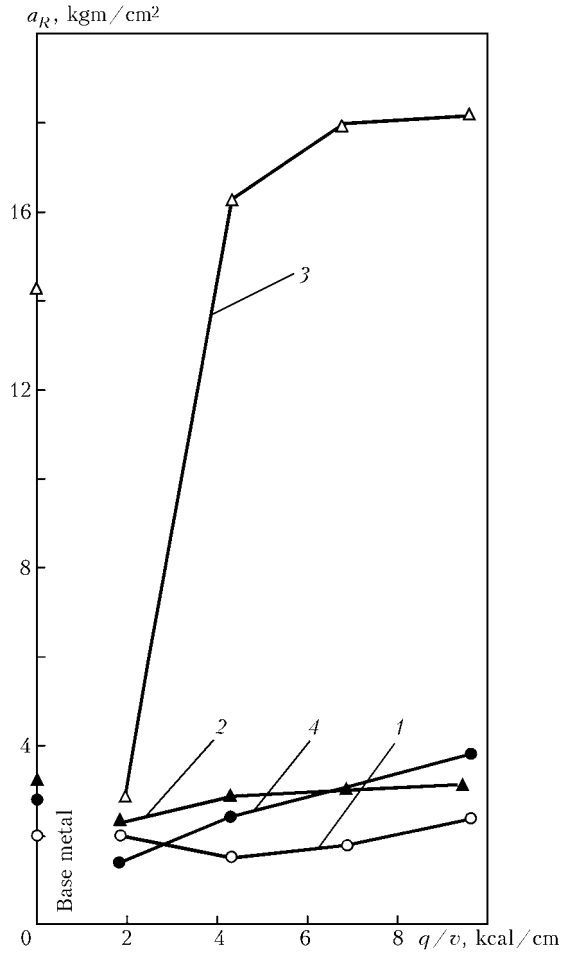

Figure 2. Effect of heat input of the arc, q/v, on impact toughness of Schnadt specimens, a, at a notch radius R of 0.025 mm to ∞, and Mesnager specimen, a_n, cut from 16 mm thick plates of steel 45 with a notch in the HAZ [5]: *1* — $a_{0.025}$; *2* — $a_{0.5}$; *3* — a_∞; *4* — a_n

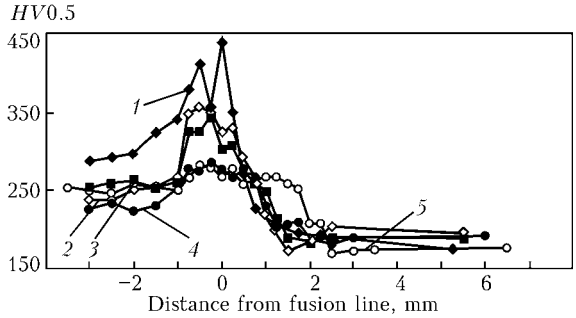

Figure 3. Hardness versus distance from the fusion zone at different preheat temperatures for 1Cr0.5Mo manual metal arc weld beads with heat input of about 0.95 kJ/mm: *1* — no preheat; *2* — preheat temperature 100 °C; *3* — 200 °C; *4* — 300 °C; *5* — 400 °C [6]

Welding of high-strength steels is accompanied by a change of properties of the weld or HAZ metal [5]. In particular, impact toughness decreases or sensitivity to brittle fracture increases, as well as cold cracks and other defects may be formed and grow to such a level that the welded joint cannot work and ensure the required performance relative to the base metal. This material is considered hard-to-weld or unweldable. Figure 1 shows an example, where the degree of changes in properties, i.e. degradation, is affected by the cooling rate. Increasing the cooling rate leads to a dramatic decrease in resistance of the HAZ of a welded joint to delayed or brittle fracture, and to a substantial redistribution of structural components. In Figure 2, the degree of degradation expressed in terms of impact toughness of the HAZ greatly differs from that of the base metal. Figure 3 shows variations in hardness (degradation) of the fusion zone in steel with 1 % Cr and 0.5 % Mo, depending upon the heating temperature.

The main difficulty in welding of stable-austenitic steels is an increased sensitivity to hot cracking of the weld and HAZ metal (Figure 4). Presence of these cracks and difficulties associated with their elimination make these materials hard-to-weld or unweldable. A substantial change in properties of metal (degradation) takes place at the presence of micro- or macrocracks.

Some structures operating under the hydrogen conditions [7] are characterised by a change of properties

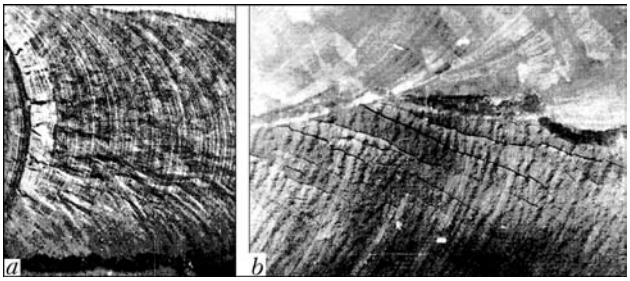

Figure 4. Appearance of specimens of steel X23N18 with solidification cracks in weld metal (*a*) and HAZ (*b*)

(degradation), and, first of all, embrittlement of the weld and HAZ metal, taking place as hydrogen is accumulated with time. This also transfers these materials to a category of hard-to-weld ones, as decrease in ductility reduces the service life. Figure 5, *a* shows an embrittlement effect of hydrogen (degradation) on titanium alloy depending upon the operating temperature. In a number of cases the degree of degradation is so high (Figure 5, *b*) that it initiates cracks in metal under static loading.

The effect of radiation on materials and their welded joints (especially the weld and HAZ metal) is well known in nuclear power engineering. This effect leads to swelling [8] and, eventually, to catastrophic decrease in performance. Because of this, the affected materials (high-nickel steels and alloys, some composites) are also categorised as having a limited weldability (Figures 6 and 7).

Proceeding from the basic notion that weldability is a property, and that this property can be controlled, it is possible to identify criteria for evaluation of degradation, i.e. weldability (joinability) of material. To achieve the certain degree of degradation, it is necessary to apply a certain energy, which can be evaluated in accepted and comprehensible physical values, i.e. in degradation of such a characteristic of material as impact or fracture toughness the energy consumed to cause a change of properties or their recovery to a level of the initial material can be quantitatively estimated.

In analogy, we can estimate the degree of degradation (weldability indicator) for conditions of hot

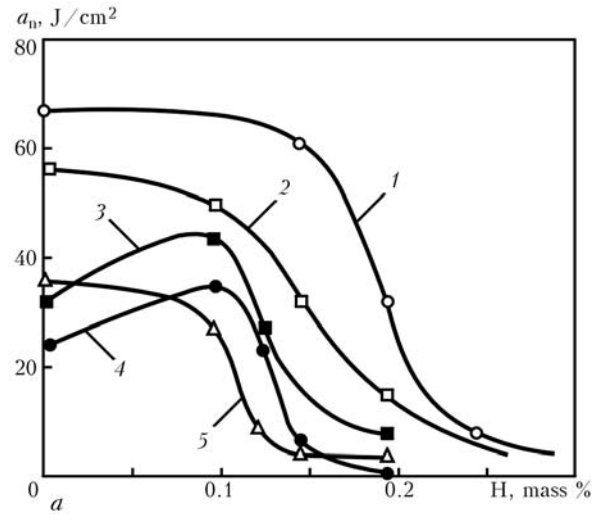

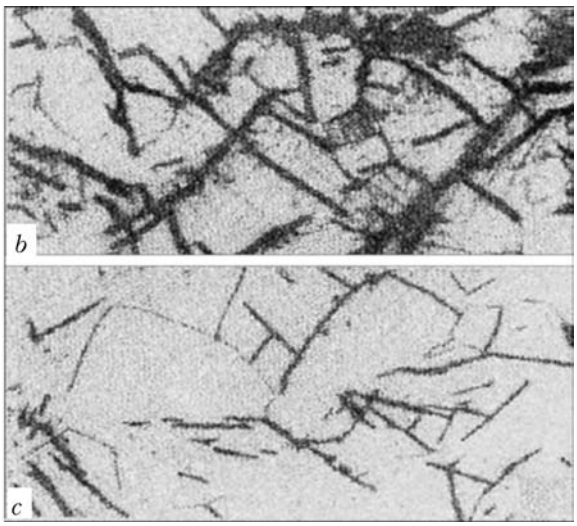

Figure 5. Effect of hydrogen on impact toughness of hardened β-alloy VT15 at different operating temperatures T_{op} (*a*) and microcracks in hardened β-alloy VT15 with 0.015 wt.% H in impact toughness (*b*) and elongation (*c*) tests at a temperature of −20 °C: *1* — T_{op} = = 20 °C; *2* — 0; *3* — −25; 4 — −50; *5* — −77 [7]

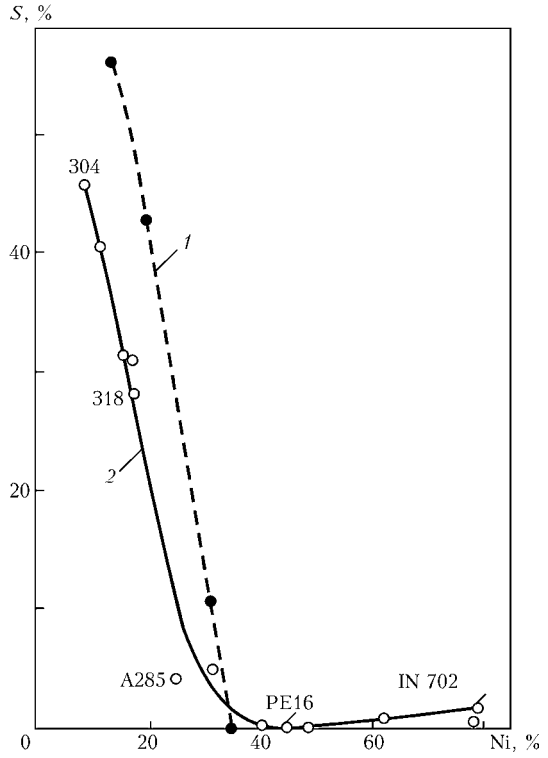

Figure 6. Dependence of swelling of laboratory (*1*) and commercial (*2*) alloys Fe–Cr–Ni upon the nickel content. Irradiation with ions Ni^{2+} (5 MeV) at 898 K to 140 displ/atom [8]

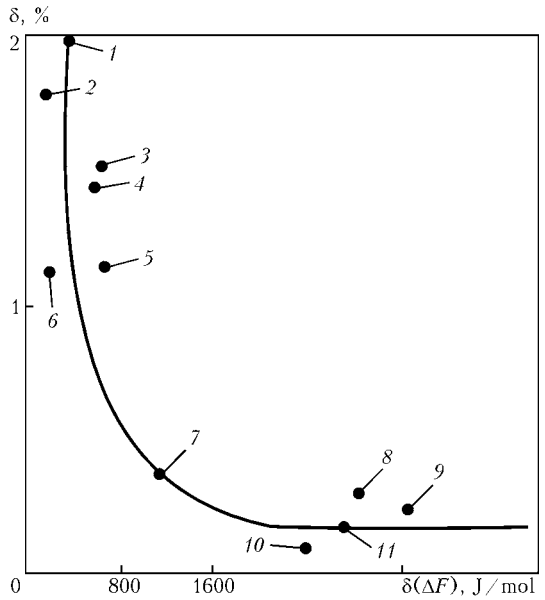

Figure 7. Dependence of elongation of specimens of alloys Fe–Cr–Ni exposed to radiation in reactor DFR to 30 displ/atom at 873 K upon variations of free energy in austenitic and ferritic states: *1* — FV548 (11.6 % Ni, 17.0 % Cr); *2* — 347 (9.1, 17.8); *3* — 316L (13.6, 16.4); *4* — 316 (12.2, 17.8); *5* — M316 (13.7, 17.2); *6* — 321 (9.5, 17.5); *7* — G68 (25.0, 13.7); *8* — PF16 (3) (43.3, 16.5); *9* — GAB (286) (42.6, 16.0); *10* — PE16 (1) (43.0, 16.6); *11* — PE16 (2) (40.3, 15.4) [8]

and cold cracking of the weld and HAZ metal, hydrogen induced embrittlement, corrosion cracking, etc. Any change of functional properties relative to the initial equilibrium state of a system as a whole can be estimated in terms of the energy criterion, i.e. specific energy required for such a change. This allows us to emphasise again that weldability is a property

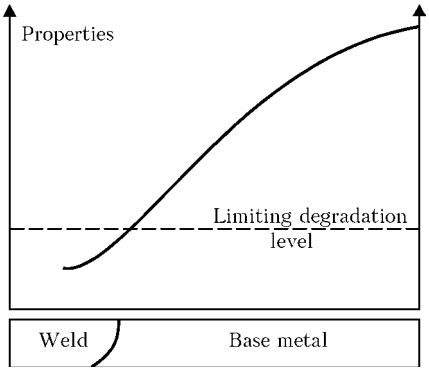

Figure 8. Schematic presentation of the ultimate level of degradation

of material. Knowing optimal conditions for equilibrium existence of the system (material) and energy consumed for its change, leading to a non-equilibrium state, including both for the joining (welding) process and the process of operation of a welded joint, the generalised indicators of weldability can and should be set as specification characteristics for a given material. In analogy with such properties as yield stress, tensile strength and others, they should be used and allowed for both in design of new structural materials and in operation. In this case, the physical point of weldability as a property is explicable and analysable in a generalised manner. We mean development of algorithms for accounting, calculation and control of weldability based on the «permissible degree of degradation» principle (Figure 8). Apparently, numerical criteria of weldability will be established in the near future for all structural materials.

In terms of its physical interpretation, energy indicators and control methods established by PWI, the degree of degradation can serve as a key to study the ageing processes, estimate potential and actual life of materials, evaluate reliability of structures and constructions under actual and potential loading, i.e. change in equilibrium of the «material–technology–structure–service conditions» system.

CONCLUSIONS

1. Weldability (joinability) is a property of material, which should be indicated in specifications.

2. The degree of degradation is a criterion of weldability (joinability) as a property of material.

3. The degree of degradation can be evaluated and controlled by using a versatile energy criterion or a set of indicators.

1. Yushchenko, K.A. (2003) Perspective processes for materials welding. In: *Proc. of Seminar dedicated to R. Dolby*. London: TWI.
2. Yushchenko, K.A. (2004) Welding processes for new materials. *IIW Doc. XII-1834–04*.
3. Yushchenko, K.A. (2004) Weldability and advanced processes for materials welding. *The Paton Welding J.*, **9**, 39–44.
4. Yushchenko, K.A., Derlomenko, V.V. (2005) Analysis of modern views on weldability. *Ibid.*, **1**, 5–9.
5. Shorshorov, M.Kh. (1965) *Metals science in welding of steel and titanium alloys*. Moscow: Nauka.
6. Storesund, J. (2002) Weld repair of creep exposed power plant components. *IIW Doc. IX-2028–02*.
7. Kolachev, B.A. (1985) *Hydrogen embrittlement of metals*. Moscow: Metalurgiya.
8. Zelensky, V.F., Neklyudov, I.M., Chernyaeva, I.M. (1988) *Radiation defects and metals swelling*. Kiev: Naukova Dumka.

PROFESSOR KUCHUK-YATSENKO IS 75

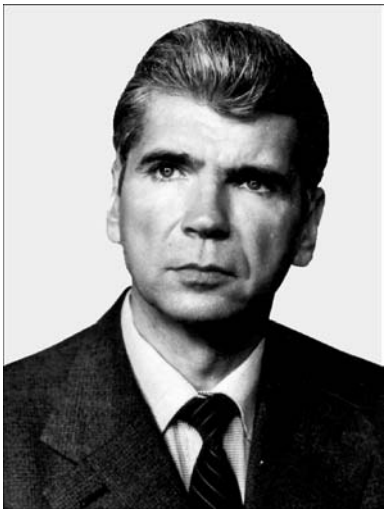

On August 2, 2005 Prof. Sergey I. Kuchuk-Yatsenko, Deputy Director of the E.O. Paton Electric Welding Institute, will celebrate his 75-year birthday anniversary.

In 1953 after the graduation from Kiev Polytechnic Institute S.I. Kuchuk-Yatsenko was assigned for work to the E.O. Paton Electric Welding Institute, where he passed the glorious working path from young engineer up to Professor, Dr. of Techn. Sci., Chief of Department of one of the leading departments, Deputy Director of the Institute on research works, academician of the National Academy of Sciences of Ukraine.

In 1960 S.I.Kuchuk-Yatsenko defended thesis for Cand. of Techn. Sci. degree, and in 1972 — for Dr. of Techn. Sci. degree. In 1978 he was elected a corresponent member of the NASU, and in 1987 was elected a full member of the NASU.

The research activity of Prof. Kuchuk-Yatsenko is connected with investigations of physical-metallurgical processes in welding of different materials in a solid phase. In particular, he obtained new data about specifics of formation of joints with the formation of a thin layer of molten metal on contacting surfaces of parts being welded, its behavior under the action of electrodynamic forces and its peculiarities of interaction with a gaseous medium in the zone of contact. It was shown for the first time that the state of molten metal in the period, preceding the deformation of parts being welded, has a dominating effect on the formation of metallic bonds between the contacting surfaces and formation of chemical non-homogeneity in the joint zone. The effect of oxide structures in molten metal on the quality of joints was studies comprehensively and ways of minimizing of oxidizing processes in the mentioned period of welding were defined.

In parallel with the above-mentioned investigations, Prof. Kuchuk-Yatsenko is carrying out over the many years a purposeful study of rapidly proceeding processes of heating and failure of single contacts at high concentrations of power. He established a number of new laws characterizing the power characteristics of the process of resistance melting of metal and defined the ways of automatic control of main parameters to create the most favorable conditions of heating and deformation of parts being welded.

The practical result of the above-mentioned fundamental research works is the development of new methods of the flash-butt welding with a continuous, pulsed and pulsing flashing, patented in the leading countries of the world. On their basis, S.I. Kuchuk-Yatsenko in collaboration with staff members has developed the technologies of welding of various products, control systems and new models of welding equipment having no analogues in the world practice. The equipment is characterized by a high efficiency, minimum consumed power and mass, provides a stable and high quality of joints. These advantages are most important in welding of intricate parts with large cross-sections. For the first time the flash-butt welding was used for the fulfillment of works in the field conditions.

Scientific and engineering activity of S.I. Kuchuk-Yatsenko is characterized by an integrated approach to the solution of problems put forward. Fundamental studies, made by him, are accompanied by the development of unique technologies of welding, automatic, and over the recent years, computer control of welding process and design of the updated welding equipment.

At his personal participation the organizing of industrial manufacturing of the new welding equipment and its mass implementation in industry have been realized. Below, the most important stages of activity of S.I. Kuchuk-Yatsenko are described.

More than 40 years Prof. Kuchuk-Yatsenko is dealing with works on rail welding. Technology and equipment, developed at his active participation and supervision, made it possible to use for the first time in the world practice the highly-efficient flash-butt welding in the field conditions that greatly promoted the railway transition to the continuous tracks. At his active participation the serial manufacture of this equipment by the PWI documentation was organized at Kakhovka Plant of Electric Welding Equipment, which since the 1970s became the world exporter of this equipment. Over the past years more than ten generations of rail welding machines were designed and manufactured, which are used in CIS countries and in many other countries of the world. S.I. Kuchuk-Yatsenko takes an active part in the updating of this equipment and technology of welding that allows maintaining of its high competitiveness. During recently, the new generations of welding machines allowing rails of infinite length to be welded in repair

of continuous tracks with a simultaneous stabilization of their stressed state were created.

In 1966 S.I. Kuchuk-Yarsenko was awarded the Levin Prize among the author's team for the development and implementation of the machine for rail flash-butt welding in repair and construction of the continuous railway tracks.

Developments of S.I. Kuchuk-Yatsenko and his associates were also used successfully at machine-building plants in manufacture of ring pre-fabrications, shafts and those of dissimilar metals. Application of multi-position flash-butt welding occurred to be very effective allowing welding of large-sized parts simultaneously in several places (engine casings, radiators of powerful transformers). Implementation of installation in the production line for manufacturing crankcases of blocks of powerful diesels at Kolomna Diesel Locomotive Building Plant allowed 70 times increasing in labour productivity and releasing 380 welders. The significant effect was also obtained as a result of multi-position welding at Zaporozhie Transformer Plant in manufacture of radiators of transformers. In 1976 S.I. Kuchuk-Yatsenko was awarded the State Prize of Ukr. SSR in the team of authors for the development and industrial implementation of the new technology and highly-efficient assembly-welding complexes for the serial manufacture of large-sized structures made from unified elements.

First in the world practice Prof. Kuchuk-Yatsenko with a team of associates has developed the unique technology of flash-butt welding of intricate products of a large section made from high-strength alloys on aluminium base, producing the joints almost equal in strength to that of the parent metal. Unique equipment was designed and manufactured on its basis which is used in manufacture of space vehicles at the plants of Russia and Ukraine. In 1986 S.I. Kuchuk-Yatsenko was awarded the State Prize of the USSR in the team of authors for the creation of technology and equipment for the flash-butt welding of structures of high-strength aluminium alloys.

A great contribution was made by S.I. Kuchuk-Yatsenko to the creation of technology and equipment for the flash-butt welding of different-purpose pipelines. At his active participation, the technologies, control systems and equipment for flash-butt welding of pipes of diameter from 60 up to 1400 mm were developed and implemented in construction of pipelines at the territory of the former USSR. More than 70,000 km of different-purpose pipelines, including 4000 km of the most powerful pipelines in the region of the Extreme North, were welded with use of this welding. The application of the flash-butt welding made it possible to increase the labor productivity and to guarantee the reliability of pipelines. This work was also awarded the Lenin Prize in 1989.

Over the recent years the equipment for welding of a out-of-standard rolled metal with a large cross-section has been developed on the basis of technology of the flash-butt welding with a pulsing flashing. This development will make it possible to increase the output of efficient products in manufacture of rolled metal at the metallurgical plants.

S.I. Kuchuk-Yatsenko takes an active part in all stage of realization of the above-mentioned works. His inventive and engineering activity is connected with numerous inventions and foreign patents.

In 1998 he was awarded the title «Distinguished person in science and technology of Ukraine».

Prof. Kuchuk-Yatsenko is the author of more than 550 scientific publications, including ten manuscripts, a large number of author's certificates, Ukrainian and foreign patents, most of which were purchased in the form of license agreements by foreign companies. In particular, in 1979 he was the supervisor of works by license agreement with company McDermott, USA, according to which the technological works were conducted on flash-butt welding of thick-walled large-diameter pipes and a specialized equipment was designed and manufactured.

At present Prof. Kuchuk-Yatsenko is continuing to deal with actual problems in the field of welding, development of challenging technologies of joining the hard-to-weld materials. He is heading one of the leading research departments of PWI and is a scientific supervisor of the Engineering Center of Pressure Welding.

S.I. Kuchuk-Yatsenko cooperates for a long time with Kakhovka Plant of Electric Welding Equipment, one of the leading enterprises-manufacturers of welding equipment in Ukraine. He took an active part in organizing a serial manufacture of flash-butt machines for welding railway rails and pipes. He was at the origin of cooperation with Canadian company E.O. Paton International Holdings, Inc., which in collaboration with PWI, ECPW and KPEWE, manufactures and services rail-welding equipment in many countries of the world.

S.I. Kuchuk-Yatsenko is a vice-chairman of the PWI scientific council, a member of editorial board of the journal «Avtomaticheskaya Svarka», a member of Interstate Scientific Council on welding and related technologies. He was the supervisor of more than ten theses for scientific degrees.

He was elected the first president of Ukrainian Welding Society and a member of its management board. He is a member of AWS.

Achievements of the scientist were awarded by Orders of the Red Banner of Labour, Badge of Honour, Prince of Yaroslav the Wise, and medals. We congratulate sincerely Sergey Ivanovich Kuchuk-Yatsenko with the 75-year birthday anniversary and wish him a strong health, every happiness and new creative achievements.

Editorial Board of «The Paton Welding Journal» of the E.O. Paton Electric Welding Institute of the NAS of Ukraine

3-GUN MACHINE KL-117 FOR ELECTRON BEAM WELDING OF DRILL BITS

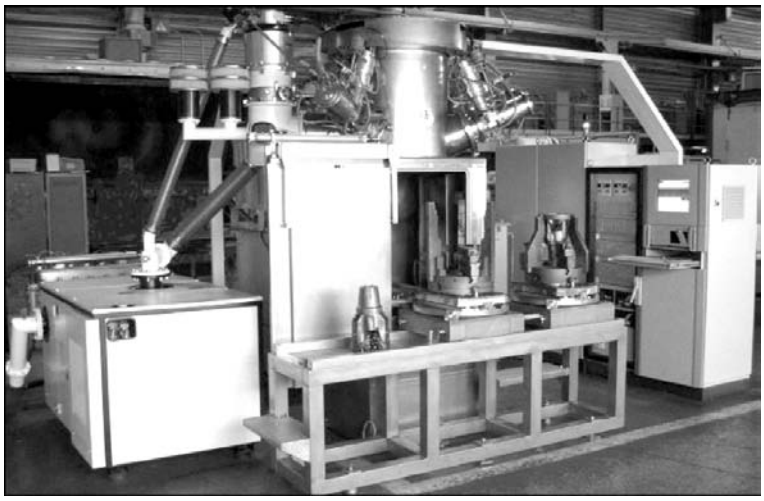

✔ Machine is intended for electron beam welding of drill bits up to 17.5" diameter with simultaneous performance of three welds, thus increasing both accuracy of drill bits dimensions and welding output.

✔ Application of a powerful control electronic tube in the accelerating voltage source prevents the arc processes in the welding gun by a short interruption of accelerating voltage, which does not lead to weld formation defects.

✔ The RASTR system, functioning on the principles of raster electron microscope, enables following the welding process and automatic coquidance of each of three electron beams to the butts of groove faces in the real time. The clear picture of the welding process is displayed on the monitor screen and is not exposed to the welded metal vapors, which is characteristic for traditional optical observing systems.

✔ Machine is provided with the electrons beam diagnostic system allowing an operator:

- to define the beam focusing plane position prior to welding;
- to periodically evaluate changes in space and energy beam parameters in order to define the necessity of the welding gun cathode replacement.

✔ Lanthanum hexaboride cathode as a tablet has service life of not less than 40 h in the welding mode at beam power of 20 kW, and the beam axis position does not change at changes in beam focusing.

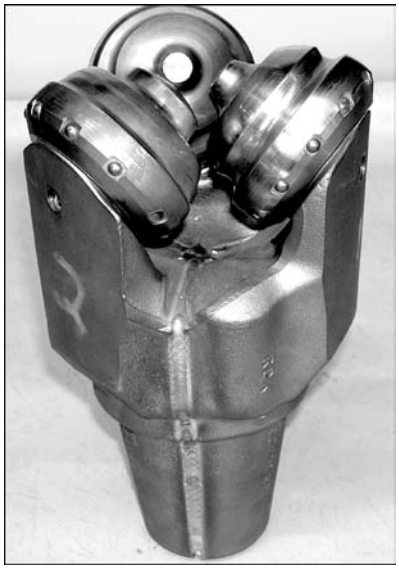

✔ Control of all equipment subsystems by means of CNC +PLC.

✔ The computer system of electron beam scanning stabilizes the molten pool state and improves the quality of face and root surfaces formation of the weld.

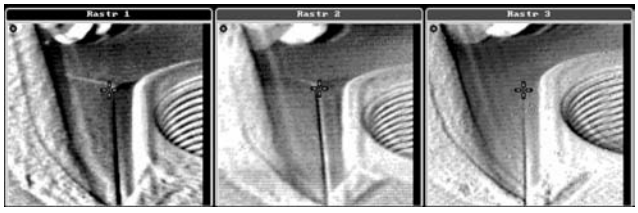

E.O. Paton Electric Welding Institute of NASU
11, Bozhenko Str., 03680, Kiev, Ukraine; Tel./fax: (38044) 525 4319
E-mail: nazarenko@technobeam.com.ua www.nas.gov.ua/pwj/beam/index.html

ADVANCE BOOK INFORMATION

FORTHCOMING BOOK INFORMATION

Vladimir I. Makhnenko, Viktor E. Pochynok. STRENGTH CALCULATION OF WELDED JOINTS WITH CRACK-LIKE IMPERFECTIONS.
Approx. 400 pp., 165×235 mm, hardback. November 2005. US$ 90

In this manuscript, the idea of the fitness-for-purpose concept is used to improve strength calculations of welded joints with crack-like imperfections caused by structural or technological factors. These include welded joints with fillet, spot, slot and butt welds having sharp fissures brought by geometry of the elements welded and limited sizes of the weld sections. Such joints are widely encountered in modern general-purpose welded structures used in civil building, shipbuilding, automobile industries, etc.

The welded joints just mentioned do not usually cause problems for structures of relatively ductile materials with small-to-medium thicknesses of component sections, and operating under predominantly static loading. However, the use of new structural materials, especially high-strength steels and aluminum alloys, etc., large cross sections of structural elements, and loading with alternate loads, requires a certain caution to be taken. Nonetheless, the technological advantages that these joints produce attract an interest in their use, of course, when it does not cause any harm to the structure safety and its residual service life.

Performing strength calculations based on the fitness-for-purpose criterion for the joints encountered in general-purpose structures, allows ensuring the requirements concerning the service life-time. However, there is a difficulty of implementing such calculations in wide engineering practice. As shown by the authors, a successful implementation of the mentioned concept for general-purpose welded joints and for wide range of users is possible only when it is based on the use of corresponding computer systems with friendly user interface, which do not require a user to have a special knowledge in fracture mechanics, deformation mechanics, numerical methods, etc. Such systems are to be portable and efficient, i.e. calculations of appropriate section sizes or verification of strength of specific joints should be done promptly. In turn, it requires development of numerical procedures and creation of specialized databases that simplify and accelerate calculations.

Viktor Ya. Kononenko. TECHNOLOGIES OF UNDERWATER WET WELDING AND CUTTING.
Approx. 140 pp., 140×200 mm, softback. December 2005. US$ 40

The book deals with the features of arcing, metal transfer and joint formation in consumable-electrode wet underwater welding. Principles of development of coated electrodes and self-shielded flux-cored wires for underwater welding and cutting are established. Characteristics of welding consumables and mechanical properties of weld metal are given. Some types of joints, procedure of preparation and fit-up for welding, possible defects of the joints and methods to prevent their formation are described.

Information on characteristic damage to the underwater metal structures is generalized, and technological solutions are given, which have been implemented during restoration of their performance, using wet processes of underwater welding and cutting. The book gives the characteristics of the equipment for implementation of underwater arc welding process.

The main processes of thermal underwater cutting are presented, and characteristics of consumable materials and equipment for its implementation are described. Examples of work performance using underwater cutting are given.

The book is designed for scientific and engineering-technical personnel, qualified welders-divers involved in design, fabrication and repair of underwater constructions.

The book is written by a specialist, who is developing electrode materials and technologies and has a vast experience of practical work under the water.

ADVANCE BOOK INFORMATION

TITANIUM: Titanium and its alloys. Technologies. Equipment. Production. Electrometallurgy. Welding

Approx. 180 pp., 200×290 mm, softback. December 2005. US$ 50

The collection presents papers on electrometallurgy and welding of titanium and its alloys published between 2002 and 2005 in «Advances in Electrometallurgy» and «The Paton Welding Journal» journals. The authors of the papers are scientists and specialists in the field of titanium and its production, known in Ukraine and abroad. The collection is designed for a broad range of readers dealing with the problems of production, processing and use of titanium.

ORDER RORM

Please return to:

International Association «Welding»,
11, Bozhenko str., Kiev, 03680, Ukraine
Tel.: (38044) 287 6757, 287 6049, 529 2623
Fax: (38044) 287 4677
E-mail: journal@paton.kiev.ua; tomik@mac.relc.com

Please send me:

❑ Vladimir I. Makhnenko, Viktor E. Pochynok «Strength Calculation of Welded Joints with Crack-Like Imperfections». US$ 90, postage included

❑ Viktor Ya. Kononenko «Technologies of Underwater Wet Welding and Cutting». US$ 40, postage included

❑ «Titanium». Collection of Scienific Paper. US$ 50, postage included

How to Pay and Payment Details

❑ By bank transfer (or mail a cheque) into our account
№ 2600801283433
UKREXIMBANK, Kiev, Ukraine
S.W.I.F.T.: EXBSUAUX
CORR. ACC. #04-094-227
Bankers Trust Company,
New York, U.S.A.
S.W.I.F.T.: BKTR US 33

❑ Please Invoice

❑ Your Details
Name _____

Organization _____

Address _____

Signed _____ Date _____

INFORMATION FOR CONTRIBUTORS TO
THE PATON WELDING JOURNAL

«The Paton Welding Journal» is an English translation of the monthly «Avtomaticheskaya Svarka» journal published in Russian since 1948.

THE PATON WELDING JOURNAL is a scientific journal publishing fundamental and applied papers and short notes in the area of:

- *weldability of structural materials*
- *welding different types of steels and cast irons*
- *welding non-ferrous metals, including aluminium, titanium, etc.*
- *joining dissimilar and composite materials*
- *welding refractory metals and alloys*
- *welding cryogenic materials*
- *arc welding*
- *flash-butt welding*
- *electron beam and laser welding*
- *explosion welding and cutting*
- *friction welding*
- *electroslag welding*
- *soldering and brazing*
- *advanced structural materials*
- *surfacing and coating deposition*
- *cutting*
- *computer technologies in welding*
- *strength of welded joints and structures*
- *residual stresses and strains*
- *calculation and design of welded joints and structures*
- *automation of welding fabrication*
- *estimation of residual life of welded structures*
- *welding for fabrication of unique structures*
- *welding and repair in thermal and nuclear power engineering*
- *advances in underwater welding, cutting and repair*

The journal accepts also advertisements and announcements of conferences and publications on related topics.

THE PATON WELDING JOURNAL is published monthly.

Subscription requests should be sent to the Editorial Office.

Manuscripts should be submitted in duplicate in English, and supplemented with a text file and figures on a diskette. An electronic copy may be submitted by e-mail.

The rules for submission of electronic copies are as follows:

- an electronic copy should be submitted on a diskette or by e-mail simultaneously with sending a hard copy of the manuscript;
- acceptable text formats: MSWord (rtf, doc);
- acceptable graphic formats for figures: EPS, TIFF, CDR. Figures created using software for mathematical and statistical calculations should be converted to one of these formats.

Manuscripts should be supplemented with:

- official letter signed by a chief manager of the institution where the work was performed. This rule does not apply to papers submitted by international groups of authors.

Title page:

- title of the paper and name(s) of the author(s);
- name of affiliated institution, full address, telephone and fax numbers, e-mail addresses (if available) for each author.

Abstract: up to 100 words, must be presented in English. Before the abstract text one should indicate in the same language: the paper title, surnames and initials of all authors.

Key words: their amount must not exceed eight word units. In the specific cases it is acceptible to use two- or three-word terms. These words must be placed under the abstract and written in the same language.

Text should be printed double-spaced on white paper (A4 format) with a 12-point font. Titles of the paper and sections should be typed with bold capitals.

Tables should be submitted on separate pages in the format of appropriate text processors, or in the text format (with columns separated by periods, commas, semicolons, or tabulation characters). Use of pseudo-graphic characters is not allowed.

List of references should be double-spaced, with references numbered in order of their appearance in the text.

Captions for figures and tables should be printed in the manuscript double-spaced after the list of references.

Pictures will be scanned for digital reproduction. Only high-quality pictures can be accepted. Inscriptions and symbols should be printed inside. Negatives, slides and transparencies are accepted.

Figures: each figure should be printed on a separate page of the manuscript and have a size not exceeding 160 × × 200 mm. For text in figures, use 10-point fonts. All figures are to be numbered in order of their appearance in the text, with sections denoted as (a), (b), etc. Placing figure numbers and captions inside figures is not allowed. On the back side, write with a pencil the paper title, author(s) name(s) and figure number, and mark the top side with an arrow.

Photographs should be submited as original prints.

Color printing is possible if its cost is covered by the authors.

For information about the rules and costs, contact the Executive Director.

No author's fee is provided for.

Publication in TPWJ is free of charge.

Manuscripts should be sent to:

Dr. Alexander T. Zelnichenko
Executive Director of
«The Paton Welding Journal»,
11, Bozhenko Str.,
03680, Kiev, Ukraine
Tel.: (38044) 287 67 57, 529 26 23
Fax: (38044) 528 04 86
E-mail: journal@paton.kiev.ua
www.nas.gov.ua/pwj